2014

Lysosomal cobalamin transport and its relevance to ageing and Alzheimer's disease

Hua Zhao
University of Wollongong

LYSOSOMAL COBALAMIN TRANSPORT AND ITS RELEVANCE TO AGEING AND ALZHEIMER'S DISEASE

A thesis submitted in (partial) fulfilment of the requirements for the award of the degree

DOCTOR OF PHILOSOPHY

from

UNIVERSITY OF WOLLONGONG

by

HUA ZHAO

SCHOOL OF BIOLOGICAL SCIENCES

FACULTY OF SCIENCE, MEDICINE AND HEALTH

2014

This thesis is dedicated to my parents.

For their endless love, support and encouragement.

DECLARATION

I, Hua Zhao, declare that this thesis, submitted in (partial) fulfilment of the requirements for the award of Doctor of Philosophy, in the School of Biological Sciences, University of Wollongong, is wholly my own work unless otherwise referenced or acknowledged. The document has not been submitted for qualifications at any other academic institution.

Hua Zhao

16 June 2014

ABSTRACT

Vitamin B_{12}, known as cobalamin (Cbl), is required for erythrocyte formation and DNA synthesis. It plays a crucial role in maintaining neurological function. As a coenzyme for methionine synthase and methylmalonyl-CoA mutase, Cbl utilisation depends on its efficient transit through the intracellular lysosomal compartment and subsequent delivery to the cytosol and mitochondria. Lysosomal function deteriorates in ageing and Alzheimer's disease (AD). Although rodent studies indicate that Cbl supplementation significantly improves cognitive performance, human trials have failed to provide a consistent beneficial effect on cognitive performance with either oral or parenteral Cbl. This thesis proposes a novel hypothesis that neuropathological conditions that impair lysosomal function, such as age-related lipofuscinosis, lysosomal storage diseases, and AD, may interrupt lysosomal Cbl transport and thereby impede Cbl utilisation. The experiments will apply, for the first time, *in vitro* and *in vivo* models of ageing and AD to define how lysosomal perturbations directly affect Cbl utilisation.

To address this question, a subcellular fractionation method was developed and western blot and gamma counting techniques were used to measure organelle marker proteins and [^{57}Co] Cbl radioactivity levels in isolated purified lysosomes, mitochondria, and cytosol that were derived from neuronal cells and mouse brain tissue. The results from cultured cells, treated with compounds to impair lysosomal protease function, revealed a ten-fold increase of [^{57}Co] Cbl in lysosomes concomitant with reduced [^{57}Co] Cbl levels in mitochondria and cytosol. Artificial

lipofuscin was synthesized and fed into cells, which also resulted in an accumulation in lysosomal [^{57}Co] Cbl levels. In addition, lysosomal [^{57}Co] Cbl transport was interrupted in lysosomal glycosphingolipid storage disease cells derived from a patient with Gaucher's disease, where lysosomal glucosylceramides had accumulated and lysosomal [^{57}Co] Cbl levels were doubled. Furthermore, C57BL/6J wild type mice and APPxPS1 AD mice were intraperitoneally injected with [^{57}Co] Cbl and the amount of [^{57}Co] Cbl radioactivity in the major organs was measured. The [^{57}Co] Cbl level in the APPxPS1 AD mouse brains demonstrated a significant increase in lysosomes and a decrease in cytosol compared to the wild type mice. These *in vivo* experiments were replicated using APP mutant cells treated with a proteasome inhibitor to induce lysosomal amyloid-beta accumulation. This similarly increased lysosomal [^{57}Co] Cbl levels.

In summary, the results from the *in vitro* and *in vivo* experiments provide a detailed understanding of the impact of lysosomal dysfunction related to brain ageing and AD on lysosomal Cbl transport at the subcellular level. These results may also explain why Cbl administration has not yielded a consistent therapeutic benefit in the ageing and AD contexts. More importantly, this thesis sheds light on this crucial issue and is a step towards identifying a clinical therapeutic target to improve neuronal Cbl utilisation and thus reduce the production of neurotoxic metabolites that accumulate when the coenzyme forms of Cbl do not reach their intracellular targets.

ACKNOWLEDGMENTS

I would like to thank my supervisor and mentor Professor Brett Garner for your invaluable support and guidance during my PhD. Thank you for all the opportunities you have given me and for all your help and advice over the last three years. You have inspired me to be a better scientist.

To Kalani Reberu and Hongyun Li, I really appreciate all the help and assistance during my study. I couldn't have done it without your support.

I would like to thank Andrew Jenner, Adena Spiro, and Sarah Abbott for your advice and assistance. I will remember the days I work with you guys.

I would like to acknowledge Anthony Don and Timothy Couttas at the University of New South Wales for using your equipment to measure glucosylceramide.

I would like to acknowledge Linda Cohen for professional proofreading some of the chapters. Thanks a lot for your time and energy.

Last but not least, to my partner and family members, thank you for all your love and endless support during my PhD.

PUBLICATIONS TO DATE

Journal articles

Zhao H, Li H, Ruberu K, Garner B (2014) "Impaired lysosomal cobalamin transport in Alzheimer's disease" J Alzheimers Dis. 43 (3).

Zhao H, Ruberu K, Li H, Garner B (2014) "Perturbation of neuronal cobalamin transport by lysosomal enzyme inhibition" Biosci Rep. 34 (1).

Zhao H, Ruberu K, Li H, Garner B (2013) **"**Analysis of subcellular [^{57}Co] cobalamin distribution in SH-SY5Y neurons and brain tissue." J Neurosci Methods. 217(1-2):67-74.

Zhao H, Brunk UT, Garner B (2011) "Age-related lysosomal dysfunction: an unrecognized roadblock for cobalamin trafficking?" Cell Mol Life Sci. 68(24):3963-9.

Conference presentations

Oral

Zhao H, Garner B (2012) "Assessing intracellular cobalamin utilisation by subcellular fractionation method" School of Biological Sciences, Kiola Postgraduate Conference, Australia.

Zhao H, Garner B (2011) "Age-related dysfunction of lysosomal cobalamin metabolism" School of Biological Sciences, Kangaroo Valley Postgraduate Conference, Australia.

Posters

Zhao H, Ruberu K, Li H, Garner B (2014) "Alzheimer's disease-related lysosomal dysfunction impairs neuronal cobalamin transport" Australian Neuroscience Society annual meeting, Adelaide, Australia.

Zhao H, Ruberu K, Li H, Garner B (2013) "Lysosomal dysfunction disrupts neuronal cobalamin transport *in vitro* and *in vivo*" Society for Neuroscience annual meeting, San Diego, USA.

Zhao H, Garner B (2013) "Age-related lysosomal alterations perturb neuronal cobalamin trafficking" Australian Neuroscience Society annual meeting, Melbourne, Australia.

Zhao H, Ruberu K, Li H, Garner B (2012) "Establishment of subcellular fractionation techniques to assess intracellular cobalamin transit in vitro and the impact of lysosomal dysfunction" Vitamin B12 International Symposium, Nancy, France. (**Winner of Young Investigator Award**)

TABLE OF CONTENTS

LIST OF TABLES

LIST OF FIGURES

ABBREVIATIONS

4-NPP	4-nitrophenyl phosphate
Aβ	Amyloid β
AdoCbl	5-deoxyadenosylcobalamin
AD	Alzheimer's disease
AL	Autophagolysosome
Amph	Amphisome
AP	Autophagosome
APP	Amyloid β precursor protein
ASGP-R	Asialoglycoprotein receptor
ATP	Adenosine-5'-triphosphate
AV	Autophagic vacuoles
BHMT	Betaine-homocysteine methyltransferase
BCA	Bicinchoninic acid
BSA	Bovine serum albumin
Cbl	Cobalamin
CBE	Conduritol B epoxide
CBS	Cystathionine-β-synthase
Con	Control
CNS	Central nervous system
cpm	Counts per minute
DAB	3,3'-Diaminobenzidine
DAPI	4',6-diamidino-2-phenylindole
DNA	Deoxyribonucleic acid

DMEM	Dulbecco's Modified Eagle Media
ECL	Enhanced chemiluminescence
EE	Early endosome
ELISA	Enzyme-linked immunosorbent assay
$FADH_2$	Flavin adenine dinucleotide hydroquinone 2
FS	Fetal bovine serum
GC	Gas chromatography
GCase	Glucocerebrosidase
GD	Gaucher disease
GlcCer	Glucosylceramide
GTP	Guanosine triphosphate
HC	Haptocorrin
HD	Huntington's disease
Hcy	Homocysteine
HHcy	Hyperhomocysteine
HoloTC	Holotranscobalamin
HRP	Horseradish-peroxidase
HS	Human serum
IF	Intrinsic factor
i.p.	intraperitoneally
LAMP1	Lysosomal-associated membrane protein 1
LAMP2	Lysosomal-associated membrane protein 2
LC-MS	Liquid chromatography-mass spectrometry
LE	Late endosome
LER	Lysosome enrichment reagent
LMBD1	Limb region 1 protein homologue (LMBR1) domain-containing protein 1

Lyso	Lysosome
MCI	Mild cognitive impairment
MeCbl	Methylcobalamin
Met	Methionine
Mito	Mitochondria
MTHFR	Methylene tetrahydrofolate reductase
MMA	Methylmalonic acid
MMACHC	Methylmalonic aciduria CblC type with homocystinuria
MMADHC	Methylmalonic aciduria CblD type with homocystinuria
MM-CoA	Methylmalonyl-CoA
MMCM	Methylmalonyl-CoA mutase
MS	Methionine synthase
MTT	3-[4,5-dimethylthiazol-2-yl]-2,5 diphenyl tetrazolium bromide
NADH	Nicotinamide adenine dinucleotide
NaOH	Sodium hydroxide
PAS	Pre-autophagic structure
PBS	Phosphate buffer saline
PD	Parkinson's diseases
PS1	Presenilin 1
ROS	Reactive oxygen species
SAM	S-adenosyl-methionine
SAH	S-adenosylhomocysteine
SDS-PAGE	Sodium dodecyl sulfate polyacrylamide gel electrophoresis
SE	Standard error
TC	Transcobalamin
TCA	Trichloro-acetic acid

TCblR	Transcobalamin receptor
TGN	Trans-Golgi network
THF	Tetrahydrofolate
ThS	Thioflavine S
TMB	3,3',5,5'-tetramethylbenzidine
VDAC1	Voltage-dependent anion channel 1

Chapter 1

Introduction

1 Introduction

1.1 Cobalamin

Cobalamin (Cbl), more commonly known as Vitamin B_{12}, has a complex chemical structure with a central cobalt atom tethered equatorially to four nitrogens donated by the corrin ring (Figure 1.1) (Hodgkin *et al.*, 1956). Cbl exists in several chemically-related forms, of which methylcobalamin (MeCbl) and 5-deoxyadenosylcobalamin (AdoCbl) are the active forms in human metabolism. Foods of animal origin are the only natural source of Cbl in the human diet. As a water-soluble vitamin, Cbl is primarily present in meat, fish and dairy products in limited amounts (2-5 µg/100 g) (Herrmann and Obeid, 2012). Cbl is required for DNA synthesis and blood cell formation in bone marrow and it plays a crucial role in maintaining neurological function and energy production.

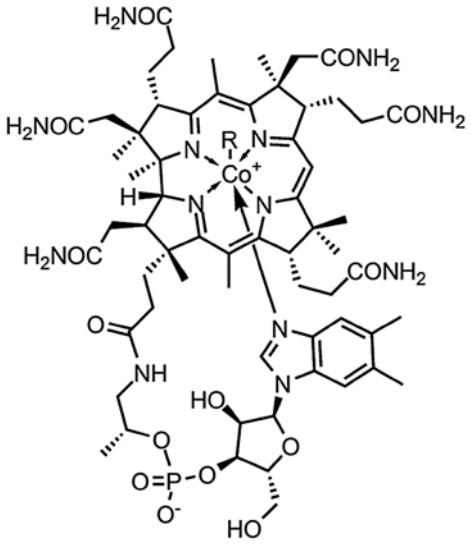

Figure 1.1 Cobalamin chemical structure

Cbl deficiency can result in haematological disorders, cognitive impairment and irreversible neurological abnormalities if untreated. Clinically, Cbl status is typically determined by examining serum Cbl concentrations. Serum Cbl levels of < 150 pmol/l are treated as a Cbl deficiency. However, low serum Cbl concentrations do not accurately reflect intracellular Cbl status. This is because most of the circulating Cbl is bound to the Cbl transporter haptocorrin (HC) with a high affinity and HC is not available for cellular uptake in tissues other than the liver. Cbl is a coenzyme in the conversion of homocysteine (Hcy) to methionine (Fernandes-Costa and Metz) and methylmalonyl-CoA (MM-CoA) to succinyl-CoA. Thus, plasma concentrations of Hcy (> 13 µmol/l) or methylmalonic acid (MMA) levels (> 0.4 µmol/l) are more reliable indicators of Cbl deficiency (Dali-Youcef and Andres, 2009). However as

there is no consensus "gold standard" value for diagnosing Cbl deficiency, the results should be interpreted individually combined with clinical symptoms.

Clinical evidence indicates that pernicious anaemia accounts for approximately 15-25% of Cbl deficiency, and is characterised by the lack of intrinsic factor (IF), a specific Cbl-binding protein that limits the body's capacity to absorb Cbl from dietary sources (Dali-Youcef and Andres, 2009). Pernicious anaemia is an autoimmune disease that affects the gastric mucosa and results in gastric atrophy, eventually leading to megaloblastic anaemia and neurological disorders. However, the most common cause of Cbl deficiency (about 60-70%) is due to food-Cbl malabsorption, especially in the elderly (Andres *et al.*, 2003; Andres *et al.*, 2005). This syndrome is characterised by the body's inability to release Cbl from food, and is usually caused by atrophic gastritis or intestinal transport proteins, even when the absorption of unbound Cbl is normal from food intake (Carmel, 1995). Oral or parenteral administration of Cbl is used clinically to treat Cbl deficiency caused by pernicious anaemia and other conditions that result in Cbl malabsorption.

1.2 Cbl absorption

Dietary Cbl is released from food proteins by gastric acid and pepsin in the stomach, where Cbl is sequestered and transported by the binding protein HC. HC is a salivary glycoprotein with broad specificity and high affinity for Cbl at both neutral and acidic pH (Fedosov *et al.*, 2002). Pancreatic proteases facilitate the degradation of HC, releasing Cbl into the intestinal lumen, where it binds to gastric IF to form the IF/Cbl complex. The receptor-mediated absorption of Cbl is a saturable process and

cubilin regulates the number of IF/Cbl binding sites and limits the capacity of Cbl absorption (Moestrup and Verroust, 2001). The IF/Cbl complex was taken to endosomes of the ileal cells by endocytosis, where it is processed via the endosomal–lysosomal pathway.

Upon endocytosis, endosomes deliver the IF/Cbl complex to the lysosomes, while cubilin is recycled back to the cell surface. Within the lysosomes, IF is degraded by lysosomal hydrolases while Cbl is released and transported out of the lysosomes into the ileum. Cbl is secreted via the basolateral membrane of the ileal cells regulated by the ATP-binding cassette (ABC) transporter MRP1/ABCC1 into the portal vein blood circulation (Beedholm-Ebsen *et al.*, 2010). From here, it binds to the primary Cbl binding protein transcobalamin (TC), a 43 kDa protein that is synthesised and secreted by the vascular endothelium in the intestinal villi (Quadros *et al.*, 1999). Cbl that is bound to TC is called holotranscobalamin (holoTC), and it is the metabolically active vitamin B_{12} fraction. The plasma concentration of holoTC < 40 pmol/l is an early and sensitive indicator for diagnosing Cbl deficiency. HoloTC consists of about 20% of the total Cbl circulating in the blood (Hall, 1977). Cbl is transported via systemic circulation to all target cells of the body, where specific cell membrane receptors are expressed and carry the holoTC into the cells (Figure 1.2).

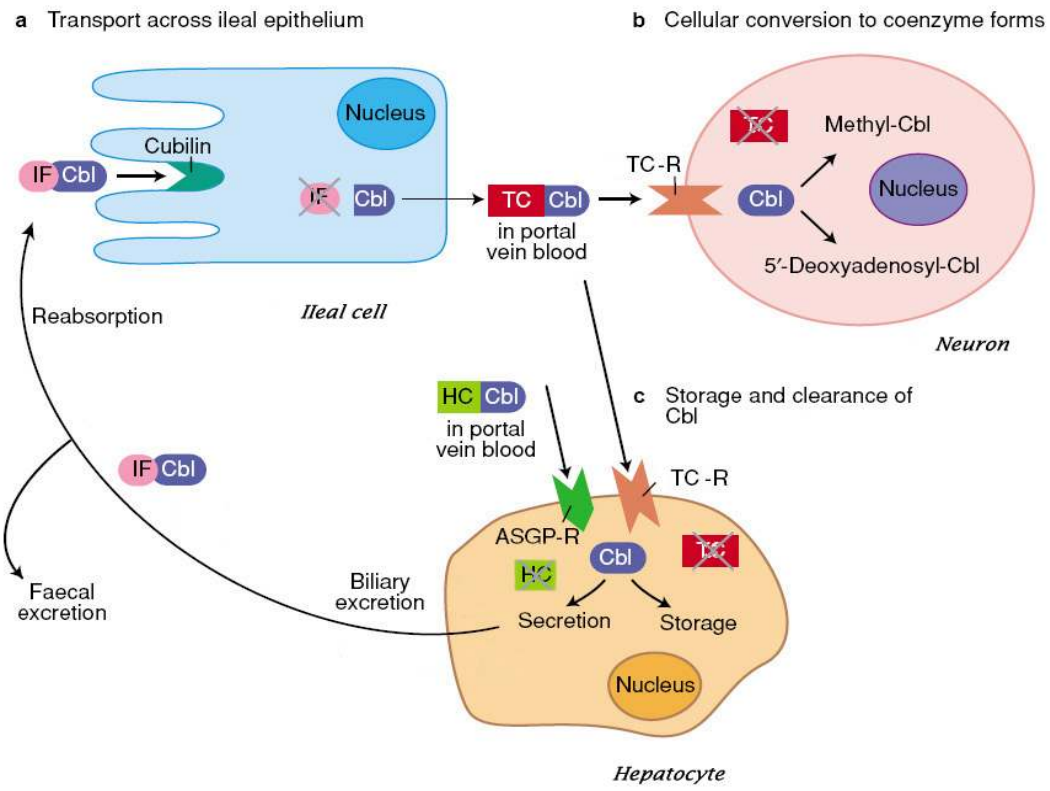

Human Cbl transport systems

Figure 1.2 Human dietary Cbl absorption systems (adapted from Seetharam and Yammani) (Seetharam and Yammani, 2003).

Approximately 80% of circulating Cbl is bound to HC and taken up by hepatocytes via the asialoglycoprotein receptor (ASGP-R) (Linnell and Bhatt, 1995; Seetharam and Yammani, 2003). In comparison to IF and TC, HC is more widely and abundantly distributed in human tissues. HC not only binds Cbl, but it also specifically binds Cbl analogues such as cobinamide with a higher affinity. In the liver, Cbl released via the degradation of the HC/Cbl complex is either stored in the form of Cbl-dependent enzymes or secreted via bile where it may be reabsorbed. Thus, while the liver contains most of the body's Cbl, the kidneys and brain are also

important organs which store Cbl (Herrmann and Obeid, 2012). The secreted Cbl binds to IF in the lumen and the IF receptor cubilin regulates the capacity of Cbl absorption. Excessive Cbl is excreted from the body through the faeces (Figure 1.2)(Seetharam and Yammani, 2003).

Within the central nervous system (CNS), holoTC rapidly passes through the blood-brain-barrier and is taken into the cerebrospinal fluid (Van den Berg *et al.*, 2003). The specific TC receptors (TCblR/CD320) expressed in cell membranes recognize and bind holoTC (Bose *et al.*, 1995). It is noteworthy that holoTC intracellular uptake in the brain is critically dependent on the availability of TCblR. Recent published data has shown that the concentration of Cbl was 92% lower in TCblR knockout mouse brains than in the controls (Fernandez-Roig *et al.*, 2012). However, no direct evidence exists that the level of TCblR expression in any tissue is related to the amount of Cbl transported to that tissue. The levels of TCblR are up-regulated to import more holoTC when the cells are in a proliferating mode or when intracellular MeCbl demand increases (Hall, 1984; Fiskerstrand *et al.*, 1998). The TCblR captures holoTC and is internalised via endocytosis to the endosomes. The empty TC receptor is recycled back to the cell surface while the endosomes escort holoTC to the lysosomes, from where TC is degraded by lysosomal hydrolases and Cbl is released into the cytoplasm (Figure 1.3).

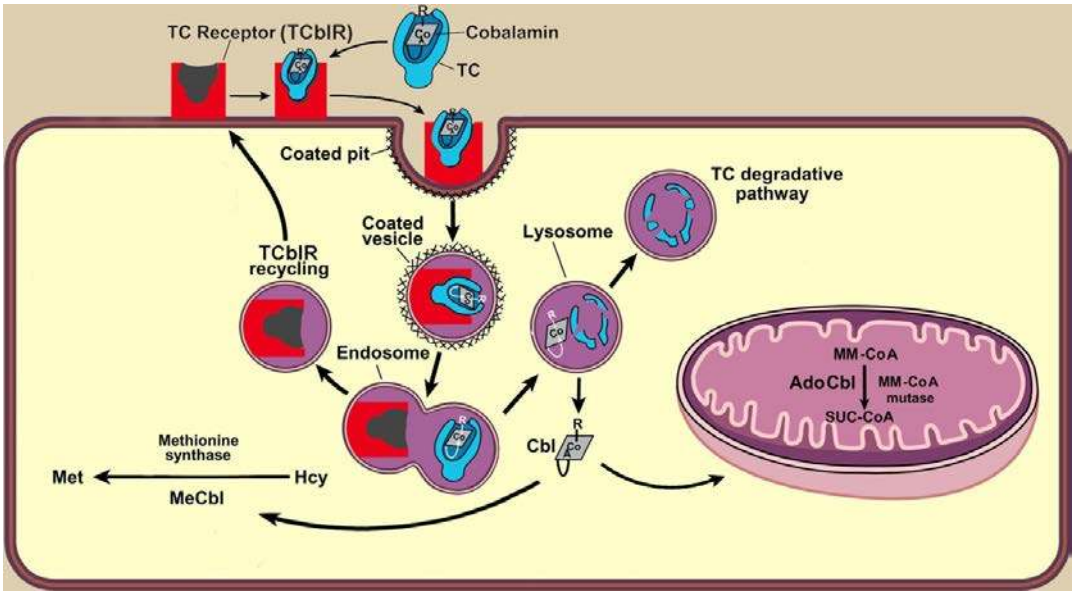

Figure 1.3 TC receptor-mediated intracellular uptake of holoTC via endocytosis (adapted from Jacobsen and Glushchenko) (Jacobsen and Glushchenko, 2009). SUC-CoA, succinyl-CoA.

In the cytosol, Cbl is converted to MeCbl and acts as a coenzyme of methionine synthase (MS) to catalyse Hcy to Met. In the mitochondria, Cbl is converted to AdoCbl, which is a coenzyme of methylmalonyl-CoA mutase (MMCM) used in the conversion of MM-CoA to succinyl-CoA. In Cbl deficiency, excess MM-CoA is converted into MMA. Therefore, the Cbl depletion increases the metabolites Hcy and MMA as their enzymatic conversions are reduced, resulting in homocysteinaemia and methylmalonic acidaemia. The concentration of holoTC in serum is an early diagnostic marker that becomes decreased before total serum Cbl level drops, whereas increased Hcy and MMA levels in the blood indicate an intracellular Cbl deficiency.

1.3 Endosomes and Lysosomes

Endosomes are endocytic membrane-bound compartments comprising early endosomes and late endosomes. Exogenous molecules are internalised to early endosomes through receptor-mediated endocytosis, pinocytosis, and phagocytosis. Early endosomes then develop into late endosomes by maturation (Figure 1.4). Lysosomal hydrolases are synthesised in the rough endoplasmic reticulum and released from Golgi apparatus. Newly produced hydrolases are taged with mannose-6-phosphate and delivered to the trans-Golgi network (TGN), where hydrolases are taken by mannose-6-phosphate receptors and transported to late endosomes. Late endosomes, known as multivesicular bodies, fuse with hydrolases and deliver them to the immature lysosomes, while the empty mannose-6-phosphate receptors are recycled back to the TGN (Mellman, 1996).

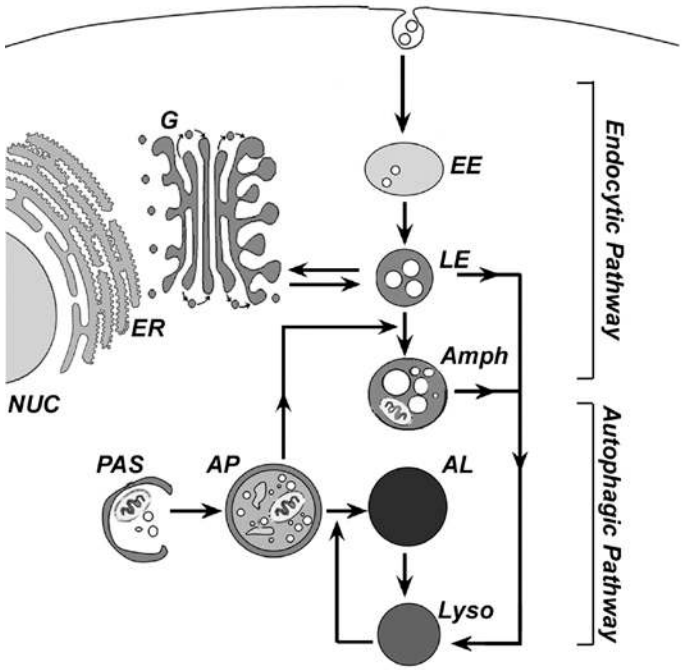

Figure 1.4 The endosome and lysosome system illustrating the endocytic and autophagic pathways (adapted from Nixon)(Nixon, 2007). In the endocytic pathway, molecules (such as proteins) are endocytosed and delivered to early endosomes (EE), which mature into late endosomes (LE). In the autophagic pathway, damaged organelles and macromolecules are surrounded by a pre-autophagic structure (PAS), which sequesters large areas of cytoplasm to become a double-membraned autophagosome (AP). This organelle receives hydrolases by fusing with either immature lysosomes to form autophagolysosomes (AL) or LE to form amphisomes (Amph), which fuse eventually with lysosomes (Lyso). ER, endoplasmic reticulum; G, Golgi; NUC, nucleus.

Lysosomes consist of acidic membrane-bound compartments and their size varies from 0.05-1 µm. The low pH (4-5) of lysosomes is generated by the action of the vacuolar H^+ membrane proton pump ATPase that acidifies the newly-created autolysosome (Mindell, 2012). Lysosomes contain over 50 soluble acid hydrolases and they are nucleases, proteases, glycosidases, lipases, phosphatases, sulphatases and phospholipases. The majority of lysosomal proteases are cathepsins that are divided into three groups according to the amino acids of their active sites that confer catalytic activity: cysteine (cathepsin B, C, F, H, K), aspartyl (cathepsin D, E), and serine (cathepsin A, G). A limiting membrane containing an abundance of glycosylated proteins surrounds these pH-sensitive lysosomal hydrolases. An intact lysosomal membrane provides the barrier necessary to maintain such a low pH environment compared with the neutral pH of the surrounding cytosol. Lysosomes play a vital intracellular role in maintaining cellular homeostasis by continually degrading and recycling cellular components for biosynthesis and energy production. Lysosomes provide the site for the terminal proteolytic degradation of misfolded proteins, defective organelles and excessive biological garbage. Lysosomal hydrolases degrade macromolecules from extracellular space through endocytosis and phagocytosis, as well as from the cytoplasm through autophagy.

Autophagy is a regulated process of degradation and includes three different mechanisms: chaperone-mediated autophagy, microautophagy and macroautophagy. Chaperone-mediated autophagy is a selective form of autophagy in which specific cytosolic proteins containing a KFERQ motif are selectively targeted by chaperone proteins to the lysosomal lumen for degradation. In microautophagy, small regions of cytoplasm are non-selectively internalised via lysosomal membrane invaginations

and continuously degraded within the lysosomal lumen. Macroautophagy regulates large-scale cytoplasm degradation and is typically referred to as autophagy. During macroautophagy, a pre-autophagic structure, known as a phagophore, encloses and sequesters a large region of cytoplasm that contains proteins and organelles such as mitochondria to become a double-membraned AP. The AP receives acid hydrolases by fusing with either an immature lysosome to form an AL or with a late endosome to form an Amph (Figure 1.4 and 1.5). Sequestered cytoplasms are degraded by acid hydrolases into amino acids in both compartments to yield a mature lysosome (autolysosome) with lysosomal hydrolases (Nixon, 2007).

Autophagy is essential to maintain cellular homeostasis through the degradation of malfunctioning organelles and protein aggregates. Autophagy in normal healthy cells is constitutively active, inducible and highly efficient. Autophagic vacuoles (AV) are intermediate autophagy-related vesicular structures including autophagosomes, amphisomes, and autophagolysosomes, and their presence in cells depends on both the rate of autophagosome formation and rate of clearance by lysosomal hydrolases. AV accumulation is rare in healthy cells because newly-formed autophagosomes are rapidly cleared by fusing with lysosomes. However, AV is rapidly accumulated when lysosomal hydrolases are inhibited by protease inhibitors (e.g leupeptin), or when the transport of lysosomal hydrolases via microtubules are disrupted (e.g vinblastine), or under neuropathological conditions (e.g AD) (Ivy *et al.*, 1984; Nixon *et al.*, 2005).

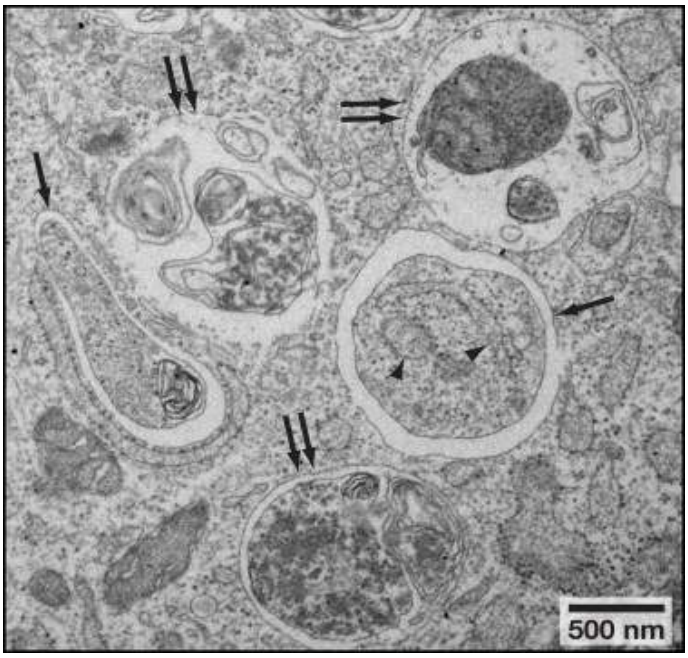

Figure 1.5 Autophagosome and autolysosome morphology. Electron microscopic analysis of nutrient-starved mouse embryonic fibroblasts. Arrows indicate autophagosomes and double arrows indicate autolysosomes/amphisomes. Arrowheads indicate fragments of endoplasmic reticulum inside the autophagosome (Mizushima *et al.*, 2010).

1.4 Lysosomal Cbl intracellular trafficking

It is currently thought that Cbl released from TC inside the lysosome is bound by another putative carrier protein that delivers Cbl to a lysosomal transporter (Probable lysosomal Cbl transporter / Limb region 1 protein homologue (LMBR1) domain-containing protein 1, LMBD1) that subsequently releases Cbl to the cytoplasm (Figure 1.6) (Gailus *et al.*, 2010). Upon export from the lysosome, Cbl is processed by the CblC gene product MMACHC (methylmalonic aciduria CblC type with

homocystinuria) and delivered to cytosolic MS and mitochondrial MMCM by the CblD gene product MMADHC (methylmalonic aciduria CblD type with homocystinuria) (Coelho *et al.*, 2008; Hannibal *et al.*, 2009).

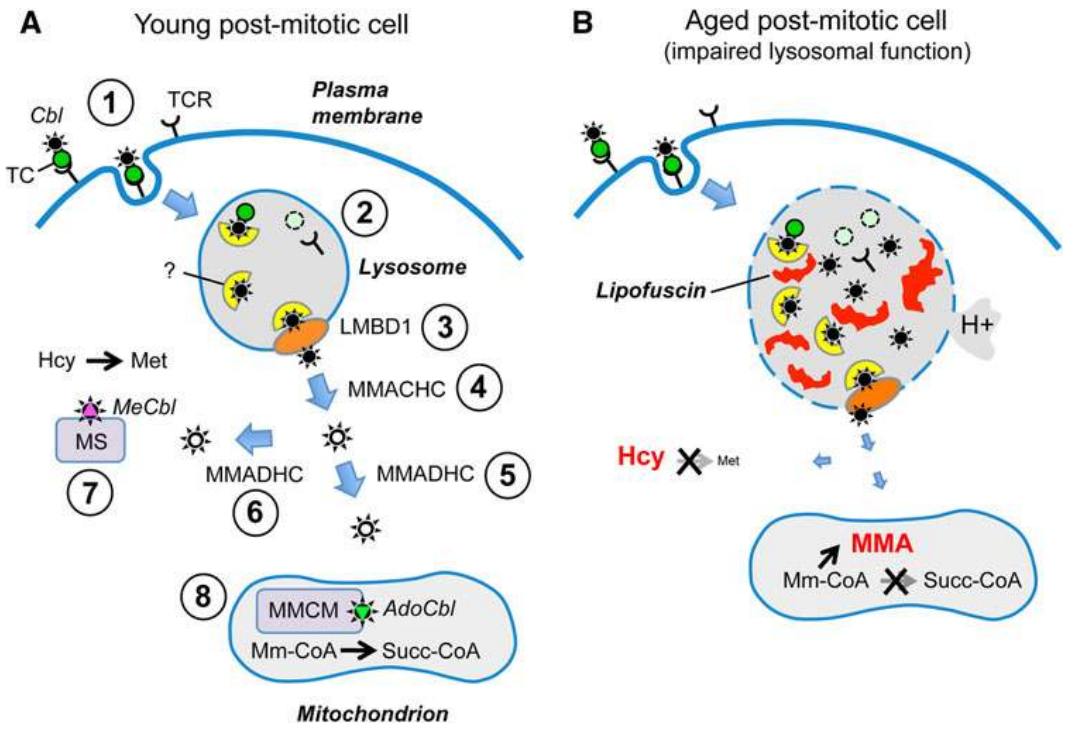

Figure 1.6 Schematic view of Cbl intracellular trafficking. Succ-CoA, succinyl-CoA; TCR, TC receptor.

The role that the lysosomes play in delivering Cbl to two important enzymes, MS in the cytosol and MMCM in the mitochondria, is demonstrated by the defect in the human *LMBRD1* gene that encodes the LMBD1 transporter (Rutsch *et al.*, 2009). Mutations in *LMBRD1* represent one of eight complementation groups of inborn errors of Cbl metabolism referred to as the CblF defect. This genetic defect in lysosomal Cbl release was discovered 25 years ago, well before the likely transporter involved was characterised (Rosenblatt *et al.*, 1985). Recent research has discovered that ABCD4 (ATP-binding cassette, sub-family D, member 4), an ATP-binding cassette transporter, is another essential component of intracellular Cbl metabolism (Coelho *et al.*, 2012). Both LMBD1 and ABCD4 co-localise with the lysosomal protein LAMP1 (lysosomal-associated membrane protein 1). The precise role of each protein in the lysosomal export of Cbl is unclear. ABCD4 may interact with LMBD1 to facilitate passive transport of Cbl across the lysosomal membrane.

It is now recognised that the acidic pH of the lysosome also influences the conversion of Cbl from the so-called “base-on” to “base-off” state in the interaction between the dimethylbenzimidazole moiety of the Cbl molecule with the central cobalt atom (Banerjee, 2006). In the base-on conformation the ligand is attached to the central cobalt atom, whereas in the base-off conformation the ligand is displaced from cobalt. It is speculated that the Cbl base-off state is important for subsequent interactions with cytosolic cargo proteins (Banerjee, 2006). It is likely that the loss of TC proteolysis and the inhibition of the conversion of Cbl to the base-off state are related to two changes in lysosomal function (impaired lysosomal proteolytic activity and increased lysosomal pH) that occur as a consequence of ageing in post-mitotic cells (Terman *et al.*, 2006; Zhao *et al.*, 2011). It is therefore plausible that the

loss of lysosomal TC proteolysis and the inhibition of the pH-dependent conversion of Cbl to the base-off state accompany such age-related changes in lysosomal function. It is noteworthy that in addition to TC, at least one additional uncharacterised lysosomal Cbl escort/transport protein is predicted to exist and this may present another point at which Cbl transit could be disrupted when lysosomal function is impaired (Banerjee *et al.*, 2009).

1.5 The consequence of MeCbl and AdoCbl deficiency

Hcy is a sulphur amino acid that is not obtained from the diet. Hcy is synthesized from methionine via a multi-step process. Hcy is converted to methionine or cysteine with the presence of vitamin B_6, vitamin B_9 (folic acid) and Cbl (Selhub, 1999). Methyl-tetrahydrofolate (methyl-THF) transfers methyl to Hcy to produce methionine and THF. This process is catalysed by MeCbl-dependent MS, which is an enzyme that in humans is encoded by the *MTR* gene (5-methyltetrahydrofolate-homocysteine methyltransferase) (Figure 1.7). Betaine-homocysteine methyltransferase (BHMT) is an another enzyme that catalyses the transfer of a methyl group from betaine to Hcy to produce dimethylglycine and methionine respectively (Obeid, 2013). However, BHMT-dependent Hcy methylation is only active in peripheral tissues, such as liver, but not in the brain.

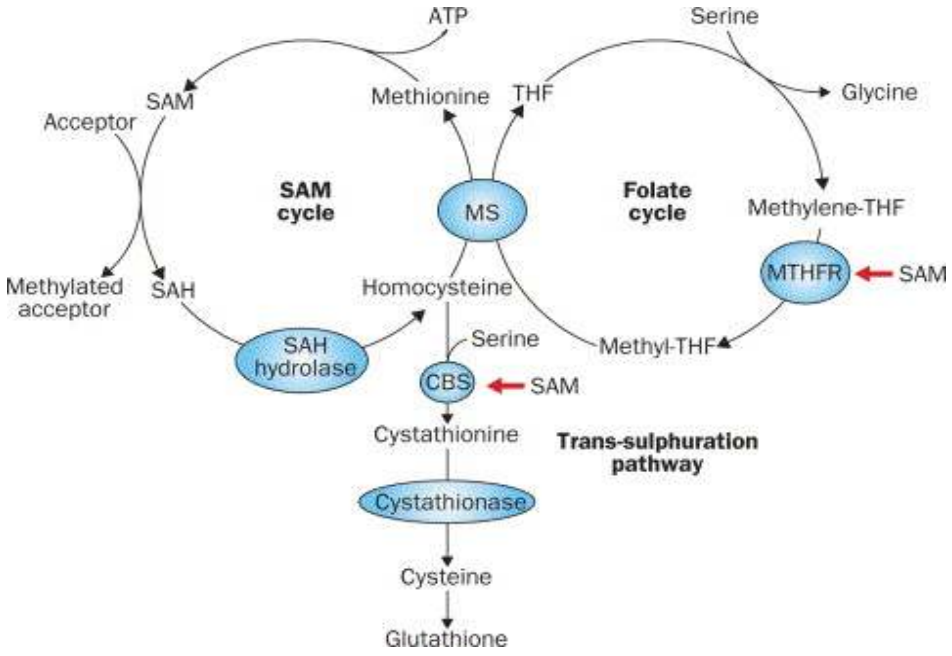

Figure 1.7 Metabolism of Hcy (adapted from Morris) (Morris, 2003).

Methionine is activated by ATP (adenosine-5'-triphosphate) to produce S-adenosyl-methionine (SAM), which is the universal donor in the transmethylation of many substrates. SAM donates a methyl group to an acceptor molecule to produce S-adenosyl-homocysteine (SAH). SAH is then catalysed by SAH hydrolase to synthesise Hcy. Folate is catalysed by dihydrofolate reductase to produce THF that enters the mitochondria and reacts with serine that is catalysed by serine hydroxymethyl transferase to form glycine and methylene-THF. Methylene-THF is catalysed by methylene tetrahydrofolate reductase (MTHFR) inhibited by SAM to produce methyl-THF. THF is a folate derivative involved in one-carbon metabolism needed for DNA synthesis. Cbl deficiency blocks the THF supply leading to impaired DNA synthesis, while elevated Hcy levels reflect the deficiency of either

Cbl or folate or both. Alternatively, Hcy reacting with serine is catalysed by B_6-dependent cystathionine-β-synthase (CBS) and activated by SAM to form cystathionine. Cystathionine is then converted to cysteine, which is a precursor of glutathione (Morris 2003).

MS plays an important role in regulating and limiting the production of methionine from Hcy in the cytosol. Failing to release Cbl from the lysosomes prevents the MeCbl intracellular conversion from Cbl, thereby reducing MS activity, inhibiting Hcy conversion, and resulting in increased Hcy concentrations. Epidemiological and clinical studies indicate that elevated plasma levels of Hcy, known as hyperhomocysteinaemia (HHcy), is recognised as a vital risk factor for developing AD and mild cognitive impairment (MCI) in the elderly (Seshadri *et al.*, 2002; Quadri *et al.*, 2004). Several clinical studies have reported HHcy in patients with AD, vascular dementia and MCI (Clarke *et al.*, 1998; Lehmann *et al.*, 1999). Evidence shows that HHcy enhances oxidative stress (Jacobsen, 2000), alters DNA methylation (Fuso *et al.*, 2005), and interferes with DNA repair mechanisms (Kruman *et al.*, 2002). HHcy concentration may increase amyloid-β (Aβ) peptide levels in the brain and could therefore accelerate AD neuropathology (Pacheco-Quinto *et al.*, 2006). More recently, Cbl deficient diet-induced HHcy was reported to increase Aβ peptide levels and Aβ deposition in the cortex and hippocampus in an AD transgenic mouse model (Zhuo *et al.*, 2010; Zhuo and Pratico, 2010). However, these deficits are reversible and the reduction in HHcy levels induced by Cbl replacement results in significantly improved cognitive performance and ameliorated brain amyloidosis (Zhuo and Pratico, 2010).

In addition, several studies have reported that plasma Hcy levels are positively correlated with brain atrophy in humans and this has led to the administration of Cbl (both with and without folate) as a therapeutic agent for MCI and AD (Sachdev *et al.*, 2002; Seshadri *et al.*, 2008). Although evidence exists that reducing Hcy levels in MCI patients slows the rate of brain atrophy, this appears to be linked to baseline Hcy levels (Smith *et al.*, 2010). Oral supplementation combining folate, vitamin B_6, and Cbl substantially lowers circulating Hcy levels, but does not appear to improve the outcome in the prevention of cardiovascular disease or dementia.

HHcy has also been identified as an independent risk factor for cardiovascular diseases including ischaemic heart disease, stroke, and peripheral vascular disease, that are rated among of the most common death in developed countries (Boers, 1994). HHcy-induced microvascular damage is associated with thrombogenesis, endothelial vasomotor function impairment, lipid peroxidation, and vascular smooth muscle proliferation (Troen *et al.*, 2008). Eventually these factors contribute to coronary heart disease and stroke (Refsum *et al.*, 1998).

In the mitochondria, AdoCbl is the coenzyme of MMCM that utilises and regulates the conversion of MM-CoA to succinyl-CoA, which is also synthesised from propionyl CoA. Propionic acid, also known as propionate, is involved in glucose formation. Propionate is efficiently taken up into cells and converted to propionyl-CoA by thiokinase and CoA, and then carboxylated by propionyl-CoA carboxylase to yield MM-CoA. Succinyl-CoA is an important intermediate of the citric acid cycle (energy production cycle) in the mitochondrial matrix. Succinyl-CoA is converted to

oxaloacetate via series of chemical reactions to generate energy through the oxidation of acetate in the form of ATP (Figure 1.8).

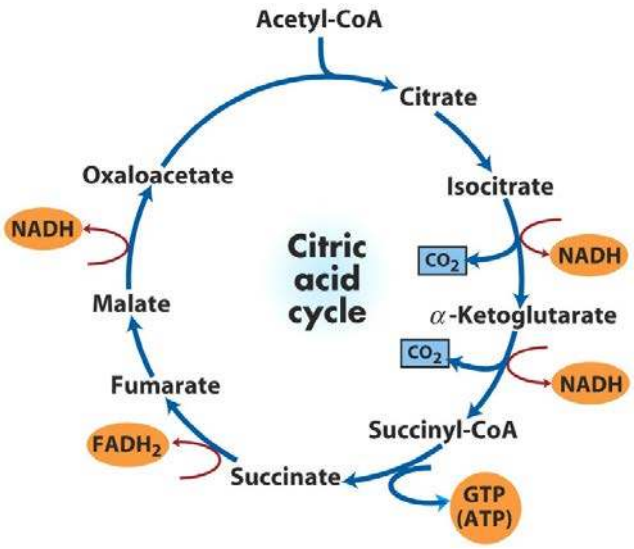

Figure 1.8 The citric acid cycle. $FADH_2$, flavin adenine dinucleotide hydroquinone 2; GTP, guanosine triphosphate; NADH, nicotinamide adenine dinucleotide.

AdoCbl intracellular deficiency can cause mitochondrial toxicity when the citric acid cycle is interrupted, thus inhibiting mitochondrial energy production and eventually leading to neuronal death (Depeint et al., 2006). On the other hand, inhibiting MMCM results in the accumulation of plasma MMA leading to the development of methylmalonic aciduria, which impairs mitochondrial respiratory chain complex activities (Brusque et al., 2002). The damage to the respiratory chain promotes

reactive oxygen species (ROS) generation causing significant oxidative stress in the mitochondria. The accumulation of oxidative stress stimulates mitochondrial DNA mutations (Richter et al., 1988), resulting in enzymatic abnormalities and further oxidative stress inducing cell death. In addtition, lysosomes are rich in low mass redox-active iron and they are very sensitive to oxidative stress (Kurz *et al.*, 2008). Lysosomal membranes are permeabilised by increased oxidative stress secondary to the Fenton reaction, leading to the rupture of the membrane and the release of lysosomal hydorlases into the cytosol, triggering apoptosis or necrosis (Kurz *et al.*, 2011).

1.6 The significance of Cbl deficiency

Cbl deficiency is a major widespread public health issue that is mainly observed during ageing, and often associated with folate deficiency during this period of life. Due to inadequate dietary intake and increasingly poor absorption (atrophic gastritis), approximately 6% of the Western population over the age of 60 has low plasma Cbl levels, with the prevalence of deficiency increasing with age (Krasinski *et al.*, 1986; Allen, 2009). Clinical studies have shown that dietary Cbl absorption is significantly reduced in healthy adults aged 55-75 years compared to young adults, with a further reduction in those older ages (Scarlett *et al.*, 1992). This contributes to a Cbl deficiency that leads to either methylmalonic aciduria or homocystinuria or both.

Data from human and animal studies indicate that Cbl deficiency impairs neuronal function; a process that is thought to contribute to age-related cognitive decline and

dementia, including AD (Calvaresi and Bryan, 2001; Seshadri *et al.*, 2002; McCaddon, 2006; Zhuo and Pratico, 2010). Plasma levels of both Hcy and MMA increase with age and elevated plasma Hcy and MMA concentrations correlate positively with cognitive decline (Herrmann *et al.*, 2000; Williams *et al.*, 2002). Cbl deficiency also results in the dysfunction of the peripheral nervous system (Reynolds, 2006). Although the biochemical pathways that are perturbed in Cbl deficient states are well understood, there is currently no clear explanation as to why such biochemical/metabolic perturbations increase with age.

Food-Cbl malabsorption is a major cause of Cbl deficiency in the elderly. Low serum Cbl levels are associated with ageing and cognitive impairment (Calvaresi and Bryan, 2001; Moore *et al.*, 2012). Studies in rodents indicate that Cbl supplementation significantly improves cognitive performance (Zhuo and Pratico, 2010). However, human trials have failed to provide a consistent beneficial effect on cognitive performance with either oral or parenteral Cbl administration (Smith, 2008; Maron and Loscalzo, 2009; McCaddon and Hudson, 2010). The fact is that both oral Cbl supplementation (by-passing problems associated with release from food components) and parenteral delivery (by-passing problems associated with both release from food as well as lack of IF) routes increase circulating Cbl to the same degree in both young and aged subjects (Nilsson-Ehle, 1998; Andres et al., 2005). This raises the possibility that other pathways independent of dietary malabsorption may contribute to suboptimal Cbl utilisation in aged individuals. One possibility that has not been previously recognised is that the lack of cognitive improvement may be due to the impaired transit of Cbl through lysosomes within the neurons of aged individuals. It is also likely that Cbl release from lysosomal TC is compromised and

the conversion to the ‘‘base-off’’ state is inhibited in neurodegenerative diseases (Nixon et al., 2008). Under these conditions, a localised Cbl deficiency would prevail despite the fact that plasma Cbl levels may have been normalised by dietary supplements or intramuscular injections.

1.7 AD and its relation to lysosomes

Dementia is the leading cause of disability in older Australians. AD is the major cause of dementia (~70% of cases) and affected 250,000 Australians in 2009. Without a significant medical breakthrough, this number is expected to reach almost 1.1 million by 2050 (Mental Health Research Institute, Australia). There is no effective cure for AD and little is known regarding the causal molecular pathways that result in AD and how they may be modulated to delay its onset.

AD is a progressive neurodegenerative disorder characterised by a gradual loss of memory, orientation, judgement and reasoning. The characteristic neuropathological alterations of AD include the loss of neurons, particularly in the cerebral cortex and hippocampus involved with memory and cognition, and the presence of abnormal intra- and extra-neuronal proteinaceous fibrous material within and around the surviving neurons (De-Paula *et al.*, 2012).

Neurofibrillary tangles, primarily abnormal paired helical filaments composed of the microtubule-associated phosphorylated protein, *Tau*, accumulate within neurons in large numbers as the disease progresses (Avila, 2006). In the extracellular space, amorphous insoluble aggregates of proteinaceous debris, termed amyloid plaques,

deposit along extraluminal surfaces of cerebral blood vessels and parenchyma (Murphy and LeVine, 2010). The main component of amyloid plaques is a highly hydrophobic 39-43 amino acid Aβ peptide. Aβ is formed after sequential cleavage of the amyloid β precursor protein (APP), a transmembrane glycoprotein expressed in many cells and tissues including neurons. APP can be cleaved by the proteolytic enzymes α-, β- and γ-secretase; Aβ peptide is generated by successive action of the β- and γ- secretases. Cleavages of APP give rise to most abundant species $A\beta_{40}$ and smaller amount of $A\beta_{42}$ (Nixon, 2007). Soluble Aβ peptide in the blood can cross the blood-brain barrier and interact with neurons in the brain (Clifford *et al.*, 2007); however, the hallmark for diagnosing AD is the accumulation of Aβ into numerous senile amyloid plaques that may induce neuronal dysfunction and cell death (Carter and Lippa, 2001).

AD is generally regarded as a sporadic disorder, while a small proportion (<5%) of familial AD (FAD) is caused by genetic defects. The pathogenic mutations in FAD genes, APP, presenilin 1 (PS1), and presenilin 2, directly cause early-onset FAD in rare families with onset of disease occurring usually 50-60 years. Together, these three genes appear to account for approximately 70% of the FAD cases (Williamson *et al.*, 2009). The inheritance of the apolipoprotein E ε4 allele is associated with an increased risk for late-onset FAD but is not sufficient to cause the disease (Kim *et al.*, 2009).

The endosomal-lysosomal pathway plays a major role in maintaining neuronal homeostasis and survival by degrading and reducing the concentration of misfolded proteins and damaged organelles to prevent aberrant protein accumulation. In AD

endosomes are a major site of Aβ production in normal cells and mediate the cellular uptake of Aβ and soluble APP (Nixon, 2007). The endocytic pathway is also responsible for the internalisation and initial processing of APP at the plasma membrane (Koo *et al.*, 1996; Nixon *et al.*, 2000). Endosomes were enlarged and increased in the neurons of the AD brain when they were labelled with the specific endosomal marker, Rab5, indicating elevated neuronal endocytosis activation (Cataldo *et al.*, 1996; Cataldo *et al.*, 1997).

Lysosomes contain over 50 acid hydrolases and the majority of lysosomal proteases are cathepsins. Lysosomal hydrolases degrade and recycle misfolded proteins and damaged organelles mainly through autophagy. The accumulation of Aβ in the lysosome has been reported in animal AD models (Langui *et al.*, 2004). Lysosomal function is continually up-regulated and the levels of lysosomal enzymes are increased in the hippocampus and frontal cortex in APPxPS1 transgenic AD mice. This possibly reflects cellular responses to the failed degradation of the accumulating Aβ (Mueller-Steiner *et al.*, 2006; Amritraj *et al.*, 2009), although residual bodies gradually accumulate as neurons become compromised when AD progresses. Lysosomal acidification is defective in AD (Wolfe *et al.*, 2013). PS1 regulates the trafficking of the vacuolar H^+-ATPase to the lysosomes and thus lysosomal proteolysis is disrupted by AD-related PS1 mutation (Lee *et al.*, 2010).

The incubation of cultured primary neurons with soluble $A\beta_{42}$ causes the accumulation of $A\beta_{42}$ in the lysosomes and intracellular $A\beta_{42}$ is relative resistant to protease degradation (Ditaranto *et al.*, 2001; Chafekar *et al.*, 2008). The increased levels of intralysosomal Aβ stimulate rapid free radical generation within lysosomes

and disrupt the lysosomal membrane proton gradient which together results in a more rapid Aβ accumulation and aggregation (Ditaranto *et al.*, 2001). This may initate a vicious cycle as neuronal oxidative stress induces further lysosomal Aβ accumulation via enhanced autophagy induction and decreased lysosomal clearance (Zheng *et al.*, 2006; Zheng *et al.*, 2006; Zheng *et al.*, 2011). Lysosomes are rich in low mass redox-active iron and they are very sensitive to oxidative stress induced by ROS via the Fenton reaction (Kurz *et al.*, 2011). Lysosomes are indeed under stress and their membrane becomes vulnerable when accumulated Aβ combines with other undegradable material to induce oxidative stress and abnormal proteolysis leading to lysosomal membrane disruption (Yang *et al.*, 1998). Consequently lysosomal membranes become destabilised and lysosomal hydrolases are released into the cytosol when lysosomal membrane permeabilisation is induced, contributing to apoptosis or necrosis (Dunlop *et al.*, 2009). Lysosomal proteases cathepsin B and cathepsin D are present extracellularly in senile plaques at high levels in the AD brain, indicating that those hydrolases may be released via lysosomal membrane rupture as neurons degenerate (Cataldo *et al.*, 1991).

1.8 Age-related impairment of lysosomal function

Ageing is one of the most significant medical challenges facing Australia and the world. The proportion of people over 60 years old is increasing faster than any other age group. At the cellular level, ageing is characterised by the increasing accumulation in long-lived post-mitotic cells of dysfunctional, usually enlarged mitochondria, lipofuscin-loaded lysosomes, and oxidatively modified cytosolic

proteins and lipids (Brunk and Terman, 2002). Lipofuscin is a brown-yellow, autofluorescent, electron-dense, intralysosomal pigment that progressively accumulates over time within non-dividing cells, such as neurons, cardiac myocytes, skeletal muscle fibres and retinal pigment epithelial cells (Strehler, 1964; Brunk and Ericsson, 1972; Brunk *et al.*, 1973; Double *et al.*, 2008). Lipofuscin consists primarily of oxidatively modified cross-linked protein residues originating from autophagocytosed cytoplasmic components (Terman and Brunk, 1998). One of the characteristic features of lipofuscin is that it is undegradable and cannot be removed via exocytosis (Terman and Brunk, 1998). The increase of lipofuscin with age may be due to an age-dependent reduction in the ability of cells to eliminate lipofuscin because of their decreased lysosomal degradative capacity and increased oxidant-induced damage. In addition, the rate of lipofuscin accumulation positively correlates with the rate of ageing, showing an almost linear dependence (Munnell and Getty, 1968; Nakano and Gotoh, 1992). Thus lipofuscin is often referred to as an age pigment and considered a hallmark of ageing (Terman and Brunk, 2004).

Lipofuscin formation can be induced under experimental conditions. It has been shown that oxidative stress promotes lipofuscin formation, whereas antioxidant treatment prevents it. In cell culture models, fibroblasts were exposed to hyperoxic conditions (40% ambient oxygen) for 6 months to promote lipofuscin accumulation (Figure 1.9), whereas growth at 8% oxygen and treatment with antioxidants reduce lipofuscin formation (Thaw *et al.*, 1984; Terman and Brunk, 1998; Quinn *et al.*, 2004).

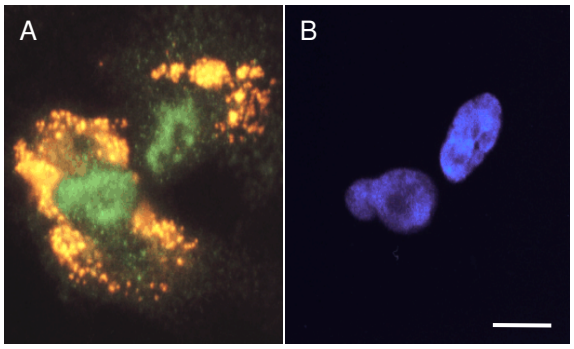

Figure 1.9 Lipofuscin accumulation induced under hyperoxic conditions. Human AG01518 fibroblasts were exposed to 40% ambient oxygen for 6 months to induce lipofuscin accumulation (A). Cell nuclei were stained with 4',6-diamidino-2-phenylindole (DAPI) and visualised as blue fluorescence (B) (Quinn *et al.*, 2004). Scale bar = 10 µm.

Alternatively, the age-related decrease in the activity of lysosomal hydrolases may contribute to the age-related increase in lipofuscin with normal brain ageing (Amano *et al.*, 1995). Lipofuscin accumulation is accelerated by prolonged protease inhibition (Ivy *et al.*, 1984; Ivy *et al.*, 1989). Conversely, the proteasome that is critical for protein metabolism/turnover is directly inhibited by lipofuscin/ceroid. Therefore, an accumulation of lipofuscin/ceroid may further aggravate the damage during ageing by inhibiting this proteasome (Sitte *et al.*, 2000). In addition, the inhibition of lysosomal hydrolases may exacerbate the oxidative stress-induced accumulation of lipofuscin. Oxidative stress and protease inhibition show synergic

pathogenic effects as hyperoxia enhances protein oxidation, while decreased protease degradation delays the removal of oxidised proteins (Terman and Sandberg, 2002). The accumulation of lipofuscin induced by the combination of oxidative stress and protease inhibition has been shown to be three times greater than that observed by either condition alone (Terman and Brunk, 1998).

Ageing is accompanied by progressive cellular accumulation of biological "garbage" and misfolded proteins (Terman and Brunk, 2006). Although damaged macromolecules and organelles are continuously degraded by lysosomes through autophagy and replaced by newly synthesised biological structures, it is clear that the proportion of waste materials, such as lipofuscin, progressively increases with age in post-mitotic cells. It is well known that cellular lipofuscin content positively correlates with oxidative stress and mitochondrial damage (Sohal and Brunk, 1989; Terman *et al.*, 2004; Terman *et al.*, 2010). ROS are generated continuously from normal mitochondrial metabolism because of unavoidable electron leakage from mitochondrial complexes during electron transport and reductive one-electron transfer processes in the cytosol. With the progressively dysfunctional senescent mitochondria, more ROS are produced and accumulated. This enhances oxidative stress that decreases the effective degradation of damaged proteins by lysosomal hydrolases and promotes lipofuscin accumulation (Terman *et al.*, 2006). Moreover, accumulating oxidative damage can then affect the efficiency of mitochondria and further increase the rate of ROS production (Stadtman, 1992).

There are compelling data to suggest that lipofuscin accumulation impairs lysosomal functions (Brunk and Terman, 2002; Terman *et al.*, 2006). Although lipofuscin-

loaded lysosomes appear to be intact under microscope, it is now recognised that the lysosomal compartment is rich in iron that partly exists in a redox-active form. This makes lysosomes sensitive to a high Fe-catalysed oxidative stress (Fenton reaction) that compromises lysosomal membrane integrity leading to the loss of the proton gradient (Yu *et al.*, 2003). The susceptibility of lysosomes to oxidative stress or potential membrane destabilisation or both is thought to play a major role in the induction of lysosomal membrane permeabilisation. Loss of lysosomal function is secondary to the abnormal permeabilisation of lysosomal membranes induced by increased mitochondrial-derived ROS. Dysfunctional lysosomes cause defective clearance and subsequent accumulation of undegraded autophagosomes, which contribute directly to neurodegeneration by subsequent release of lysosomal hydrolases into the cytoplasm triggering apoptosis or necrosis (Yuan *et al.*, 2002). Lysosomal heterogeneity exists both within cells and between cells, however it can be seen that the net function of the lysosomal compartment is severely compromised with ageing (von Zglinicki *et al.*, 1995).

Lysosomal enzymes are produced in the trans-Golgi network and are transported by mannose-6-phosphate receptors to late endosomes that acidify and mature into lysosomes. The continual fusion and fission of the lysosomal vacuoles ensures the distribution of acid hydrolases within the lysosomal compartment. Senescent post-mitotic cells contain large numbers of lipofuscin-containing lysosomes, to which a progressively greater proportion of lysosomal enzymes are directed in a futile attempt to degrade lipofuscin. These lysosomal enzymes are essentially lost for useful purposes (e.g. for the degradation of newly autophagocytosed material),

resulting in a delayed enzyme turnover and the accumulation of waste products (Terman and Brunk, 2006).

In addition to the impact of lysosomal lipofuscin accumulation, there are several age-related settings in which lysosomal function is compromised. Neurodegenerative diseases including AD, Parkinson's disease (PD) (and other Lewy body disorders), and Huntington's disease all involve the accumulation of aggregated proteins/peptides that eventually overwhelm lysosomal capacity for degradation (Cuervo *et al.*, 2004; Rubinsztein, 2006; Levine and Kroemer, 2008; Nixon *et al.*, 2008). There is strong evidence that in these conditions the degradative capacity of the lysosomes is impaired and the lysosomal membrane is destabilised (Nixon *et al.*, 2008). In addition, lysosomal pH may be increased in specific lysosomal storage diseases (e.g. mucolipidosis Type IV), even in dividing cells (Bach *et al.*, 1999).

1.9 Gaucher disease – a lysosomal storage disease

Gaucher disease is the most common lysosomal glycosphingolipid storage disease. It is a genetic disease caused by mutations in the GBA gene that result in an inherited deficiency in the lysosomal enzyme glucocerebrosidase (GCase) (Sillence and Platt, 2003; Jmoudiak and Futerman, 2005). This in turn causes the accumulation of lysosomal glucosylceramide (GlcCer) mostly in the macrophage-derived cells and neurons (Martin *et al.*, 1989; Vitner and Futerman, 2013). GlcCer can also accumulate in the spleen, liver, lungs, bone marrow, and brain (Beutler, 2004). Three clinical types of GD have been identified. Type 1 (non-neuropathic type) is the most common form and mostly occurs in individuals of Ashkenazi Jewish heritage with

haematological complications. Type 2 (acute neuropathic form, most in infantile) and type 3 (Chronic neuropathic form, most in juvenile) show neurological symptoms. All types of GD are characterised by an enlarged liver and spleen (Grabowski, 2008; Martins *et al.*, 2009). A recent study showed that GlcCer was present in the endolysosomal membrane and modulated endolysosomal pH in lymphocytes, suggesting that lysosomal function may be disrupted in GD (Sillence, 2013).

Conduritol B epoxide (CBE) is a competitive, irreversible inhibitor of GCase. Previous studies found that treating cells with CBE causes GlcCer accumulation, while other lysosomal hydrolase levels are unaffected (Daniels *et al.*, 1980; Das *et al.*, 1987). CBE-treatment of macrophages induced many morphological features of GD cells, including whole cell enlargement, oriented fibrils and vacuolated cytoplasm, eccentric nucleus and enlarged vacuoles with membranous structures (Newburg *et al.*, 1988). Moreover, CBE specifically elevated GlcCer levels in macrophages as well as in neurons without affecting the levels of other glycolipids (Yatziv *et al.*, 1988; Schwarz *et al.*, 1995). This *in vitro* system displayed many essential biological parameters relevant for studying the cellular events responsible for the neurological damage that occurs in some types of GD. Thus, CBE treatment has proved an invaluable tool in providing a chemically induced GD phenotype model.

1.10 Overview

Lysosomes play an important intracellular role maintaining cellular homeostasis by continually degrading and recycling cellular components for biosynthesis and energy production. It is possible that lysosomal Cbl intracellular transport may also be interrupted by aged or impaired lysosomes in ageing and AD. Given the fact that Cbl utilisation is critically dependent on its efficient transit through the intracellular lysosomal compartment, it seems reasonable to suggest that Cbl probably does not reach its intended intracellular targets in aged/lysosome-compromised neurons, even with an adequate Cbl supply. If the hypothesis is correct, this would result in an escalating cytotoxic trajectory from the lack of available MeCbl and AdoCbl to act as cofactors in the two important intracellular pathways.

The available evidence points towards the hypothesis that age-related or neurodegenerative impairments of lysosomal function represent a novel ‘‘roadblock’’ that prevents Cbl from reaching its target intracellular enzymes in long-lived post-mitotic cells such as neurons. This may represent a significant cause of ‘‘functional Cbl deficiency’’ in ageing and neurodegenerative diseases even when oral/parenteral Cbl supplementation maintains plasma Cbl levels within a healthy range. This roadblock could contribute to the deleterious increases in Hcy and MMA levels that occur in the ageing brain and thereby directly accelerate neurodegeneration. As there is already great interest in the provision of dietary supplements of Cbl and other B-group vitamins in the ageing and neurodegenerative diseases, detailed studies of intracellular Cbl transport under these conditions relevant to impaired lysosomal function are needed to elucidate the mechanism.

1.11 Aim of this study

This study aims to investigate the impact that lysosomal dysfunction has on Cbl intracellular transport in the context of ageing and AD. Suboptimal lysosomal processing of Cbl plays a significant role in the age-related loss of neurological function associated with both ageing and AD. Defining the mechanisms by which Cbl may confer protection in the AD setting will provide the required information to use broad scale Cbl administration for the prevention of AD in the ageing population. I propose that a significant factor responsible for the lack of cognitive improvement in aged and AD patients is the impaired transit of Cbl through lysosomes, particularly in long-lived post-mitotic cells such as neurons.

This project will primarily use *in vitro* models to define how lysosomal dysfunction directly affects Cbl transport and key metabolic sequelae. *In vitro* manipulations and mutant cell models with inhibited lysosomal function may be useful experimental approaches to investigate the changes in Cbl distribution in different subcellular compartments. These cell models include those known to induce lysosomal lipofuscin accumulation, the impairment of lysosomal function due to pathogenic (e.g. Aβ-induced) lysosomal membrane perturbations, and lysosomal storage disease. An *in vivo* APPxPS1 transgenic AD mouse model will also be assessed for alterations in lysosomal Cbl metabolism. If this hypothesis is correct it may explain why Cbl administration has not yielded a consistent therapeutic benefit in the ageing and dementia contexts. More importantly, this study may identify a pathway that could improve neuronal Cbl utilisation and reduce the production of neurotoxic

metabolites that accumulate when the coenzyme forms of Cbl do not reach their correct intracellular targets.

Chapter 2

General methods

2 General methods

2.1 Cell culture

The experiments were performed using human fibrosarcoma cells (HT1080, ATCC #CCL-121) and human neuroblastoma cells (SH-SY5Y, ATCC #CRL-2266), which were obtained from the American Type Culture Collection (ATCC, Manassas, VA, USA). The cells were cultured in Dulbecco's modified eagle medium (DMEM, Life Technologies, USA, Cat #12800-017), and supplemented with 10% (v/v) foetal calf serum (FCS, Interpath, USA, Cat #SFBS), 100 µg/ml penicillin/streptomycin (Sigma, USA, Cat #P4333), and 2 mM glutamine (Invitrogen, USA, Cat #15140122) at 37°C in a humidified atmosphere containing 5% CO_2. The cells were grown in four 175 cm^2 plastic flasks until they reached approximately 70% confluence. The experiments also used 1-year-old human healthy foreskin fibroblasts (AG01518) and human Gaucher's disease fibroblasts (GM00877, Lysosomal Storage Disease) obtained from the Coriell Institute (New Jersey, USA).

2.2 [^{57}Co] Cbl incorporation into cultured cells

As described previously, Cbl cellular uptake requires the Cbl binding protein TC that exists in the serum. The HT1080 fibroblasts and SH-SY5Y cells were metabolically labeled with [^{57}Co] Cbl (0.025 µCi/ml, MP Biomedicals, USA, Cat #06B-430002) in DMEM with 10% (v/v) human serum (HS, Sigma, USA, Cat #H4522) for 48 h at 37°C to maximise [^{57}Co] Cbl uptake. The cells were then rinsed with cold (10°C)

phosphate buffered saline (PBS), harvested with 1% (w/v) trypsin, and centrifuged at 600 × *g* for 5 min at 4°C. A small portion of the cells were stained with 1% trypan blue to determine the number of viable cells.

2.3 Cell homogenisation

A lysosome enrichment kit (Pierce, USA, Cat #89839) was applied to perform subcellular fractionation. An 800 µl aliquot of extraction buffer Lysosome Enrichment Reagent (LER) "A", containing 1% (w/v) protease inhibitors (Sigma, USA, Cat #P8340), was added to the cell pellets. The pellets were gently re-suspended and incubated on ice for no more than 2 min. The cell suspension was transferred to a ball-bearing cell homogeniser (Isobiotec, Germany) and homogenised on ice. To confirm lysis efficiency, 10 µl of cell lysate was stained with 1% (w/v) trypan blue and viewed under a light microscope. Homogenisation was continued until 95% cell membrane breakage was achieved (typically 15 passages through the homogeniser). Next, the lysed cells were transferred into a 2 ml Eppendorf tube, and 800 µl of LER "B", containing 1% (w/v) protease inhibitors, was mixed with the lysed cells. The mixed cell lysates were then centrifuged at 600 × *g* for 10 min at 4°C to remove nuclei and membranous debris, and the supernatant (1,500 µl) containing lysosomes, mitochondria and cytosol was collected.

2.4 Density gradient ultracentrifugation

To prepare a discontinuous density gradient, five gradient solutions were prepared by mixing gradient dilution buffer (a 1:1 mixture of LER A and LER B) with the OptiPrep medium (cell separation media as a 60 % solution of iodixanol-5,5´-[(2-hydroxy-1,3-propanediyl)-bis(acetylamino)]bis(N,N´-bis(2,3-dihydroxypropyl-2,4,6-triiodo-1,3-benzenecarboxamide)) as described in Table 2.1.

OptiPrep medium volume (µl)	Gradient dilution buffer volume (µl)	Final volume (µl)	OptiPrep final concentration (%)
283.3	716.7	1000	17
333.3	666.7	1000	20
191.7	308.3	500	23
450	550	1000	27
500	500	1000	30

Table 2.1 OptiPrep density gradient preparation.

The diluted OptiPrep density gradient solutions were carefully overlaid in descending concentration order (i.e. 30% OptiPrep solution first and then 27%, 23%, 20%, and 17%) in a 7 ml ultracentrifuge tube (Hitachi Koki, Japan). Next, the prepared 1,500 µl supernatants from the cell extracts described above were mixed with 500 µl of OptiPrep medium to make a final concentration of 15% OptiPrep, and this solution was overlaid on top of the density gradient (Figure 2.1). The tube was centrifuged at 145,000 × *g* for 4 h at 4°C using a Sorvall MTX 150 ultracentrifuge and a Sorvall S50-ST swinging bucket rotor (Thermo Scientific, USA). After

centrifugation, two distinct bands appeared in the gradient solution. A total of 10 fractions of 600 µl each were carefully withdrawn from the tops of the gradients using extra-long micropipette tips (Finntip 200, Thermo Scientific, USA). The amount of [^{57}Co] Cbl in each fraction was measured using a Wallace Gamma Counter (PerkinElmer, Finland). Next, each isolated fraction was mixed with 1,000 µl PBS and centrifuged at 20,000 × *g* for 30 min at 4°C to separate the lysosomes and mitochondria from the cytosol. After centrifugation, the supernatant of each fraction was collected and labelled as cytosolic fractions, while the pellets from each fraction were mixed with 400 µl PBS and labelled as lysosomal and mitochondrial fractions (subsequent to the identification of organelle markers using western blot analyses as described below). Both the pellet and supernatant fractions were assessed for [^{57}Co] Cbl radioactivity using a gamma counter, and for organelle/cytosolic markers using western blotting. An overview of this procedure is illustrated in Figure 2.1.

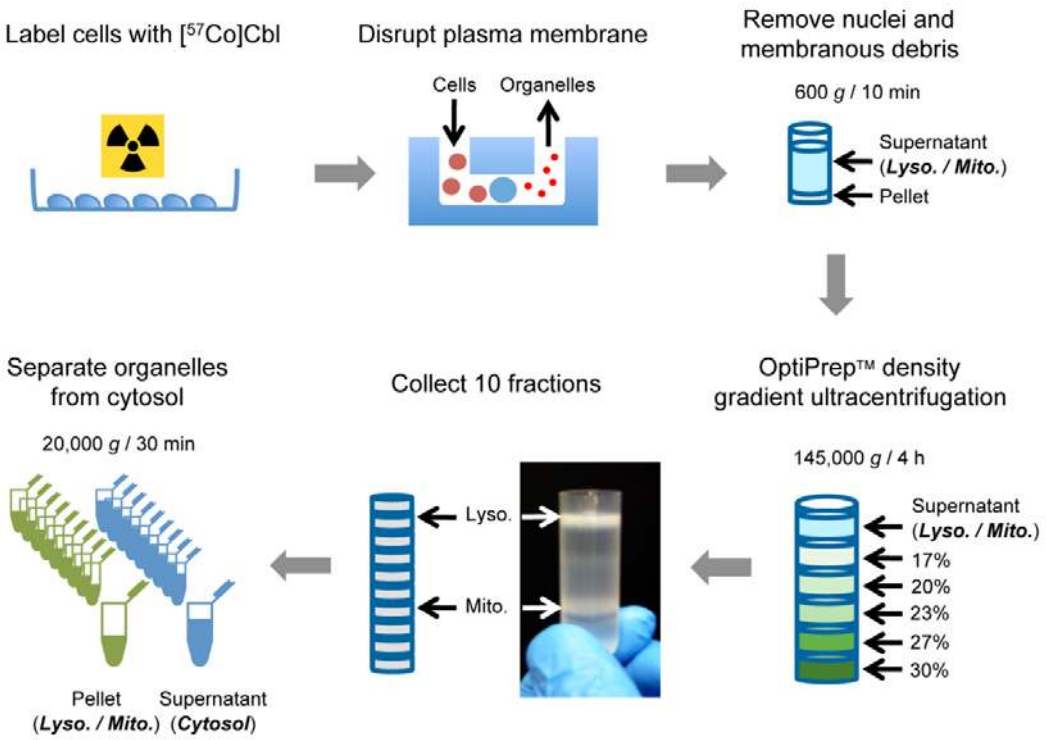

Figure 2.1 Overview of [^{57}Co] Cbl labelling and subcellular fractionation procedures. Cultured cells were incubated with 0.025 µCi/ml [^{57}Co] Cbl in DMEM with 10% (v/v) HS for 48 h. The cells were then homogenised and membrane debris and nuclei were removed. The supernatant samples overlayed on top of an OpitPrep density gradient. After ultracentrifugation at 145,000 *g* for 4 h, a total of 10 fractions of 600 µl each were collected and the lysosomal/mitochondrial (Lyso/Mito) fractions were separated from the cytosol by mixing with PBS followed by further centrifugation at 20,000 *g* for 30 min. The organelle and cytosol fractions were thereafter assessed for appropriate markers and [^{57}Co] Cbl radioactivity.

2.5 Western blotting

To identify the fractions containing lysosomes, mitochondria, and cytosol, western blot was performed using appropriate antibodies for marker proteins: lysosomes were marked with lysosomal-associated membrane protein 2 (LAMP2, Southern Biotech, USA); mitochondria were marked with voltage-dependent anion channel 1 (VDAC1, Abcam, USA); and cytosol was marked with β-actin (Sigma, USA) and methionine synthase/5-methyltetrahydrofolate-homocysteine methyltransferase (MS, Abnova, USA). Briefly, sample proteins from each fraction were separated on 12% sodium dodecyl sulfate polyacrylamide gel electrophoresis (SDS-PAGE) gels using a Mini-Protean II system (Bio-Rad, USA) at 150 V for 70 min and then transferred at 100 V for 30 min onto 0.45 μm nitrocellulose membranes using a Mini-Trans-Blot Electrophoretic Transfer cell (Bio-Rad, USA). The membranes were blocked in 5% (w/v) non-fat milk powder in PBS for 1 h at 22°C and then probed with an anti-LAMP2 mouse monoclonal antibody (1:4,000), an anti-VDAC1 rabbit polyclonal antibody (1:4,000), an anti-β-actin rabbit polyclonal antibody (1:10,000), and an anti-MS goat polyclonal antibody (1:300) for 16 h at 4°C. They were then incubated with the respective horseradish-peroxidase (HRP)-conjugated goat anti-mouse (1:4,000, Dako, Australia), goat anti-rabbit (1:4,000, Dako, Australia), and rabbit anti-goat (1:2,000, Dako, Australia) IgG antibodies for 1 h at 22°C. The blots were rinsed in PBS, and the proteins were detected using enhanced chemiluminescence (ECL, Amersham Biosciences, USA). The membranes were exposed to ECL hyperfilm (Amersham Biosciences, USA), which was developed and scanned, and the signal intensity was quantified using NIH Image software.

2.6 Bicinchoninic acid (BCA) protein assay

The BCA assay measures the total protein concentration compared to a protein standard. It uses a colour change in the sample solution from green to purple in proportion to the protein concentration that is measured using colorimetric techniques (Walker, 1994). In the experiments, the cell fractions (25 µl) were diluted in distilled water (25 µl), and 10 µl of each diluted sample/blank was added (in triplicate) to a non-sterile 96-well plate (Table 2.2). Similarly, 10 µl of each protein standard of bovine serum albumin (BSA) was added to the same 96-well plate in triplicate. The protein standards were prepared by diluting BSA with distilled water as described in Table 2.3.

10 µl of Standards (mg/ml) ⟺ 10 µl of Control (C) & Samples (S)

0	0	0	C	C	C
0.125	0.125	0.125	S 1	S 1	S 1
0.25	0.25	0.25	S 2	S 2	S 2
0.5	0.5	0.5	S 3	S 3	S 3
1	1	1	S 4	S 4	S 4
2	2	2	S 5	S 5	S 5

Table 2.2 The samples preparation.

Volume of BSA (µl)	Volume of water (µl)	Final BSA concentration (mg/ml)
400 of 2 mg/ml	0	2.0
200 of 2 mg/ml	200	1.0
200 of 1 mg/ml	200	0.5
200 of 0.5 mg/ml	200	0.25
200 of 0.25 mg/ml	200	0.125
0	400	0

Table 2.3 Preparation of BCA standards.

Finally, the BCA working solution (200 µl) was prepared by mixing Reagent A (Pierce, USA, Cat #23223) and Reagent B (4% cupric sulfate) in a 50:1 ratio, and added to each test well using a multi-channel pipette. The plate was covered with aluminum foil and incubated for 30 min at 37°C. A colour change from green to purple was observed in proportion to the total protein concentration. The absorbance was measured at 570 nm using a microtitre plate reader (Spectra Max, Bio Strategy, USA). The protein standard curve was created to analyse the data set.

2.7 Statistical analysis

The data were presented as means ± SE of three independent experiments unless stated otherwise. Statistical significance was assessed using the two-tailed unpaired Student's t test with $P < 0.05$ considered significant. All graphs were prepared with KaleidaGraph (Synergy Software, USA). In addition, the results for [^{57}Co] Cbl were

presented as counts per minute (cpm). The radioactive tracer molecule [^{57}Co] Cbl was provided by the supplier in batches of 10.5 µCi in a volume of 1 ml H_2O containing 0.9% (v/v) benzyl alcohol. On the reference date provided by the manufacturer, 0.1 ml from each batch of [^{57}Co] Cbl yielded 2.0×10^6 cpm. After evaporation and reconstitution in the cell culture medium (or saline for i.p. injection), the [^{57}Co] Cbl radioactivity was measured in a 0.1 ml aliquot to confirm the radioactivity prior to its experimental use. For the experiments described herein, the [^{57}Co] Cbl tracer was routinely used within 2 months of the reference date, and the radioactivity per 0.1 ml on the day of preparation for addition to cells or animals was $1.52 \times 10^6 \pm 0.04 \times 10^6$ cpm (mean ± SE, n = 8). The values ranged from 1.37×10^6 to 1.65×10^6 cpm in these experiments. As an approximation, when 300 µCi/µg [^{57}Co] Cbl was used in experiments, 1,000 cpm equated to ~2.4 pg of [^{57}Co] Cbl. In all experiments, the [^{57}Co] Cbl was used within two months of the reference date and the radioactivity of [^{57}Co] Cbl may have decreased by up to a maximum of 14%. This decrease needs to be considered when directly comparing cpm values from different experiments.

Chapter 3

Development and application of subcellular fractionation method

3 Development and application of subcellular fractionation method

3.1 Introduction

As reviewed in Chapter 1, once Cbl is released from the lysosome, it acts as a coenzyme that is converted to MeCbl in the cytosol and AdoCbl in the mitochondria, respectively. Cbl thus locates in three main intracellular compartments: lysosome, mitochondria and cytosol. To accurately assess Cbl transit through these intracellular compartments, it was essential to develop a fast and efficient procedure that can separate these three compartments into fractions in which labeled Cbl can be unambiguously quantified. The following steps were therefore processed to achieve this purpose: (1) the fibroblast and neuronal cells were labeled with [^{57}Co] Cbl; (2) the cells were disrupted in a ball-bearing homogeniser; (3) the isolated organelles were separated from the cellular membrane debris and nuclei; (4) the density-based organelles were separated over an OptiPrep density gradient using ultracentrifugation; (5) ten fractions were collected from the gradient; and (6) the fractions were separated into pellet (organelle) and supernatant (cytosol) fractions. The methodological detail for each of these steps is described in Chapter 2, section 2.2-2.4, and an overview is illustrated in Figure 2.1. The purified fractions were then analyzed for specific organelle markers using western blotting and [^{57}Co] Cbl radioactivity was measured in each fraction.

3.2 Methods

3.2.1. Western blotting

The detail for identifying the fractions containing lysosomes, mitochondria, and cytosol using appropriate antibodies for marker proteins was described in Chapter 2, section 2.5.

3.2.2. Acid phosphatase assay

During cell homogenisation and ultracentrifugation, lysosomal membranes are susceptible to pressure and may be broken; thus, as a consequence, lysosomal hydrolases may be leaked into the cytosol. Acid phosphatase is one of the acid hydrolases that is present in lysosomes and is thus a classical marker for the identification of lysosomes in subcellular fractionation studies. An acid phosphatase assay kit (Sigma, USA, Cat #CS0740) was applied to detect lysosomal membrane integrity in each fraction. Briefly, a substrate solution was prepared by dissolving one 4-nitrophenyl phosphate tablet in 5 ml of citrate buffer, and the solution was equilibrated at 37°C. The standard solution was prepared by diluting 5 µl of the 10 mM nitrophenol standard solution in 995 µl of 0.5 M sodium hydroxide (NaOH). The reaction components and samples were added to 96-well microtitre plates according to the manufacturer's instructions, and the samples were analysed in triplicate. The plates were incubated for 10 min at 37°C and then 200 µl of 0.5 M NaOH was added to all of the wells (except the standard) to stop the reaction. The absorbance was measured at 405 nm using a microtitre plate reader (Spectra Max,

Bio Strategy, USA), and the results were expressed as acid phosphatase Units/ml (where 1 Unit of enzyme activity will hydrolyse 1 μM of 4-nitrophenyl phosphate per min at pH 4.8 at 37°C).

3.3 Results

3.3.1. Isolation of lysosomes, mitochondria and cytosol from fibroblasts

The initial experiments focused on the HT1080 fibroblast cell line. Western blot analysis of the organelle fractions for LAMP2 and VDAC1 (lysosomal and mitochondrial markers, respectively) revealed that lysosomes were recovered from the top of the OptiPrep gradient, particularly in fraction #1 (Figure 3.1 A). Because LAMP2 was also detected at lower levels in fractions #2 – #5, these combined fractions (fractions #1 – #5) were considered to represent the lysosomal content of the cells. In contrast, VDAC1 was detected in fractions #7 – #9 and thus represented the mitochondrial fractions. Importantly, β-actin was detected at very low level; if at all, in the isolated organelle fractions, and MS was not detected in any of the organelle fractions (Figure 3.1 A), indicating that pure lysosomes can be separated from mitochondria and that both organelles were essentially free of cytosolic contaminants that may spuriously contribute to apparent organelle Cbl levels. The cytosolic components of each of the ten OptiPrep gradient fractions were also assessed using western blotting. Neither LAMP2 nor VDAC1 was detected in the cytosolic fractions, whereas β-actin was clearly detected in fractions #1 – #8, with particularly high levels in fractions #1 – #4 (Figure 3.1 B). In addition, MS was detected in fractions #1 – #3, with particularly high levels in fraction #2.

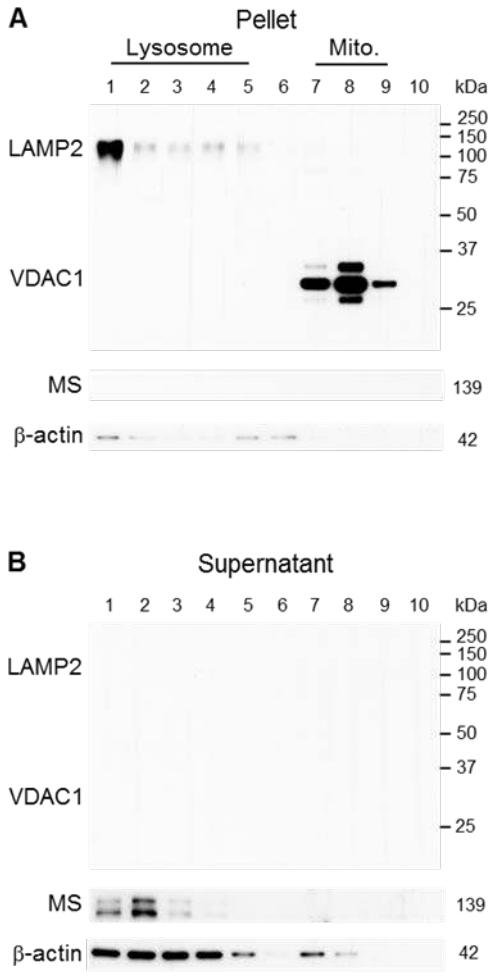

Figure 3.1 Separation of lysosomes, mitochondria, and cytosol in fibroblast fractions. Approximately 16 × 10^6 cells were metabolically labeled with [^{57}Co] Cbl for 48 h. The radiolabeled cells were disrupted using a ball-bearing homogeniser and the lysosomes, mitochondria, and cytosolic fractions were separated using an OptiPrep gradient. The appearance of the markers LAMP2 (lysosomal), VDAC1 (mitochondrial), β-actin and MS (both cytosolic) were probed by western blotting in all of the fractions (Note: fraction #1 is the least dense from the top of the gradient). (A) In the pellet fractions, a clear separation was observed for lysosomes (fractions #1 – #5) and mitochondria (Mito, fractions #7 – #9). Cytosolic markers were either absent or present only at trace amounts. (B) In the supernatant portion of the fractions, lysosomal and mitochondrial markers were not detected; however, strong signals for cytosolic markers, β-actin (fractions #1 – #8) and MS (fractions #1 – #3) were detected. Data are representative of three independent experiments.

3.3.2. Isolation of lysosomes, mitochondria and cytosol from neuronal cells

The same method was also used to purify lysosomes and mitochondria from the SH-SY5Y neuronal cell line. Similar to the results obtained from fibroblast studies, pure lysosomal and mitochondrial preparations were recovered from fractions #1 – #5 and from fractions #7 – #9, respectively (Figure 3.2 A). Most of lysosomal LAMP2 expression was found at fraction #1, which is the least dense from the top of the gradient. Neither β-actin nor MS was detected in the organelle fractions. Assessment of the cytosolic fractions revealed a lack of contamination of the cytosol with lysosomes or mitochondria, as assessed by the absence of LAMP2 and VDAC1 signals, respectively (Figure 3.2 B). Moreover, β-actin was clearly detected in fractions #1 – #9, with particularly high levels in fractions #1 – #6, whereas MS was detected predominantly in fractions #2 – #5. Thus, the established subcellular fractionation method is suitable for isolation of pure lysosomal, mitochondrial and cytosolic fractions from fibroblasts and neuronal cells. The method was also applied to other mutant cell lines and mouse brain tissues to investigate the alteration of subcellular [^{57}Co] Cbl distribution in those conditions.

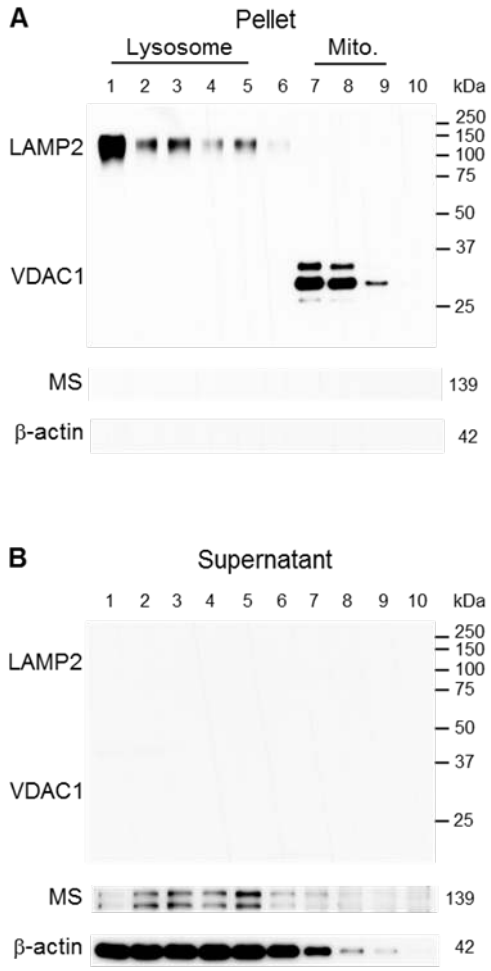

Figure 3.2 Separation of lysosomes, mitochondria, and cytosol in neuronal cell fractions. Approximately 16×10^6 cells were metabolically labeled with [^{57}Co] Cbl for 48 h. The radiolabeled cells were disrupted using a ball-bearing homogeniser and the lysosomes, mitochondria, and cytosolic fractions were separated using an OptiPrep gradient. The appearance of the markers LAMP2 (lysosomal), VDAC1 (mitochondrial), β-actin and MS (both cytosolic) were probed by western blot in all fractions (Note: fraction #1 is the least dense from the top of the gradient). (A) In the pellet fractions, a clear separation was observed between the lysosomes (fractions #1 – #5) and mitochondria (fractions #7 – #9). The expression of cytosolic markers was absent. (B) In the supernatant portion of the fractions, lysosomal and mitochondrial markers were not detected; however, strong signals for the cytosolic markers β-actin (fractions #1 – #8) and MS (fractions #2 – #5) were detected. Data are representative of three independent experiments.

3.3.3. Lysosomal membrane integrity after subcellular fractionation

The subcellular fractionation procedure requires several differential centrifugations with various speeds. A suspension of cell organelles subjected to a series of increasing centrifugal force cycles may generate enormous pressure to their membranes. Unlike mitochondrial membranes, lysosomal membranes are susceptible to pressure and may be broken during ultracentrifugation. Lysosomal hydrolases may be leaked into the cytosol as a consequence. To confirm that the membrane of isolated lysosomes remained intact during the homogenisation and ultracentrifugation procedures, all of the organelle and cytosolic fractions were assessed for acid phosphatase activity. Acid phosphatase is one of the acid hydrolases that normally reside in lysosomes. It is a classical marker for the identification of lysosomal membrane integrity in subcellular fractionations.

The results demonstrated that acid phosphatase activity was closely correlated with the expression of LAMP2 in the lysosomal fractions from both fibroblasts and neuronal cells (Figure 3.3 A and B, respectively). The majority of acid phosphatase was detected in the fraction #1, at which lysosomal LAMP2 showed highest intensity in all fractions in the western blots. Although acid phosphatase was also detected in the fractions #7 and #8, the amount is at very low range and no LAMP2 expression was found in these fractions. Furthermore, acid phosphatase activity was detected only at minimal level in any of the cytosolic fractions and thus was negligible (Figure 3.3). Importantly, the buffers used in the acid phosphatase assay were adjusted to pH 4.8 so that even if the enzyme was located in the cytosol (normally close to neutral pH), we would still be able to detect its activity in the 4-nitrophenyl

phosphate (4-NPP) hydrolysis assay. The result indicates that the isolated lysosomes remain structurally intact during the ultracentrifugation procedure and that the lysosomal membranes are not compromised.

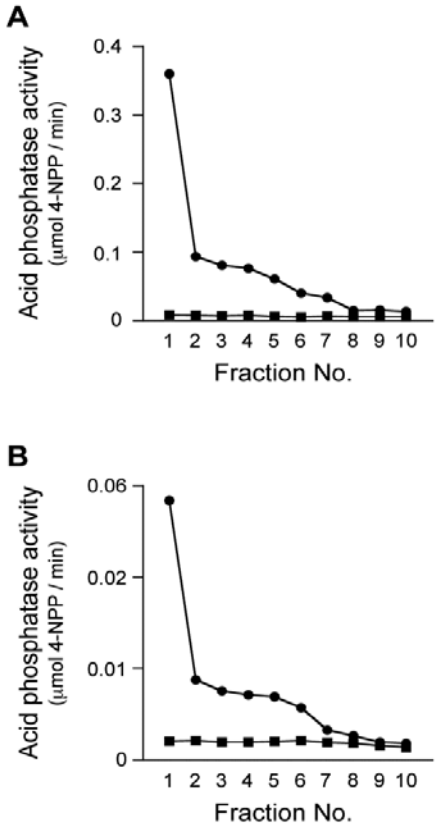

Figure 3.3 Acid phosphatase activity in fibroblast and neuronal cell fractions. Acid phosphatase activity (indicating the presence of lysosomes with an intact membrane) was measured in all pellet fractions (circles) and cytosolic fractions (squares) using 4-NPP as a colorimetric substrate. Acid phosphatase activity in fibroblast fractions (A) and neuronal cell fractions (B) indicated that lysosomes were predominantly found at the top of the density gradient (fraction #1) and were structurally intact (high acid phosphatase activity). The acid phosphatase activity in the supernatant fractions was negligible. Data are representative from three independent experiments.

3.4 Discussion

In the present study I developed a [^{57}Co] Cbl metabolic labeling / subcellular fractionation method that permits the separation of the two major pools of intracellular Cbl (in the cytosol and mitochondria) from the presumably more transient lysosomal pool. Subcellular fractionation by differential centrifugation was first described in 1955 (De Duve *et al.*, 1955) and has subsequently been applied for isolating organelles from various cultured cells and tissues (Maric *et al.*, 1994; Ferrari *et al.*, 1997; Nothwang *et al.*, 2003). However, those early studies lacked of detailed evidence whether the isolated organelle fractions were free of contamination from other organelles. Without this prerequisite, any result from further measurement or test was questionable. The current method builds on many previous studies that have separately analysed cellular [^{57}Co] Cbl metabolism in cells and mice (Mellman *et al.*, 1978; Youngdahl-Turner *et al.*, 1978; Yassin *et al.*, 2000; Hannibal *et al.*, 2008; Yamani *et al.*, 2008) or aspects of lysosome function in cells and mice (Manunta *et al.*, 2007; Yang *et al.*, 2011). The isolated lysosomal, mitochondrial and cytosolic fractions from this method were examined by appropriate antibodies for marker proteins to confirm that every single fraction was purified.

During ultracentrifugation, the loaded cell organelles on the top of the gradient move down through the density gradient. Cell organelles with different densities or sizes in a suspension will sediment at different rates, with the larger and denser particles, e.g. mitochondria, moving faster. Because the density of the mitochondria is greater than the density of the gradient, all the mitochondria will eventually move down and form

a solid pellet zone at the lower level of the gradient. The majority of lysosomes with lighter density, on the other hand, will stay up on the top of the gradient (Figure 2.1). However, the morphology and density of lysosomes varies depending on the cell and tissue source. A couple of fractions close to at the lower level of the gradient may contain both lysosomes and mitochondria in some cases. This may be due to small amount of specific lysosomes that have similar density with light mitochondria and sediment together in the standard condition, or when lysosomal function is inhibited, or in some pathological conditions where lysosomal autophagy is activated and up-regulated, resulting in more autophagic vacuoles formation to increase the density of lysosomes. Therefore, it is necessary to optimize the gradient concentration, centrifugation speed and time for desired results.

Lysosomes maintain cellular homeostasis by continually degrading cellular waste, dysfunctional organelles and potential toxic protein aggregates. An intact lysosomal membrane provides the barrier necessary to maintain such a low pH environment compared with the neutral pH of the surrounding cytosol. Thus, it is essential to maintain lysosomal membrane integrity after subcellular fractionation. The results from acid phosphatase activity indicate that the majority of isolated lysosomes remained structurally intact. It is noteworthy that a lower level in acid phosphatase activity was present with the major mitochondrial fraction (Fraction #7 and #8). LAMP2 expression was not detected in these fractions so lysosomal contamination seems unlikely. One possible explanation could be that one or more of the several known mitochondrial phosphatases may have residual activity at pH 4.8 and thus act upon the 4-NPP is our assay (McBride *et al.*, 2006).

3.5 Conclusion

The development of subcellular fractionation method provides a useful tool for isolating purified lysosomes, mitochondria and cytosol. It is a prerequisite procedure before further investigating intracellular [^{57}Co] Cbl trafficking in fibroblast and neuronal cell lines. Using this method I will also assess cell lines and animal models that are known to have impaired lysosomal function due to, for example, accumulation of the age-related pigment lipofuscin, substrate accumulation in lysosomal storage diseases, and accumulation of AD-derived Aβ. Future studies may adapt the method to assess subcellular distribution of other specific metals and their impact on lysosomes and mitochondria *in vitro* and *in vivo*.

Chapter 4

Impaired lysosomal function inhibits lysosomal cobalamin transport

4 Impaired lysosomal function inhibits lysosomal cobalamin transport

4.1 Subcellular [^{57}Co] Cbl distribution in the standard culture condition

4.1.1. Introduction

As reviewed in Chapter 1, Cbl utilisation as an enzyme cofactor is dependent on its efficient transit through lysosomes to the cytosol and mitochondria. I propose that pathophysiological perturbations in lysosomal function may inhibit intracellular Cbl transport with consequences for down-stream metabolic pathways. Having established subcellular fractionation method for the isolation of pure lysosomes, mitochondria and cytosol, I will use both HT1080 fibroblast and SH-SY5Y neuronal cells to address fundamental questions related to lysosomal Cbl transport. The subcellular distribution of [^{57}Co] Cbl is assessed in the standard cultured fibroblasts and neuronal cells subsequent to a [^{57}Co] Cbl metabolic radiolabelling. Several trial experiments are conducted to optimise the conditions for [^{57}Co] Cbl incorporation in these cells before performing [^{57}Co] Cbl metabolic labeling / subcellular fractionation.

4.1.2. Results

4.1.2.1 **The effect of serum on [^{57}Co] Cbl incorporation into the cells**

The concentration of 0.025 µCi/ml [^{57}Co] Cbl was applied to all experiments as suggested in trial experiments and previous studies (Moras *et al.*, 2007; Hannibal *et al.*, 2009). Cbl cellular uptake requires metabolically active Cbl transporter TC from the serum delivering to the cell surface, where specific cell membrane receptors are expressed and carry the TC-Cbl complex into the cells. Mixed previous reports suggest that [^{57}Co] Cbl incorporation into cells takes place from the medium containing either FCS (Rosenberg *et al.*, 1975; Berliner and Rosenberg, 1981; Hannibal *et al.*, 2009) or HS (Mellman *et al.*, 1978; Amagasaki *et al.*, 1990; Moras *et al.*, 2007). In the current experiment, The SH-SY5Y cells were seeded into 6-well cell culture plates and incubated with 0.025 µCi/ml [^{57}Co] Cbl in DMEM containing either 10% (v/v) FCS or 10% (v/v) HS for 48 h at 37˚C. The cells were collected and measured for radioactivity after incubation. It was observed that FCS substantially reduced the incorporation of [^{57}Co] Cbl into cells (Figure 4.1), whereas HS promoted [^{57}Co] Cbl uptake into cells and thus HS was applied to all experiments.

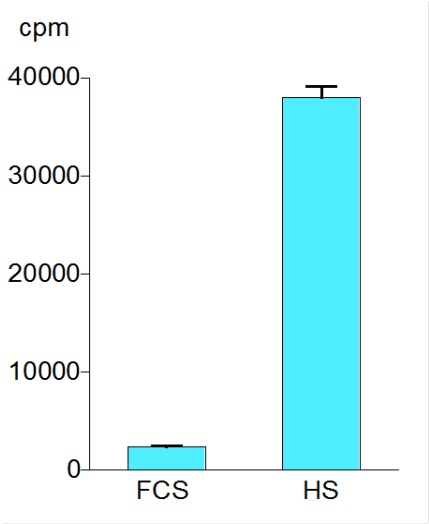

Figure 4.1 Cellular [^{57}Co] Cbl uptake affected by the serums. Approximately 90,000 cpm of [^{57}Co] Cbl was added to the same number of SH-SY5Y cells in DMEM containing either 10% (v/v) FCS or 10% (v/v) HS for 48 h at 37˚C. The cells incubated with 10% (v/v) FCS had only 2,300 ± 100 cpm radioactivity reading, whereas the cells with 10% (v/v) HS expressed 38,000 ± 1,600 cpm radioactivity reading. Data are representative and expressed as mean ± SE (represented by the error bars) from three independent experiments.

4.1.2.2 The effect of incubation period on [^{57}Co] Cbl incorporation into the cells

The period of [^{57}Co] Cbl metabolic radiolabelling is an important factor for effective cellular [^{57}Co] Cbl uptake. Longer or shorter incubation time means that cellular [^{57}Co] Cbl uptake may not reach its maximal rate and lead to inadequate [^{57}Co] Cbl radioactivity reading. To determine the optimal incubation period for [^{57}Co] Cbl incorporation into cells, the time-course of cellular [^{57}Co] Cbl uptake was examined. The fibroblasts and neuronal cells were seeded into 6-well cell culture plates and incubated with 0.025 µCi/ml [^{57}Co] Cbl in DMEM containing 10% (v/v) HS at 37˚C

for 16, 24, 48, and 72 h. The cells were collected and measured for radioactivity after incubation. It was found that the cellular uptake of [^{57}Co] Cbl was time-dependent and reached its summit at 48 h (Figure 4.2).

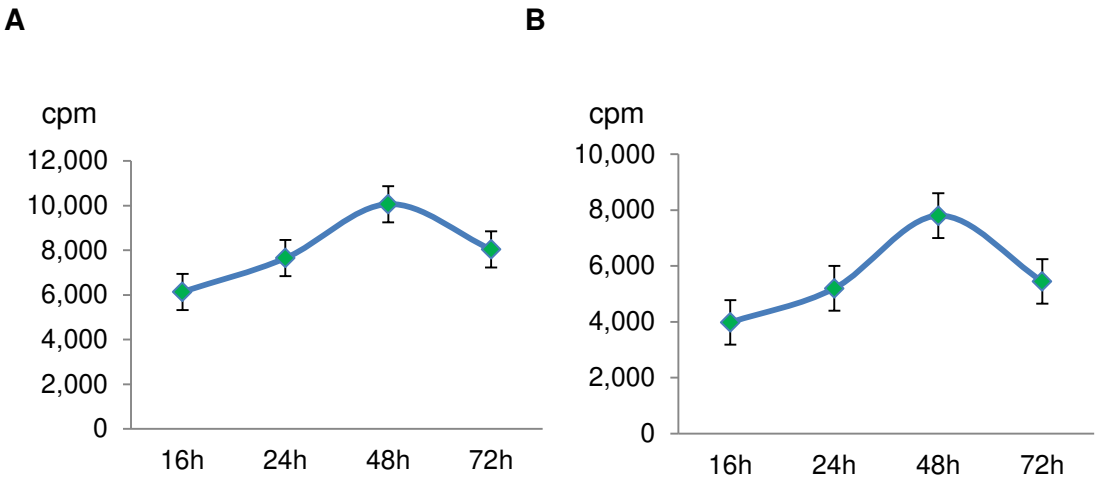

Figure 4.2 The period of cellular [^{57}Co] Cbl uptake in fibroblasts and neuronal cells. The same number of fibroblasts (A) and neuronal cells (B) were incubated with approximately 40,000 cpm of [^{57}Co] Cbl in DMEM containing 10% (v/v) HS for various periods at 37˚C. The cells incubated for 48 h had the highest radioactivity readings of 10,100 ± 500 and 7,800 ± 300 cpm, respectively. Data are representative and expressed as mean ± SE (represented by the error bars) from three independent experiments.

4.1.2.3 The effect of cell growth confluence on [^{57}Co] Cbl incorporation into the cells

The extent of [^{57}Co] Cbl incorporation under various cell growth confluences was also examined to maximise cellular [^{57}Co] Cbl uptake. The SH-SY5Y cells were seeded into 6-well cell culture plates and grown in DMEM containing 10% (v/v) FCS to reach 60%, 80%, and 100% of confluence, and then incubated with 0.025 µCi/ml [^{57}Co] Cbl in DMEM containing 10% (v/v) HS for 48 h at 37˚C. The cells were collected and measured for radioactivity after 48 h. The results indicated that neuronal cells with 80% confluence incorporated more [^{57}Co] Cbl than other conditions (Figure 4.3).

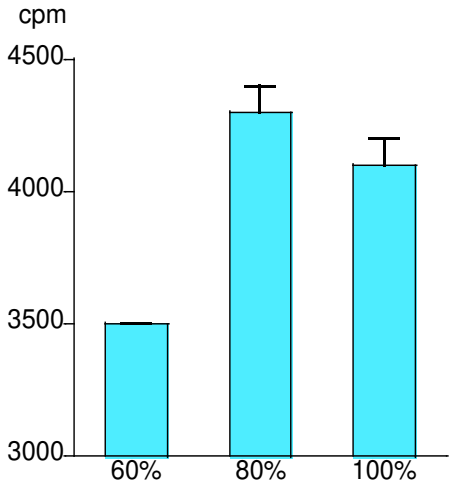

Figure 4.3 [^{57}Co] Cbl incorporation under various neuronal growth confluences. SH-SY5Y cells that were grown to 60%, 80%, and 100% confluence were incubated with same amount of [^{57}Co] Cbl in DMEM containing 10% (v/v) HS for 48 h at 37˚C. The neuronal cells grown with 80% confluence had the highest radioactivity reading of 4,200 ± 100 cpm. Data are representative and expressed as mean ± SE (represented by the error bars) from three independent experiments.

4.1.2.4 Isolated cellular fractions probed by western blotting

Once the optimal conditions for cellular [^{57}Co] Cbl uptake were determined, I assessed subcellular [^{57}Co] Cbl distribution in the cultured fibroblasts and neuronal cells based on those conditions. Both cells were grown to reach 80% confluence and then incubated with 0.025 μCi/ml [^{57}Co] Cbl in DMEM containing 10% (v/v) HS for 48 h at 37°C. The cells were then homogenised and cell fractions were collected, followed by subcellular fractionation as described previously (Chapter 2, section 2.4). Isolated cellular fractions containing lysosomes, mitochondria, and cytosol were probed for appropriate organelle markers by western blotting: lysosome: LAMP2; mitochondria: VDAC1; and cytosol: MS.

Consistent with the results from the established methods in Chapter 3, the separation of fibroblast and neuronal cell organelles through an OptiPrep gradient yielded pure lysosomes (LAMP2-positive fractions #1 – #5 and #1 – #6, respectively) and mitochondria (VDAC1-positive fractions #7 – #9) as demonstrated by western blotting (Figure 4.4 A and B). Neither LAMP2 nor VDAC1 signal was detected in the cytosolic fractions (Data are not shown). The organelle fractions were free of detectable MS whereas a clear MS signal was detected in the cytosolic fractions (#1 – #5).

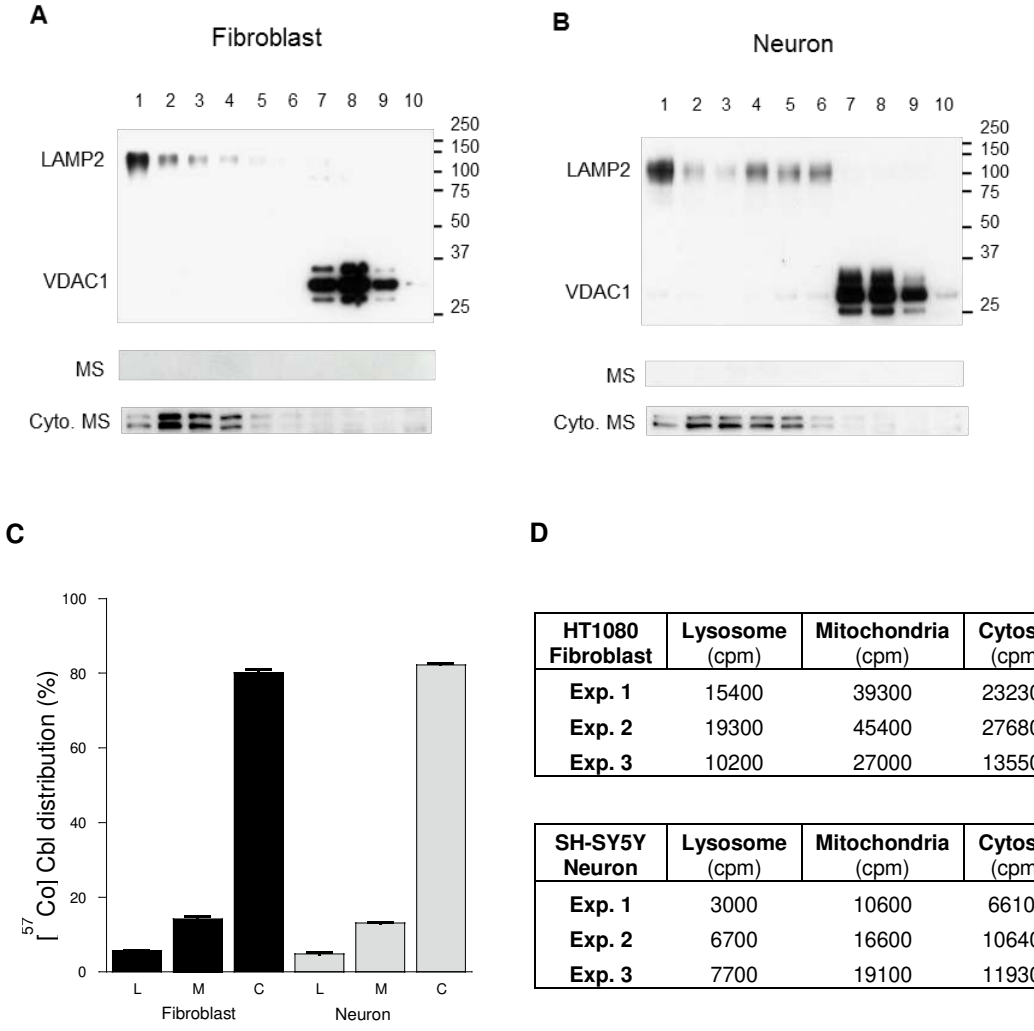

HT1080 Fibroblast	Lysosome (cpm)	Mitochondria (cpm)	Cytosol (cpm)
Exp. 1	15400	39300	232300
Exp. 2	19300	45400	276800
Exp. 3	10200	27000	135500

SH-SY5Y Neuron	Lysosome (cpm)	Mitochondria (cpm)	Cytosol (cpm)
Exp. 1	3000	10600	66100
Exp. 2	6700	16600	106400
Exp. 3	7700	19100	119300

Figure 4.4 Distribution of [^{57}Co] Cbl in lysosomes, mitochondria, and cytosol. The fibroblasts and neuronal cells were incubated separately with 0.025 µCi/ml [^{57}Co] Cbl in DMEM with 10% (v/v) HS for 48 h at 37 °C. The cells were then homogenised, followed by subcellular fractionation. The lysosomal, mitochondrial, and cytosolic fractions were separated and probed for marker proteins LAMP2 (lysosomal), VDAC1 (mitochondrial), and MS (cytosolic) by western blotting in all fractions from fibroblasts (A) and neuronal cells (B). The proportional distribution of [^{57}Co] Cbl was expressed as the percentage of cpm values in each organelle fraction for both cell types (C). Data are representative and expressed as mean ± SE (represented by the error bars). The cpm data for each of the organelles in the three independent experiments was obtained for each cell type shown in "C" (Figure 4.4 D). L, lysosome; M, mitochondria; C, cytosol.

4.1.2.5 Subcellular [^{57}Co] Cbl distribution in the fibroblasts and neuronal cells

After the 48 h [^{57}Co] Cbl radiolabelling period, 18.3 ± 0.9% of the total radioactivity was incorporated into the fibroblasts (mean ± SE, n = 3), whereas under the same culture condition only 6.0 ± 1.2% of the total radioactivity was uptaken into the neuronal cells (mean ± SE, n = 3). Despite the relatively low level of isotope incorporation, this amount was clearly sufficient to assess [^{57}Co] Cbl distribution in lysosomes, mitochondria and cytosol (Figure 4.4 D).

The data presented in Figure 4.4 C indicate the distribution of [^{57}Co] Cbl in each organelle fraction expressed as a percentage of cpm values. As a proportion of total cellular [^{57}Co] Cbl, the relative distribution of [^{57}Co] Cbl in fibroblasts was as follows: lysosomes, 5.7 ± 0.1%; mitochondria, 14.2 ± 0.7%; and cytosol, 80.1 ± 0.8% (all means ± SE, n = 3). The corresponding data for the neuronal cells were as follows: lysosomes, 4.8 ± 0.5%; mitochondria, 13.1 ± 0.3%; and cytosol, 82.2 ± 0.4% (all means ± SE, n = 3). There was no obvious deference in terms of [^{57}Co] Cbl distribution in lysosomes, mitochondria and cytosol between fibroblasts and neuronal cells. Although there was some variability in the absolute cpm values for [^{57}Co] Cbl in each of the organelles assessed over three independent experiments (Figure 4.4 D), the proportional distribution of [^{57}Co] Cbl in the intracellular compartments was remarkably constant (Figure 4.4 C).

4.2 Lysosomal pH alteration interrupts lysosomal [^{57}Co] Cbl transport

4.2.1. Introduction

Early studies described the defective transfer of lysosomal Cbl to the cytosol in fibroblasts derived from a human patient with inborn error of Cbl metabolism, chloroquine was used to retard intralysosomal proteolysis in control fibroblasts in order to model lysosomal Cbl trapping (Rosenblatt *et al.*, 1985). The maintenance of acidic pH and efficient protease activity is critical for lysosomal Cbl transport. Chloroquine, a traditional anti-malarial drug, raises intralysosomal pH above its physical level by disrupting the H^+ gradient across the lysosomal membrane and thereby neutralising the normally acidic lysosomal pH (Gonzalez-Noriega *et al.*, 1980). Chloroquine alters the lysosomal acidic compartments, causes inhibition of lysosomal hydrolase activities, and induces accumulation of autophagosomes (Geng *et al.*, 2010), which prevents the release of Cbl from TC and also blocks the transport of lysosomal Cbl to both MS and MMCM (Rosenblatt *et al.*, 1985).

The acidic pH of the lysosome also influenced the conversion of Cbl from the "base-on" to "base-off" state, i.e. the interaction of the dimethylbenzimidazole moiety of the Cbl molecule with the central Co atom (Banerjee, 2006). The Cbl base-off state is thought to be important for subsequent interactions of Cbl with cytosolic cargo proteins. Thus, it is possible that chloroquine could at least partly inhibit Cbl intracellular transport by blocking its conversion to the base-off state. In addition, chloroquine-treated cells under transmission electron microscope showed a changed

lysosomal morphology with increased enlarged multilaminar autophagic vacuole formation in the cytoplasm (Myers *et al.*, 1995). This effect was dose-dependent and was more pronounced with the higher doses. In the present study, I utilised both fibroblast and neuronal cells and investigated the effect of chloroquine treatment on their lysosomal Cbl transport.

4.2.2. Methods

4.2.2.1 Inhibition of lysosomal function with chloroquine

As chloroquine at high concentration is toxic to cells and an overdose of chloroquine may be lethal, the optimal concentration of chloroquine treatment was determined before cellular [^{57}Co] Cbl radiolabeling. The fibroblasts were incubated with chloroquine (Sigma, USA, Cat #C6628) at different concentrations in DMEM with 10% (v/v) FCS for 48 h at 37°C. The cellular viability was assessed by 3-[4,5-dimethylthiazol-2-yl]-2,5 diphenyl tetrazolium bromide (MTT) assay and 1% (w/v) trypan blue cell staining. Once the concentration of chloroquine was determined, the fibroblasts and SH-SY5Y cells were incubated separately with 0.025 µCi/ml [^{57}Co] Cbl in DMEM containing 10% (v/v) HS in the presence of chloroquine (25 µM) for 48 h at 37°C. The cells were then homogenised and cell fractions were collected, followed by subcellular fractionation as described previously (Chapter 2, section 2.4).

4.2.2.2 Western blotting

The details for identifying the fractions containing lysosomes, mitochondria, and cytosol using appropriate antibodies for marker proteins were described in Chapter 2, section 2.5.

4.2.2.3 MTT activity assay

The MTT assay is based on the conversion of soluble yellow MTT into insoluble purple formazan crystals by living cells that determine mitochondrial activity (van Meerloo *et al.*, 2011). For most cell populations, total mitochondrial activity is related to the number of viable cells. The MTT assay is used to measure the *in vitro* cytotoxic effects of drugs on cells. In this experiment, it was used to detect mitochondrial activity in those cells with chloroquine treatment. Briefly, after 48 h incubation with chloroquine, the fibroblasts were rinsed with PBS, harvested with 1% (w/v) trypsin, and centrifuged at 600 × *g* for 5 min. The cell suspension was mixed with 0.5 mg/ml MTT stock solution. The mixture was then incubated in a water bath for 30 min at 37°C. A sample of viable cells was suspended in PBS and used as a positive control. Next, the samples were centrifuged at 16,000 × *g* for 5 min. The supernatant was discarded and the pellet was mixed thoroughly with 300 µl of dimethyl sulfoxide. Each sample (90 µl, in triplicate) was transferred to a non-sterile 96-well plate and incubated for 10 min at 37°C. The absorbance was measured at 570 nm using a microtitre plate reader (Spectra Max, Bio Strategy, USA).

4.2.3. Results

4.2.3.1 The toxicity of chloroquine on cellular viability

The viability of living cells was demonstrated using the MTT assay and trypan blue staining. The same numbers of fibroblasts were seeded into 6-well cell culture plates and incubated with chloroquine at 5, 10, 15, 20 and 40 µg/ml in DMEM containing 10% (v/v) FCS for 48 h at 37˚C. The cells were then collected and either measured by the MTT assay (Figure 4.5 A) or stained by trypan blue (Figure 4.5 B) to evaluate cell viability. Both results demonstrated that exposure to chloroquine resulted in a rapid reduction in the number of living cells and that this decrease was dose-dependent. Thus, the concentration of 25 µM (~15 µg/ml) chloroquine was selected for this experiment because it is estimated that approximately 80% of the cells survive with this comparatively high dose and it allows comparison with previous relevant studies.

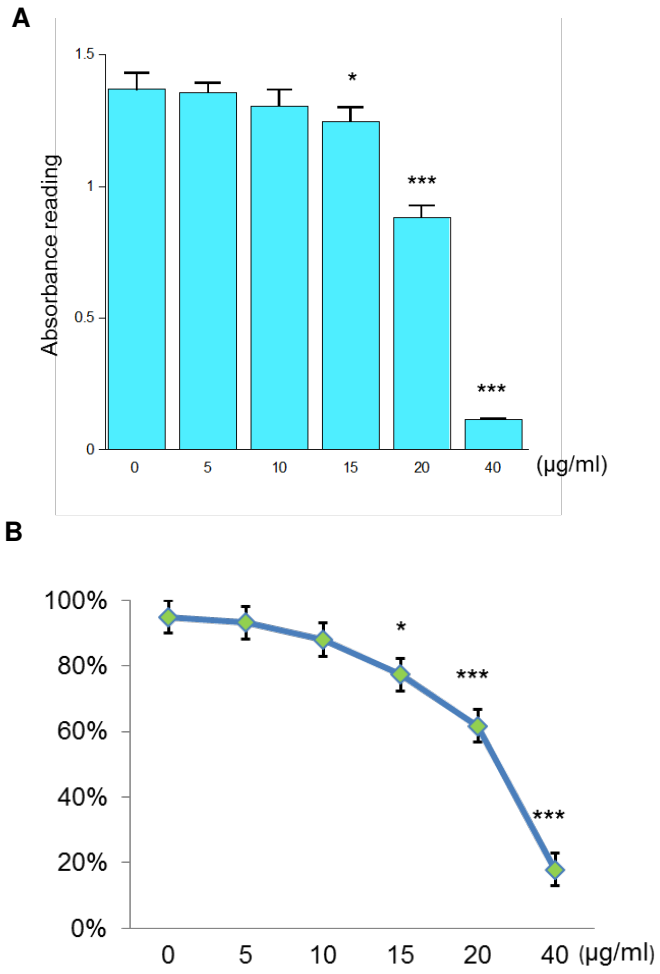

Figure 4.5 The effect of chloroquine treatment on cell viability. The same number of fibroblasts was treated with chloroquine at various concentrations in DMEM containing 10% (v/v) FCS for 48 h at 37˚C. The cells were then collected and either measured by the MTT assay (A) or stained by trypan blue (B) to evaluate cell viability. Both results showed that exposure to chloroquine resulted in a reduction in the number of living cells and that this decrease was dose-dependent. Data are expressed as mean ± SE (represented by the error bars). * $P < 0.05$, ***$P < 0.001$.

4.2.3.2 Isolated cellular fractions probed by western blotting

Next, the fibroblasts and SH-SY5Y cells were incubated separately with 0.025 µCi/ml [^{57}Co] Cbl in the presence of 25 µM chloroquine. Isolated cellular fractions were collected after subcellular fractionation and probed for appropriate organelle markers by western blotting. Although chloroquine increased the lysosomal pH and inhibited lysosomal function, the western blot results from chloroquine-treated fibroblasts and neuronal cells demonstrated a distribution of organelle markers that was consistent with the cells incubated under control culture condition (Figure 4.4 A and B). Pure lysosomes (LAMP2-positive fractions #1 – #5) were separated from mitochondria (VDAC1-positive fractions #6 – #10) in the fibroblasts (Figure 4.6 A). In the SH-SY5Y cells, pure lysosomes were located in fractions #1 – #5 and mitochondria dominated in fractions #6 – #10, with a minor contamination from lysosomes in fractions #6 – #8 (Figure 4.6 B). With chloroquine treatment, the appearance of fibroblast and neuronal cell fractions showed a higher intensity in the LAMP2 band in comparison to the control condition (Figure 4.4 A and B). The organelle fractions from both fibroblasts and neuronal cells were free of detectable MS signal (Figure 4.6 A and B). In the cytosolic fractions, LAMP2 and VDAC1 signals were not seen in any fraction, while a clear MS signal was detected in the cytosolic fractions (#1 – #5) (Figure 4.6 A and B).

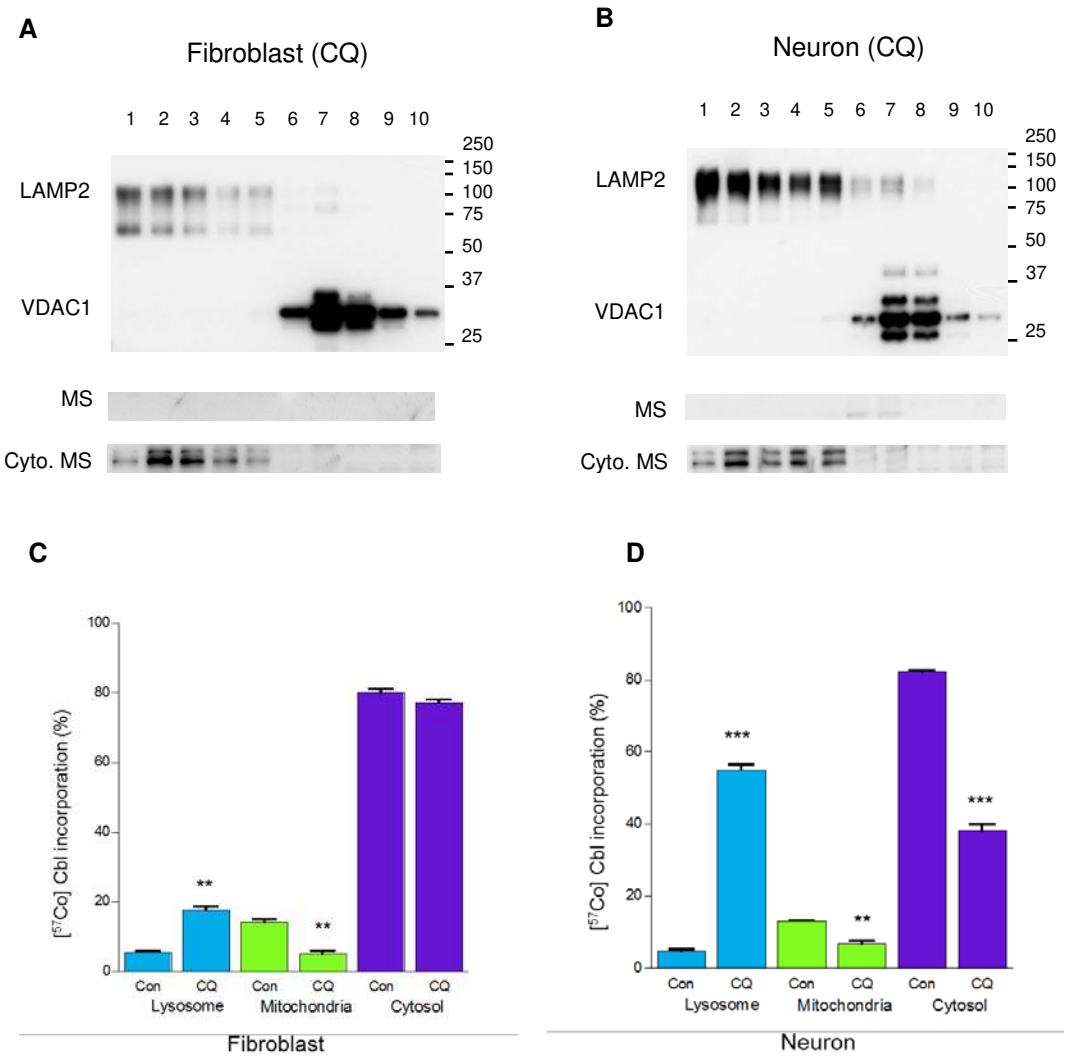

Figure 4.6 Subcellular [^{57}Co] Cbl distribution after chloroquine treatment. The fibroblasts and neuronal cells were incubated separately with 0.025 µCi/ml [^{57}Co] Cbl in DMEM with 10% (v/v) HS in the presence of 25 µM chloroquine for 48 h. The cells were then homogenised and cell fractions were collected, followed by subcellular fractionation. The lysosomal, mitochondrial, and cytosolic fractions were separated and probed for marker proteins LAMP2 (lysosomal), VDAC1 (mitochondrial), and MS (cytosolic) by western blotting in all fractions from fibroblasts (A) and neuronal cells (B). The proportional distribution of [^{57}Co] Cbl was expressed as the percentage of cpm values in each chloroquine-treated organelle fraction compared to the control condition for both cell types (C and D). Data are representative and are expressed as mean ± SE (represented by the error bars) from three independent experiments. ** $P < 0.01$, *** $P < 0.001$. Con, control; CQ, chloroquine.

4.2.3.3 Chloroquine treatment impairs lysosomal [^{57}Co] Cbl transport

The data presented in Figure 4.6 C and D indicated the distribution of [^{57}Co] Cbl in each organelle fraction expressed as a percentage of cpm values between control and chloroquine-treated cells. As a proportion of total cellular [^{57}Co] Cbl, lysosomes in the fibroblasts contained 5.7% of cellular [^{57}Co] Cbl under control culture conditions and this increased 3.1-fold to 17.6% with chloroquine treatment (Figure 4.6 C). This retention of [^{57}Co] Cbl in the lysosomes was concomitant with a significant 63% decrease (from 14.3% to 5.2% of total cellular levels) in mitochondrial [^{57}Co] Cbl and a trend (P = 0.07) for a 4% decrease (from 80.1% to 77.1% of total cellular levels) in cytosolic [^{57}Co] Cbl. However, the lysosomal [^{57}Co] Cbl level in the neuronal cells with chloroquine treatment dramatically increased more than 10-fold from 4.8% to 55.0%. This remarkable increase was inversely associated with a decrease in the mitochondrial and cytosolic [^{57}Co] Cbl levels, at which [^{57}Co] Cbl was significantly reduced to 50% (from 13.1% to 6.8% and from 82.2% to 38.8%, respectively). Therefore, chloroquine treatment on fibroblasts and neuronal cells neutralises lysosomal pH and inhibits lysosomal function, resulting in [^{57}Co] Cbl accumulation in the lysosomes. Lysosomal dysfunction may impair subcellular [^{57}Co] Cbl transit by inhibiting the release of [^{57}Co] Cbl into mitochondria and cytosol.

4.3 Lysosomal protease inhibition impairs lysosomal [^{57}Co] Cbl transport

4.3.1. Introduction

I have shown that chloroquine inhibits lysosomal proteolysis and causes lysosomal [^{57}Co] Cbl accumulation. As chloroquine can also theoretically modulate the transition of lysosomal Cbl to the "base-off" state (as explained above), I further assessed whether a lysosomal hydrolase inhibitor that does not operate through neutralizing lysosomal pH could also lead to a trapping of Cbl in the lysosome. In the current experiment, a broad specificity competitive transition state inhibitor, leupeptin (inhibits cysteine, serine and threonine proteases, but does not alter lysosomal pH), was given to the cells to examine the impact of lysosomal protease inhibition on lysosomal Cbl transport.

4.3.2. Results

4.3.2.1 Isolated cellular fractions probed by western blotting

The fibroblasts and neuronal cells were incubated separately with 0.025 μCi/ml [^{57}Co] Cbl in DMEM containing 10% (v/v) HS in the presence of 40 μM leupeptin (Sigma, USA, Cat #L2884) for 48 h at 37°C. The cells were then homogenised and cell fractions were collected, followed by subcellular fractionation as described previously (Chapter 2, section 2.4). Isolated cellular fractions containing lysosomes,

mitochondria, and cytosol were probed for appropriate organelle markers by western blotting: lysosome: LAMP2; mitochondria: VDAC1; and cytosol: MS.

The western blot results from leupeptin-treated fibroblasts and neuronal cells demonstrated a different distribution of organelle markers from the cells incubated under control culture conditions (Figure 4.4 A and B). In the fibroblasts, pure lysosomes were localised in LAMP2-positive fractions #1 – #6 with intense signals in fractions #1 and #6, while the mitochondria were distributed through VDAC1-positive fractions #7 – #9 (Figure 4.7 A). In neuronal cells, pure lysosomes appeared in fractions #1 – #5, the mitochondria and lysosomes were colocalised in fractions #6 – #8, and pure mitochondria appeared in fractions #9 – #10 (Figure 4.7 B). Among the neuronal lysosomal fractions, fractions #5 and #7 seemed to have the strongest signal. The organelle fractions from both fibroblasts and neuronal cells were free of detectable MS signal (Figure 4.7 A and B). In the cytosolic fractions, LAMP2 and VDAC1 signals were not seen in any fraction, while a clear MS signal (#1 – #5) was detected from both conditions. Interestingly, both chloroquine and leupeptin treatment with neuronal cells were associated with the appearance of LAMP2 through a broader range of density fractions isolated from the OptiPrep gradient (compare Figure 4.4 B to Figure 4.6 B and Figure 4.7 B). This may result from both an expansion of the lysosomal compartment and an increase in the size and density of a subpopulation of lysosomes; both of which would be predicted to occur as intralysosomal substrates accumulate.

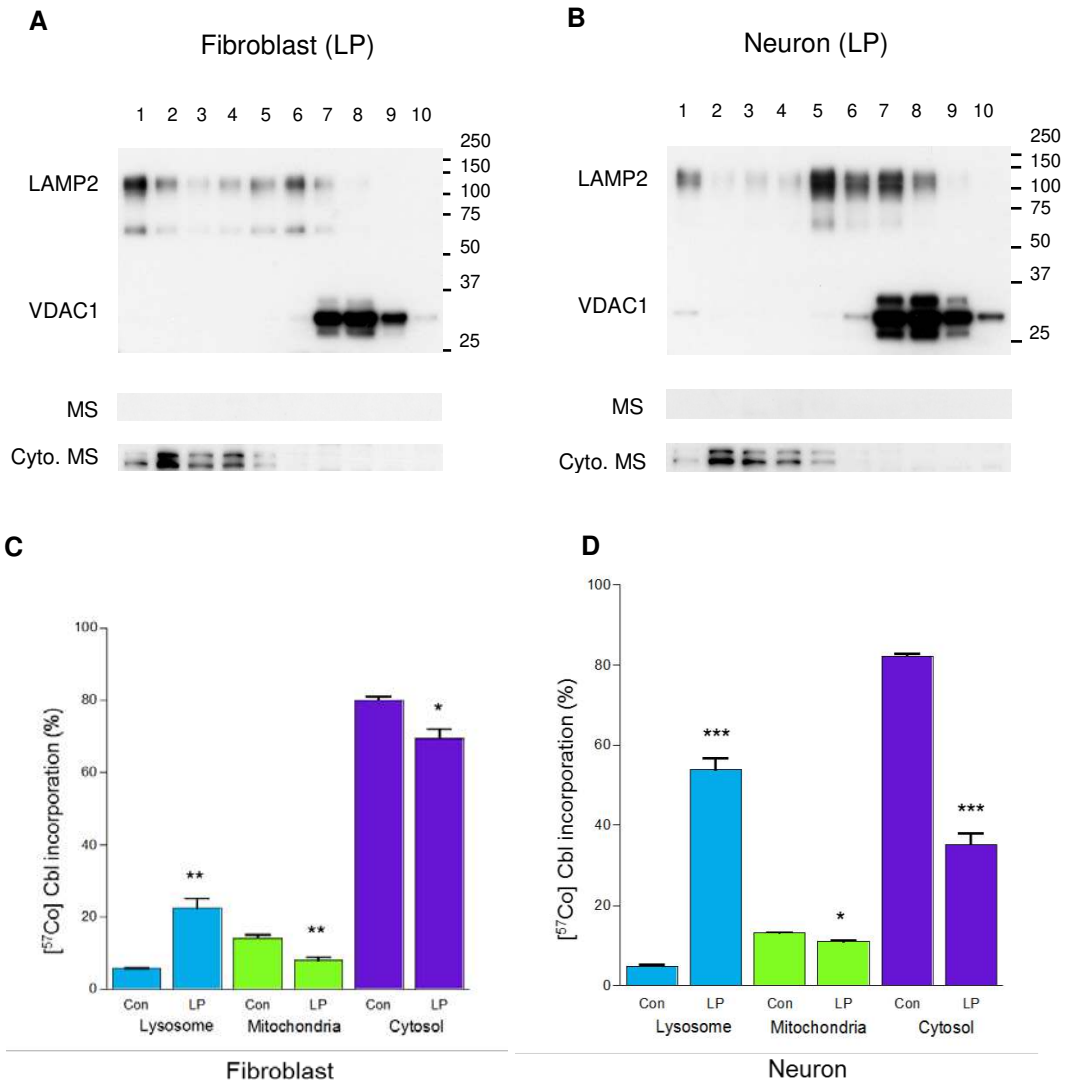

Figure 4.7 Subcellular [^{57}Co] Cbl distribution after leupeptin treatment. The fibroblasts and neuronal cells were incubated separately with 0.025 µCi/ml [^{57}Co] Cbl in DMEM with 10% (v/v) HS in the presence of 40 µM leupeptin for 48 h. The cells were homogenised and cell fractions were collected, followed by subcellular fractionation. The lysosomal, mitochondrial, and cytosolic fractions were separated and probed for marker proteins LAMP2 (lysosomal), VDAC1 (mitochondrial), and MS (cytosolic) by western blotting in all fractions from fibroblasts (A) and neuronal cells (B). The proportional distribution of [^{57}Co] Cbl was expressed as the percentage of cpm values in each luepeptin-treated organelle fraction compared to the control condition for both cell types (C and D). Data are representative and are expressed as mean ± SE (represented by the error bars) from three independent experiments. * $P < 0.05$, ** $P < 0.01$, *** $P < 0.001$. Con, control; LP, leupeptin.

4.3.2.2 Leupeptin treatment impairs lysosomal [^{57}Co] Cbl transport

In conditions where neuronal proteolysis was inhibited by leupeptin, the density of lysosomes in 2 of the 8 LAMP2-positive fractions (i.e. fractions #7 and #8) became so similar to the mitochondria that it was not possible to completely separate them. In this case the cpm values in those two fractions were estimated based on the LAMP2 optical density and compared with the closest "clean" LAMP2 fractions (i.e. fractions #5 and #6). After subtracting the estimated lysosomal radioactivity (cpm) in fractions #7 and #8, the remaining radioactivity (cpm) was assigned as mitochondrial. Using this method, both the leupeptin and chloroquine (in the latter the LAMP2/VDAC1 overlap was not pronounced) treatments gave similar results for lysosomal Cbl levels.

The data presented in Figure 4.7 C and D indicated the distribution of [^{57}Co] Cbl in each organelle fraction expressed as a percentage of cpm values between control and leupeptin-treated cells. Similar to the results using choroquine, the fibroblasts treated with leupeptin showed a significant 3.9-fold increase (from 5.7% to 22.4%) in lysosomal [^{57}Co] Cbl level, which was associated with a significant reduction in both mitochondrial and cytosolic [^{57}Co] Cbl levels (reduced by 44% and 13%, respectively, Figure 4.7 C). Likewise, the neuronal cells treated with leupeptin showed that 53.8% of total [^{57}Co] Cbl was trapped in the lysosomes, an 11-fold increase compared to the control cells, whereas the cellular levels of [^{57}Co] Cbl in the mitochondria and cytosol significantly decreased (from 13.1% to 11.0% and from 82.2% to 35.2%, respectively) ($P < 0.05$ and $P < 0.001$). Therefore, leupeptin treatment of fibroblasts and neuronal cells inhibits lysosomal proteases without

disturbing lysosomal pH, a mechanism different from choloquine treatment, causes lysosomal [^{57}Co] Cbl accumulation. This may impair subcellular [^{57}Co] Cbl transit by preventing the release of [^{57}Co] Cbl into mitochondria and cytosol.

4.3.2.3 Comparison of chloroquine and leupeptin treatment on fibroblasts and neuronal cells

In comparing the experiments conducted with fibroblasts and neuronal cells, there were striking differences in the degree of lysosomal accumulation of [^{57}Co] Cbl and the cytosolic depletion of [^{57}Co] Cbl, with both parameters being much more severe in the neuronal cells (Figure 4.8). In addition, associated with the more pronounced lysosomal [^{57}Co] Cbl accumulation, the change in LAMP2 distribution through the OptiPrep density gradient was also more pronounced in the neuronal cells (compare Figure 4.6 C with D; Figure 4.7 C with D); possibly reflecting a more extensive enlargement of the lysosomal compartment and a greater increase in average lysosome size and density distribution. It was also clear that there were differences in the extent to which mitochondrial [^{57}Co] Cbl levels were modulated by chloroquine and leupeptin treatment in the different cell types and this did not necessarily follow changes in lysosomal [^{57}Co] Cbl retention. For example, the leupeptin treatment of neuronal cells resulted in an approximate 11-fold increase in lysosomal [^{57}Co] Cbl, and an approximate 57% decrease in cytosolic [^{57}Co] Cbl, whereas in the same experimental condition, the mitochondrial [^{57}Co] Cbl levels were reduced by only 16% (Figure 4.7 D).

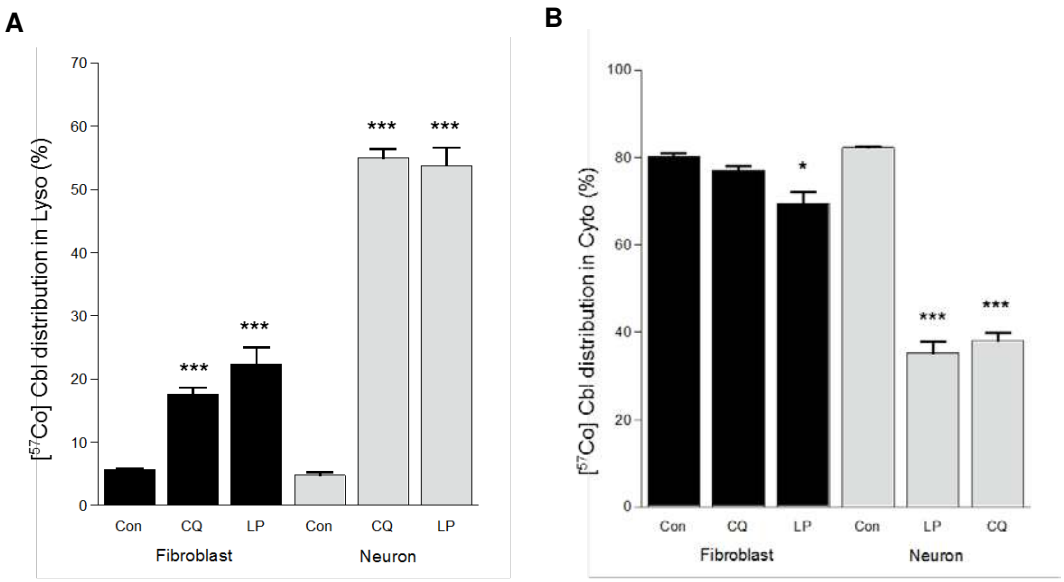

Figure 4.8 Comparison of [^{57}Co] Cbl level in lysosomes (A) and cytosol (B). The lysosomal and cytosolic [^{57}Co] Cbl levels from fibroblasts and neuronal cells were compared under control, chloroquine, and leupeptin treatment conditions. Data are representative and expressed as mean ± SE (represented by the error bars) from three independent experiments. * $P < 0.05$, *** $P < 0.001$. Lyso, lysosome; Cyto, cytosol; Con, control; CQ, chloroquine; LP, leupeptin.

4.4 [^{14}C] propionate incorporation into fibroblasts and neuronal cells

4.4.1. Introduction

Propionate is efficiently taken up into cells and converted to propionyl-CoA by thiokinase and CoA, and then carboxylated by propionyl-CoA carboxylase to yield MM-CoA (Figure 4.9) (Ballhausen *et al.*, 2009). AdoCbl is the coenzyme of MMCM that regulates the conversion of MM-CoA to succinyl-CoA in the mitochondria. As an indirect measurement of MMCM activity, the incorporation of extracellular [^{14}C] propionate into cellular macromolecules such as proteins that are precipitated by trichloro-acetic acid (TCA) *in vitro* is thus an established clinical and basic research tool for evaluating the Cbl-dependent activity of MMCM (Willard *et al.*, 1976; Zhao *et al.*, 2014).

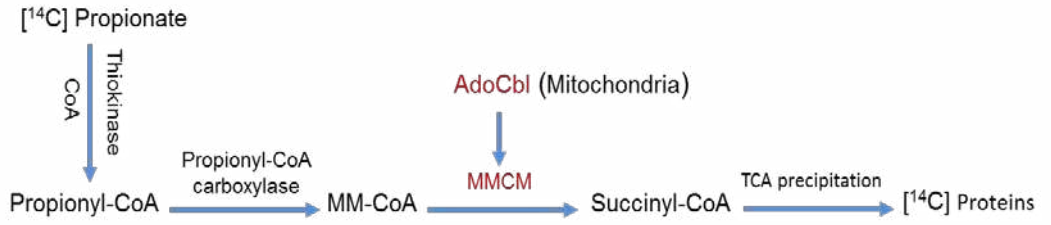

Figure 4.9 [^{14}C] propionate utilisation pathway.

The importance of the role that the lysosome plays in the delivery of Cbl to MS and MMCM has been highlighted by the discovery of two inborn errors of Cbl metabolism referred to as *cblF* and *cblJ* (Rosenblatt *et al.*, 1985; Rutsch *et al.*, 2009; Coelho *et al.*, 2012). These life-threatening conditions are caused by a loss of function in either LMBD1 or ABCD4, lysosomal membrane proteins that normally promote Cbl efflux from the lysosome to the cytosol (Rutsch *et al.*, 2009; Coelho *et al.*, 2012). In *cblF* and *cblJ* subjects, Cbl accumulates in lysosomes and levels of toxic metabolites Hcy and MMA increase (Rutsch *et al.*, 2009; Coelho *et al.*, 2012).

When lysosomal function is inhibited by chloroquine and leupeptin treatment, intracellular Cbl utilisation might be affected because of the reduction in delivering Cbl from lysosomes to mitochondria and cytosol. This inhibits the conversion of MM-CoA to succinyl-CoA, resulting in less succinyl-CoA being converted from propionate. In order to assess whether the variation in mitochondrial [^{57}Co] Cbl levels related to chloroquine or leupeptin treatment was associated with changes in MMCM activity, the incorporation of [^{14}C] propionate into TCA-precipitated proteins / macromolecules was measured.

4.4.2. Methods

The same number of fibroblasts and neuronal cells were seeded into two 6-well cell culture plates with 6 wells as control; 3 wells treated with chloroquine (25 µM); and 3 wells treated with leupeptin (40 µM). The cells were incubated in DMEM with 10% (v/v) FCS for 48 h at 37°C. Next, the cells were washed with PBS and incubated with [^{14}C] propionate (1 µCi/ml, MP Biomedicals, USA, Cat #11221750)

in Puck's saline containing 15% (v/v) FCS and 0.05 M glucose for 8 h at 37°C. The cells were then washed with PBS and incubated with 5% TCA (Sigma, USA, Cat #9159) for 10 min at 4°C. The cells were collected with a cell scraper and centrifuged at 6,000 × g for 5 min at 4°C. Finally the supernatants were removed and the pellets were dissolved with 1 M NaOH. The amount of [^{14}C] propionate in the cell pellets was measured using a Tri-Carb Liquid Scintillation Counter (PerkinElmer, Finland). The cell protein concentrations in each condition were determined using BCA protein assay.

4.4.3. Results

The data presented in Figure 4.10 A indicated the incorporation of [^{14}C] propionate in the cell pellets expressed as a percentage of the control conditions. Chloroquine treatment resulted in a significant inhibition of [^{14}C] propionate incorporation into TCA-precipitated pellets in both fibroblasts and neuronal cells (by 25.5% and 15.7% reduction, respectively). Similarly, leupeptin treatment significantly reduced [^{14}C] propionate incorporation in fibroblasts (by 24.6%), and there was a trend for reduced [^{14}C] propionate incorporation in neuronal cells (5.7%, $P = 0.07$). When the variation in mitochondrial [^{57}Co] Cbl levels associated with chloroquine or leupeptin treatment was compared to the relative [^{14}C] propionate incorporation values, a significant positive correlation ($R^2 = 0.88$, $P = 0.003$) was detected (Figure 4.10 B). These results suggest that the accumulation of lysosomal Cbl causes the decrease of AdoCbl in the mitochondria and may have downstream consequences on cellular physiology. The inhibition of lysosomal function disrupts intracellular Cbl utilisation

and results in reduced level of mitochondrial [^{57}Co] Cbl that is correlated with impaired MMCM activity, leading to the increased production of neurotoxic metabolites.

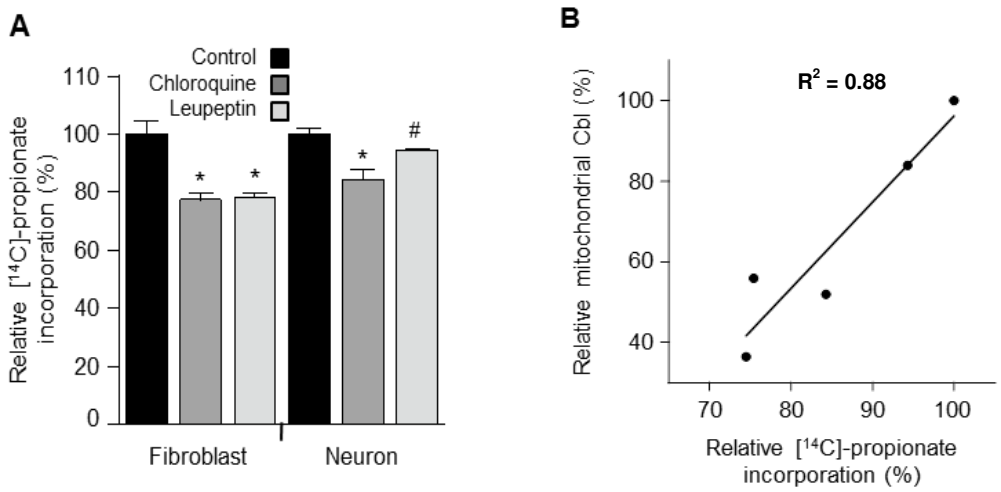

Figure 4.10 Lysosomal protease inhibitors reduce cellular [^{14}C] propionate incorporation. The fibroblasts and neuronal cells were seeded into 6-well plates and metabolically labeled with [^{14}C] propionate under control culture conditions or in the presence of either chloroquine (25 μM) or leupeptin (40 μM) for 48 h. The cells were then subjected to 5% (w/v) TCA, and [^{14}C] propionate in the cell pellets was determined and expressed as a percentage of the control conditions (A). Pearson correlation analysis was conducted to assess the potential associations between changes in relative mitochondrial [^{57}Co] Cbl levels (derived from experiments shown in Figure 4.6 and 4.7) and [^{14}C] propionate incorporation into TCA-precipitated cell pellets (B). * $P < 0.05$, # $P = 0.07$.

4.5 Inhibition of lysosomal hydrolase pathway may interrupt lysosomal [^{57}Co] Cbl transport

4.5.1. Introduction

Lysosomal hydrolases are synthesised at the rough endoplasmic reticulum and travel along the secretory pathway until they reach the TGN, from which hydrolases are taken by mannose-6-phosphate receptors to form vesicles that deliver them to immature lysosomes (Coutinho *et al.*, 2012). Microtubules are primary components of the cytoskeleton and they are composed of a single type of globular protein, tubulin. Microtubules provide platforms for intracellular transport and are involved in a variety of cellular processes, including the movement of secretory vesicles, organelles, and intracellular substances (Copper, 2000). Vinblastine is commonly used for cancer treatment and it is also a microtubule-depolymerising compound that disrupts cytoskeletal-dependent vesicular transport and inhibits subsequent fusion of autophagosomes with endosomal and lysosomal compartments (Marzella *et al.*, 1980; Dhamodharan *et al.*, 1995). Vinblastine treatment induces autophagy and causes extensive AV accumulation, as well as disrupts lysosomal hydrolase transport on microtubules, subsequently delaying the formation of mature lysosomes and inhibiting lysosomal proteolysis (Oliva *et al.*, 1992; Boland *et al.*, 2008). Thus, the role of vinblastine treatment was investigated in this experiment to assess the impact of impaired lysosomal enzymes delivery on lysosomal Cbl intracellular transport.

4.5.2. Results

4.5.2.1 Isolated cellular fractions probing by western blotting

Vinblastine is toxic to cells and differential toxicity was observed when cells were subjected to 4 h exposure (Ferguson *et al.*, 1984). Furthermore, it has been reported that fibroblasts are more susceptible to vinblastine toxicity (Boland *et al.*, 2008). Thus, SH-SY5Y cells were treated with vinblastine and incubation period was reduced to 24 h. As a supplementary experiment to support the above results (lysosomal protease inhibition by chloroquine and leupeptin), one experiment for each concentration of vinblastine treatment was conducted. The SH-SY5Y cells were incubated with 0.025 µCi/ml [^{57}Co] Cbl in DMEM with 10% (v/v) HS in the presence of 1 µM or 10 µM vinblastine (Sigma, USA, Cat #V1377) for 24 h at 37°C. The cells were then homogenised and cell fractions were collected, followed by subcellular fractionation method as described previously (Chapter 2, section 2.4). Isolated cellular fractions containing lysosomes, mitochondria, and cytosol were probed for appropriate organelle markers by western blotting: lysosome: LAMP2; mitochondria: VDAC1; and cytosol: MS.

The western blot results from both vinblastine concentrations demonstrated a similar distribution of organelle markers that was consistent with the cells incubated under control culture conditions (Figure 4.4 A and B). Pure lysosomes (LAMP2-positive fractions #1 – #2) were separated from mitochondria (VDAC1-positive fractions #6 – #8) with 1 µM vinblastine treatment (Figure 4.11 A). When vinblastine concentration was increased to 10-fold, pure lysosomes were located in fractions #1 – #5 and mitochondria dominated in fractions #7 – #9 (Figure 4.11 B). The different pattern of lysosomal location may result from an expansion of the lysosomal

compartment or an increase in the size and density of a subpopulation of lysosomes, possibly indicating that more cellular [^{57}Co] Cbl were entrapped in the lysosomes with the increased concentration of vinblastine. The organelle fractions from both conditions were free from detectable MS. In the cytosolic fractions, LAMP2 and VDAC1 signals were not seen in any fraction, while a clear MS signal (#2 – #5) was detected from both conditions (Figure 4.11 A and B).

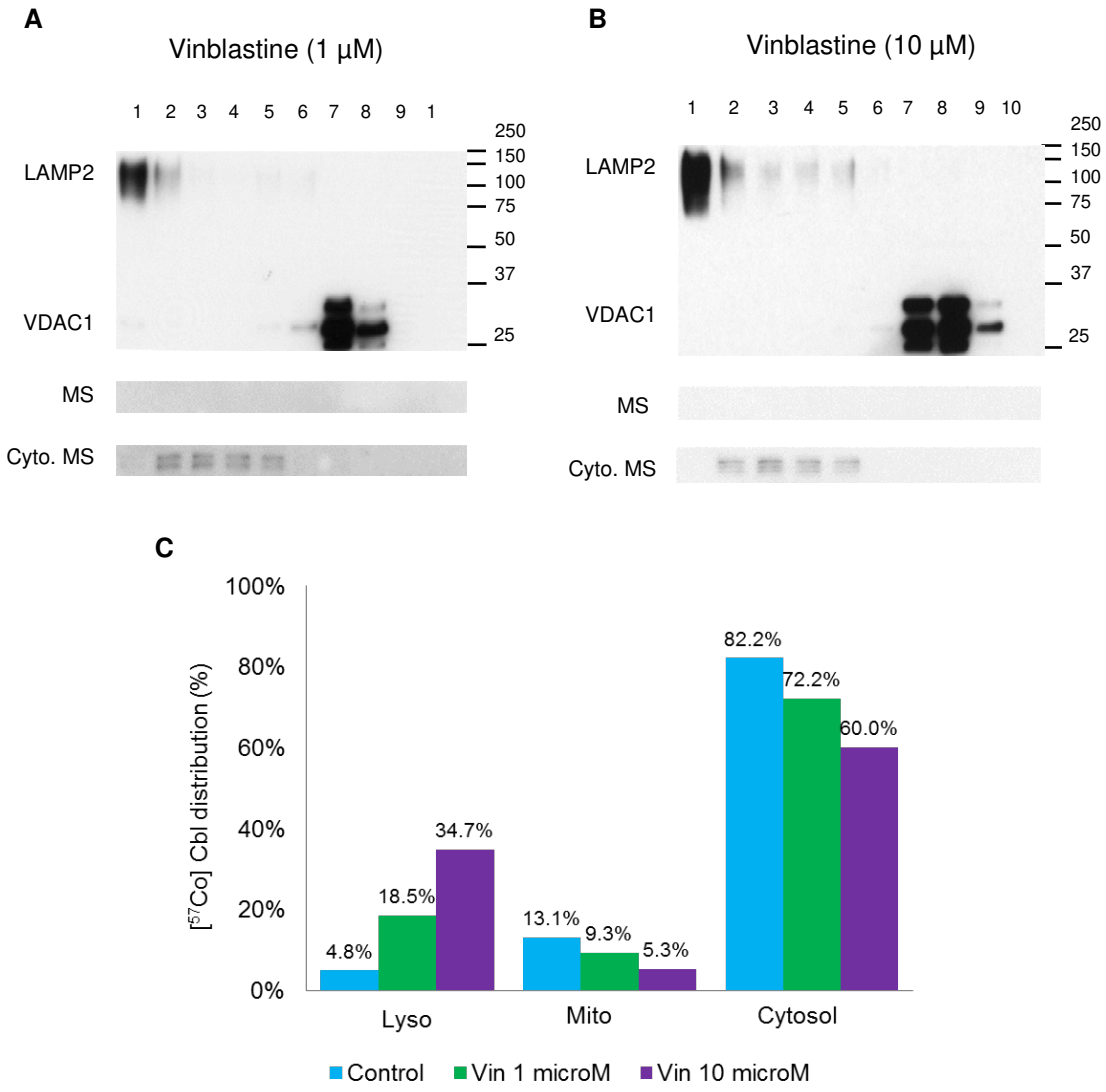

Figure 4.11 Subcellular [^{57}Co] Cbl distribution after vinblastine treatment in SH-SY5Y cells. The SH-SY5Y cells were incubated with 0.025 µCi/ml [^{57}Co] Cbl in DMEM with 10% (v/v) HS in the presence of 1 µM or 10 µM vinblastine for 24 h. The cells were then homogenised and cell fractions were collected, followed by subcellular fractionation. The lysosomal, mitochondrial, and cytosolic fractions were separated and probed for marker proteins LAMP2 (lysosomal), VDAC1 (mitochondrial), and MS (cytosolic) by western blotting in all fractions: 1 µM vinblastine (A) and 10 µM vinblastine (B). The proportional distribution of [^{57}Co] Cbl was expressed as the percentage of cpm values in each organelle fraction in the vinblastine-treated cells and compared to the control cells (C). Data are from a single experiment using two vinblastine concentrations (1 µM and 10 µM). Lyso, lysosome; Mito, mitochondria; Vin, vinblastine.

4.5.2.2 Vinblastine treatment may impair lysosomal [^{57}Co] Cbl transport

The data presented in Figure 4.11 C indicated the distribution of [^{57}Co] Cbl in each organelle fractions expressed as a percentage of cpm values between control and vinblastine-treated cells. As a proportion of total cellular [^{57}Co] Cbl, there was a definite trend for increased lysosomal [^{57}Co] Cbl that was concomitant with an increasing concentration of vinblastine. There was a simultaneous decreased trend for the mitochondrial and cytosolic [^{57}Co] Cbl compared to the control condition. The lysosomes contained 4.8% of the cellular [^{57}Co] Cbl under the control culture condition and this increased to 4-fold or 8-fold (18.5% or 34.7%) with 1 µM or 10 µM vinblastine treatment, respectively. This retention of [^{57}Co] Cbl in the lysosomes was associated with a 29.0% or 59.5% decrease (from 13.1% to 9.3% and 5.3% of total cellular levels) in mitochondrial [^{57}Co] Cbl, and a 12.2% or 27.0% decrease (from 82.2% to 72.2% and 60.0% of total cellular levels) in cytosolic [^{57}Co] Cbl. These results suggest that although only one experiment from each vinblastine concentration is performed, there is an obvious trend underlying the fact, which is that the disruption of lysosomal hydrolase transport on microtubules inhibits lysosomal proteolysis and causes [^{57}Co] Cbl build-up in the lysosomes and may inhibit intracellular [^{57}Co] Cbl transit.

4.6 Discussion

The present results have shown that inhibition of lysosomal proteolysis using both pH-dependent (chloroquine) and -independent (leupeptin and vinblastine) approaches suppress lysosomal function, cause lysosomal [^{57}Co] Cbl accumulation, and interrupt intracellular [^{57}Co] Cbl transit. The results provide the first detailed analysis of the effects that physiologically relevant impairments of lysosomal function have on intracellular Cbl transport. Moreover, lysosomal [^{57}Co] Cbl trapping is correlated with decreased incorporation of [^{14}C] propionate into cellular macromolecules, which is a physiological marker of mitochondrial MMCM activity. The increasing amount of [^{57}Co] Cbl in the lysosomes impairs Cbl-dependent utilisation of [^{14}C] propionate.

The results from western blotting for LAMP2 in OpitPrep gradient fractions suggests that such lysosomal Cbl "trapping" is associated with an enlargement of the lysosomal compartment and an increase in a subpopulation of lysosomes with increased size and/or density distribution. When the [^{57}Co] Cbl cpm values were compared with LAMP2 signal in the pure lysosome fractions, a close correlation was generally observed. However, when lysosomal [^{57}Co] Cbl was increased to a 10-fold with chloroquine or leupeptin treatment in the neuronal cells, the change in LAMP2 signal from western blot did not reach to the same magnitude. For example, a semi-quantitative comparison of the LAMP2 western blot suggested chloroquine treatment increased LAMP2 levels approximately 2-fold, whereas lysosomal [^{57}Co] Cbl level was increased approximately 10-fold. The recent report suggests that lysosomal protease inhibitors (including chloroquine) have a dual effect on autophagy as they

initiate early autophagic processes while suppressing autophagic degradation (Li *et al.*, 2013). This is predicted to result in an expansion of the lysosomal compartment that may be mechanistically related to our current observations. Therefore lysosomal Cbl accumulation that is induced by protease inhibition seems due to a combination of both an enlargement of the lysosomal compartment and an increase in lysosomal Cbl concentration. This along with a failed release of Cbl from the TC-Cbl complex could together contribute to the impaired transit of [^{57}Co] Cbl through the lysosomal compartment. Although lysosomal morphology clearly changes in human AD tissues (Cataldo *et al.*, 1994; Cataldo *et al.*, 1996), future studies utilising electron microscopy techniques might clarify the extent to which lysosomal morphology changes under current experimental conditions.

4.7 Conclusions

Three different experimental approaches by inhibiting lysosomal function are conducted with fibroblasts and neuronal cells to assess the impact on the subcellular [^{57}Co] Cbl transport *in vitro*. These results indicate that inhibition of lysosomal hydrolases suppresses lysosomal function and results in lysosomal [^{57}Co] Cbl accumulation, consequently interrupting intracellular [^{57}Co] Cbl transit. Moreover, preventing lysosomal Cbl from the release reduces the amount of Cbl to enter cytosol and mitochondria, thus, it may have impact on downstream cellular metabolites and cause cytotoxic accumulation. Lysosomal [^{57}Co] Cbl trapping is correlated with decreased incorporation of [^{14}C] propionate into cellular macromolecules. Lysosomal protease inhibition causes reduced mitochondrial [^{57}Co] Cbl that is correlated with impaired MMCM activity. An important role of lysosome

function on Cbl intracellular transport and utilisation is established which may be affected in conditions associated with lysosomal dysfunction, e.g. age-related lipofuscin accumulation, lysosomal storage disorders, and AD.

Chapter 5

Impact of lipofuscin accumulation and Gaucher's disease on subcellular cobalamin distribution

5 Impact of lipofuscin accumulation and Gaucher's disease on subcellular cobalamin distribution

5.1 Artificial lipofuscin induction and effect of its accumulation on lysosomal [^{57}Co] Cbl transport

5.1.1. Introduction

Ageing is accompanied by progressive cellular accumulation of biological "garbage" and misfolded proteins (Terman and Brunk, 2006). Although damaged macromolecules and organelles are continuously degraded by lysosomes through autophagy and replaced by newly synthesized biological structures, it is clear that some material progressively accumulates in post-mitotic cells. One of the characteristics of ageing is the increasing accumulation of lipofuscin-loaded lysosomes in long-lived post-mitotic cells such as cardiac myocytes and neuronal cells. Lipofuscin is an autofluorescent and undegradable intralysosomal pigment that consists primarily of oxidatively modified cross-linked protein residues originating from autophagocytosed cytoplasmic components (Terman and Brunk, 1998; Double *et al.*, 2008).

Previous studies indicated that lipofuscin accumulation impaired lysosomal functions (Brunk and Terman, 2002; Terman *et al.*, 2006). Lipofuscin-loaded lysosomal compartment is rich in iron that partly exists in a redox-active form. This makes lysosomes sensitive to a high Fe-catalysed oxidative stress (Fenton reaction) that compromises lysosomal membrane integrity resulting in the loss of the proton

gradient (Yu *et al.*, 2003). The resulting increase in lysosomal pH significantly reduces protease action and if the lysosomal membrane is sufficiently damaged, cathepsins may be released to the cytosol and trigger apoptosis (Yuan *et al.*, 2002). Oxidative stress decreases the effective degradation of damaged proteins by lysosomal hydrolases and promotes lipofuscin accumulation (Terman *et al.*, 2006; Terman *et al.*, 2010). To examine whether age-related lipofuscin accumulation affect intracellular Cbl transport in the cultured cells, artificial lipofuscin was generated in the current experiment and then fed to fibroblasts and neuronal cells in attempt to induce lipofuscin accumulation in the lysosomal compartment.

5.1.2. Methods

5.1.2.1 Artificial lipofuscin induction

In the current experiment artificial lipofuscin was generated by exposing cell lysates that are enriched in lysosomes and mitochondria to UV light as described in an established method (Nilsson and Yin, 1997). Artificial lipofuscin was then fed to HT1080 fibroblasts and SH-SY5Y neuronal cells that endocytosed the material and transported it to the lysosomes. Briefly, the fibroblasts were grown in twelve 175 cm^2 plastic flasks until the cells were grown to 100% confluent. The cells were then rinsed with cold PBS and harvested with 1% (w/v) trypsin. The cell suspension was transferred to a ball-bearing cell homogeniser and homogenised on ice. Next, the mixed cell lysates were centrifuged at 600 × *g* for 10 min at 4°C to isolate the pellets containing nuclei and membranous debris. The supernatant was centrifuged at 20,000 × *g* for 30 min at 4°C. After centrifugation, the pellets containing

mitochondria and lysosomes were collected. The pellets were suspended with PBS and then loaded into petri dishes (5 ml/100 mm dish) without lids, and placed under UV light in a Laminar Air Flow fume hood for up to 24 h to allow peroxidation to take place. Finally, the resulting dried, lipofuscin-like materials were resuspended in sterile water to sample original volume. Further homogenisation was conducted by sonication to make artificial lipofuscin.

5.1.2.2 Artificial lipofuscin measurement

Next, artificial lipofuscin was fed into fibroblasts and neuronal cells. The extent of lipofuscin "loading" in these cells was measured using flow cytometry technique. Briefly, the fibroblasts and neuronal cells were incubated with prepared artificial lipofuscin at different concentrations for 48 h at 37°C to determine the optimal condition for cellular uptake. After 48 h, a small portion of cells was washed with PBS, trypsinised, and analysed using a BD LSR-II flow cytometer (BD Biosciences, USA). A population of highly fluorescent cells was detected at emission 575 nm when excited at 488 nm using autofluorescence parameters. In addition, the cells that were fed artificial lipofuscin were subcultivated onto 22 mm cover slips in a 12-well cell culture plate. Once the cells settled and spread on the cover slips, they were fixed in 4% (w/v) formaldehyde in PBS for 30 min. The cover slips were then inverted onto micro-culture slides before they were assessed with a Nikon TE2000 fluorescence microscope, equipped with a SPOT digital camera (Diagnostic Instruments, USA), and Image-Pro Plus 6.1 software (Media Cybernetics, USA).

5.1.2.3 [^{57}Co] Cbl labelling and western blotting

After artificial lipofuscin loading concentration was determined, the accumulation of artificial lipofuscin in the cells was induced and its effect on intracellular Cbl transport was assessed. The fibroblasts and neuronal cells were treated with artificial lipofuscin (200 µg/ml) for 48 h at 37°C, and then incubated with 0.025 µCi/ml [^{57}Co] Cbl in DMEM with 10% (v/v) HS for 48 h at 37°C. The cells were then homogenised and cell fractions were collected, followed by subcellular fractionation as described previously (Chapter 2, section 2.4). Isolated cellular fractions containing lysosomes, mitochondria, and cytosol were probed for appropriate organelle markers by western blotting: lysosome: LAMP2; mitochondria: VDAC1; and cytosol: MS. Only one experiment from each condition was performed with subcellular fractionation and assessed by western blotting.

5.1.3. Results

5.1.3.1 Artificial lipofuscin cellular uptake was inefficient

The fibroblasts and neuronal cells were fed with artificial lipofuscin (50 µg/ml and 200 µg/ml) and those highly fluorescent cells were detected by fluorescence-activated cell sorting (FACS) using a flow cytometer. The cells were also examined on glass slides using a fluorescence microscope to assess the efficiency of lipofuscin cellular uptake. The results from FACS indicated a group of highly fluorescent cells after lipofuscin treatment were separated with non-fluorescent cells (Figure 5.1 A). Approximately 8% and 40% of both fibroblasts and neuronal cells contained

fluorescent lipofuscin compared to control cells when loading concentrations were at 50 µg/ml and 200 µg/ml, respectively. However, after subcultivating lipofuscin-loaded neuronal cells onto cover slips, only a small percentage (< 5%) of neuronal cells filled with fluorescent inclusions were observed with 200 µg/ml lipofuscin loading concentration (Figure 5.1 C) compared to control neuronal cells (Figure 5.1 B), indicating that the artificial lipofuscin cellular uptake was not satisfactory. Further increasing lipofuscin loading concentration to 400 µg/ml may promote lipofuscin cellular uptake, but large amount of exogenous artificial lipofuscin results in inhibition of the proteasome and eventually induce neuronal apoptosis (Powell *et al.*, 2005). Thus, 200 µg/ml lipofuscin loading concentration was selected in the current experiment to assess its impact on intracellular Cbl transport in fibroblasts and neuronal cells.

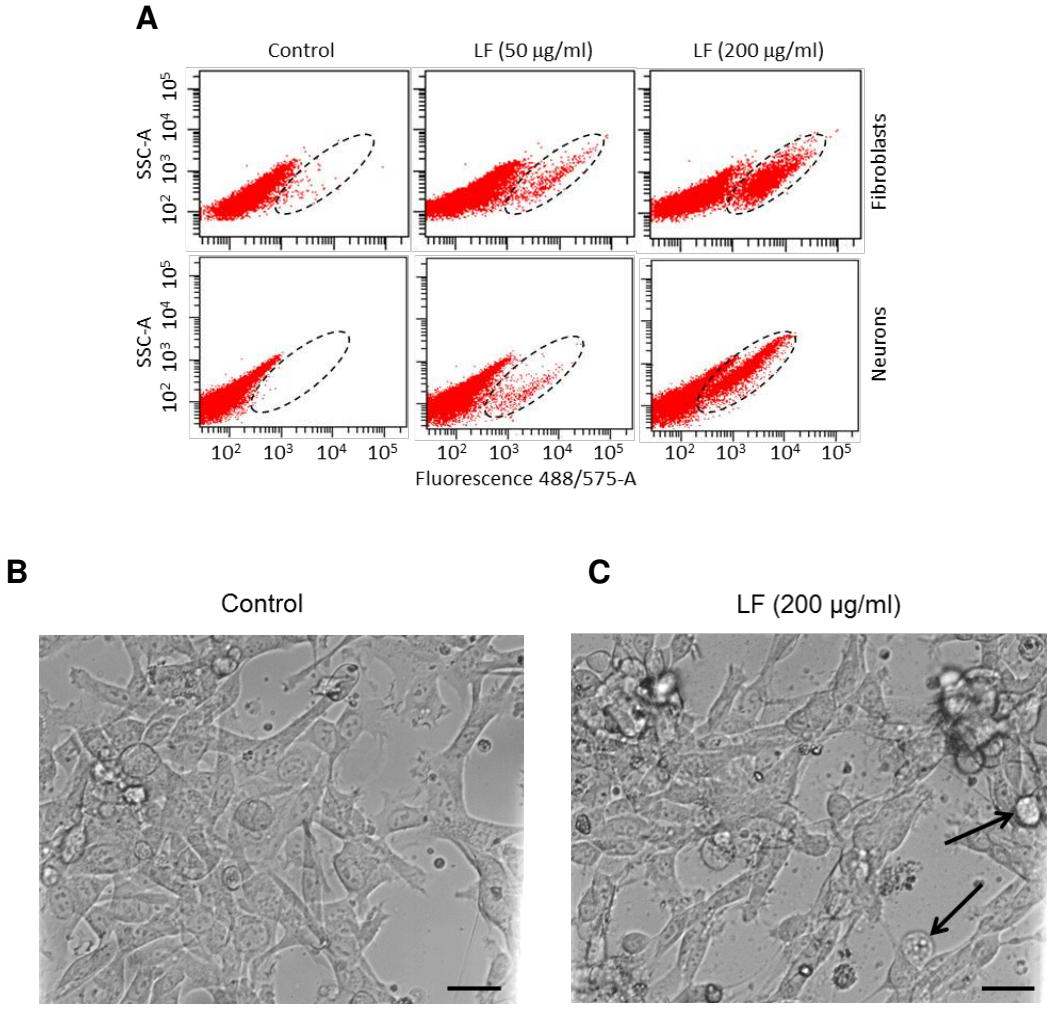

Figure 5.1 Artificial lipofuscin cellular uptake. The fibroblasts and neuronal cells were incubated with artificial lipofuscin at 50 µg/ml and 200 µg/ml for 48 h. A population of highly fluorescent cells (detected by the FACS using autofluorescence parameters Ex 488/Em 575) is circled. This population has increased granularity as shown by side scatter (SSC), consistent with lysosomal lipofuscin accumulation (A). The neuronal cells were fed with artificial lipofuscin and subcultivated onto 22 mm cover slips. The cover slips were inverted onto micro-culture slides and assessed using a fluorescence microscope. A representative image from control (B) and lipofuscin (200 µg/ml) treated (C) neuronal cells is shown. A couple of lipofuscin-treated neuronal cells containing fluorescent inclusions are shown (arrows). LF, lipofuscin. Scale bar = 200 µm.

5.1.3.2 Isolated cellular fractions probing by western blotting

The western blot results from lipofuscin-treated fibroblasts and neuronal cells demonstrated a similar distribution of organelle markers compared to the cells incubated under control conditions (Figure 4.4 A and B). Pure lysosomes (LAMP2-positive fractions #1 – #6) were separated from mitochondria (VDAC1-positive fractions #7 – #10) in fibroblasts (Figure 5.2 A), whereas in neuronal cells pure lysosomes were located in fractions #1 – #5 and mitochondria dominated in fractions #7 – #10 with minor contamination from lysosomes in fractions #7 (Figure 5.2 B). Interestingly, the appearance of fraction #5 in neuronal cells showed highest intensity of LAMP2 band among all fractions, this change may derive from an expansion of the lysosomal compartment or an increase in the size and density of a subpopulation of lysosomes. The organelle fractions from both fibroblasts and neuronal cells were free of detectable MS whereas a clear MS signal was detected in the cytosolic fractions (#2 – #5) (Figure 5.2 A and B).

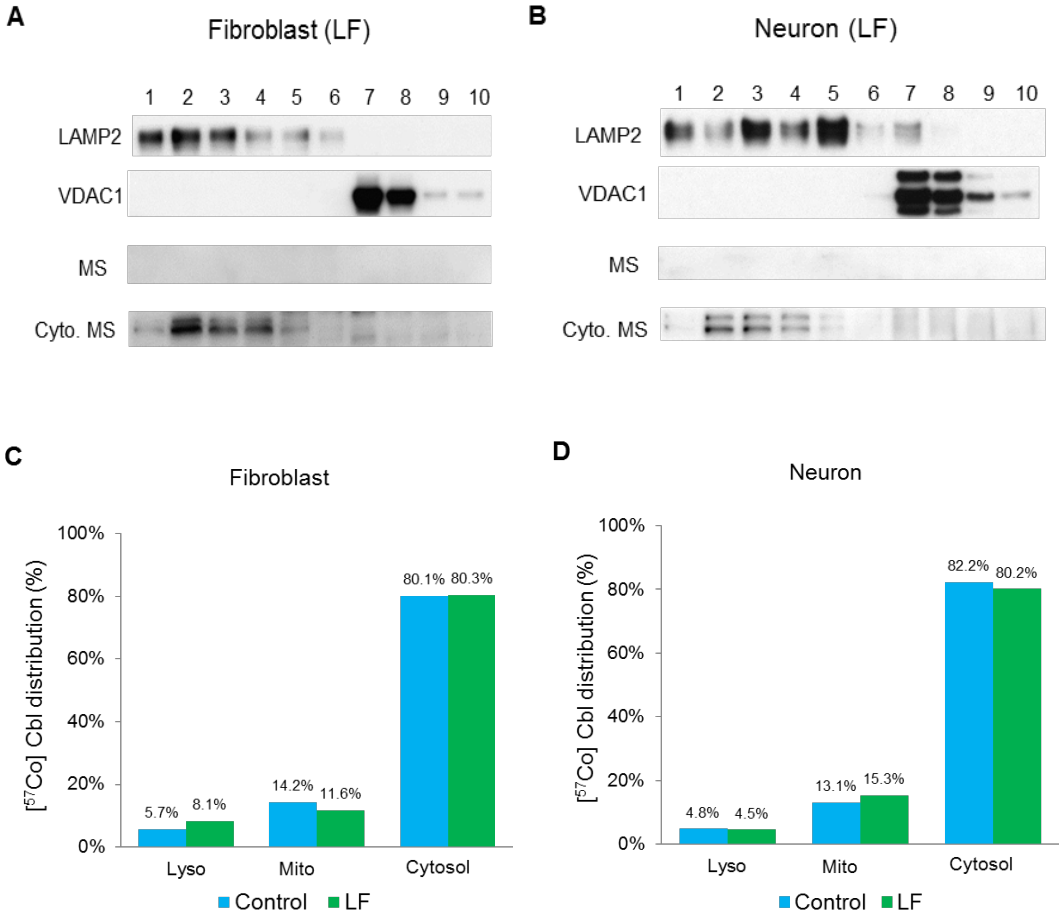

Figure 5.2 Subcellular [^{57}Co] Cbl distribution after artificial lipofuscin treatment. The fibroblasts and neuronal cells were treated separately with artificial lipofuscin (200 µg/ml) for 48 h, followed by incubation with 0.025 µCi/ml [^{57}Co] Cbl in DMEM with 10% (v/v) HS for 48 h. The lysosomal, mitochondrial, and cytosolic fractions in the fibroblast (A) and neuronal cell (B) were separated and probed for marker proteins LAMP2 (lysosomal), VDAC1 (mitochondrial), and MS (cytosolic) by western blotting. The proportional distribution of [^{57}Co] Cbl was expressed as the percentage of cpm values in the fibroblast (C) and neuronal cell (D) and compared to the control cells. Data are expressed as a single experiment. LF, lipofuscin; Lyso, lysosome; Mito, mitochondria.

5.1.3.3 Subcellular [^{57}Co] Cbl distribution in artificial lipofuscin-loaded cells

The results indicated the distribution of [^{57}Co] Cbl in each artificial lipofuscin-loaded organelle fraction expressed as a percentage of cpm values in each experiment. As a proportion of total cellular [^{57}Co] Cbl, lysosomes in the fibroblasts contained 5.7% of [^{57}Co] Cbl under control culture conditions and this was slightly increased to 8.1% with artificial lipofuscin treatment (Figure 5.2 C). The mitochondrial [^{57}Co] Cbl level was concomitantly reduced from 14.2% to 11.6% of total cellular [^{57}Co] Cbl levels. There was no obvious change observed in the cytosolic [^{57}Co] Cbl level. On the other hand, the lysosomal [^{57}Co] Cbl level in neuronal cells with artificial lipofuscin treatment was slightly decreased from 4.8% to 4.5%. The mitochondrial [^{57}Co] Cbl level had increased from 13.1% to 15.3% and this was associated with a slight reduction of cytosolic [^{57}Co] Cbl level (from 82.2% to 80.2%). The results suggest that there is only a trend that lysosomal [^{57}Co] Cbl level in fibroblasts may increase with artificial lipofuscin treatment. Given that only small changes were found in the subcellular [^{57}Co] Cbl distribution in these cells in comparison to chloroquine and leupeptin treatment, this experimental approach was not pursued further.

5.1.4. Discussion

For the first time, I assessed the subcellular Cbl distribution in the cells that are induced with age-related lysosomal artificial lipofuscin. From the literature review in Chapter 1.8, it was expected that lysosomal [^{57}Co] Cbl level would be significantly increased due to impaired lysosomal function that was caused by accumulation of

artificial lipofuscin in the lysosomal compartment (Brunk and Terman, 2002). However, the results showed that lysosomal [^{57}Co] Cbl level was not dramatically changed in fibroblasts and neuronal cells. The slight increase in the lysosomal [^{57}Co] Cbl level in fibroblasts is opposite to the change in neuronal cells, which have an unexpectedly slight decrease in the amount of lysosomal [^{57}Co] Cbl. The induced artificial lipofuscin in fibroblasts and neuronal cells has not obviously affected lysosomal [^{57}Co] Cbl transport.

It is noteworthy that the current method was not efficient for the induction of artificial lipofuscin in this experiment. The procedure requires twelve 175 cm^2 plastic flasks with 100% confluent cells so they can generate the minimum amount of artificial lipofuscin when the mixed lysosomal and mitochondrial pellets were exposed to UV light for peroxidation. Furthermore, the incorporation rate of artificial lipofuscin into the cells was also not satisfactory. Only less than 5% of SH-SY5Y cells were filled with fluorescent inclusions when lipofuscin loading concentration was increased to 200 µg/ml. This may arise from the fact that HT1080 fibrosarcoma cells and SH-SY5Y neuroblastoma cells are cancer cells, which are in a constant proliferating and dividing state. The speed of division and overturning rate in these cells is much faster than post-mitotic cells. The amount of induced artificial lipofuscin in these proliferative cells may not be enough to accumulate in the lysosomes and impair lysosomal function. This may explain the lack of obvious change in lysosomal [^{57}Co] Cbl level in fibroblasts and neuronal cells with lipofuscin treatment. Further increasing lipofuscin loading concentration is expected to not only promote lipofuscin cellular uptake, but also become toxic to cells and trigger cellular apoptosis or necrosis. The current experimental method was, therefore, time-

consuming and inefficient. Developing a novel technique that can more easily produce and deliver artificial lipofuscin into the cells is vital to investigate the effect of age-related lipofuscin on the Cbl intracellular transport in the near future.

5.2 Lysosomal [^{57}Co] Cbl transport is impaired in Gaucher's disease

5.2.1. Introduction

GD is the most common lysosomal glycosphingolipid storage disease. GD is a genetic disease caused by mutations in the GBA gene that result in an inherited deficiency in the lysosomal enzyme GCase (Sillence, 2007). This in turn causes the accumulation of lysosomal GlcCer mostly in the macrophage-derived cells and neurons (Martin *et al.*, 1989; Jmoudiak and Futerman, 2005; Molano *et al.*, 2012; Vitner and Futerman, 2013). It has been reported that GlcCer was located in the endolysosomal membrane and modulated endolysosomal pH in lymphocytes (Sillence, 2013). Thus, lysosomal function may be perturbed by the lysosomal pH change in GD due to the accumulation of GlcCer, and that may impact on lysosomal Cbl transport. I have shown that inhibition of lysosomal proteolysis in fibroblasts and neuronal cells using both pH-dependent and -independent approaches suppresses lysosomal function and causes lysosomal [^{57}Co] Cbl accumulation, leading to impaired lysosomal Cbl intracellular transport. Cbl intracellular transport is critically dependent on its efficient transit through the intracellular lysosomal compartment. As lysosomal function is affected by the accumulation of GlcCer, it is possible that lysosomal Cbl transport may also be interrupted by dysfunctional lysosomes in GD.

In addition, CBE is a competitive, irreversible inhibitor of GCase that is commonly applied to induce acute GlcCer accumulation and pathologically mimic GD phenotype (Newburg *et al.*, 1988). Previous studies found that treating cells with CBE specifically elevated GlcCer levels and caused GlcCer accumulation, while other lysosomal hydrolase levels were unaffected (Daniels *et al.*, 1980; Das *et al.*, 1987; Yatziv *et al.*, 1988; Schwarz *et al.*, 1995). CBE-treatment of macrophages induced many morphological features of GD cells, including whole cell enlargement, oriented fibrils and vacuolated cytoplasm, eccentric nucleus and enlarged vacuoles with membranous structures (Newburg *et al.*, 1988). This *in vitro* system displayed many essential biological parameters relevant for studying the cellular events responsible for the neurological damage that occurs in some types of GD. Thus, CBE treatment has proved to be an invaluable tool in providing a chemically induced GD phenotype. In the current experiment, I used CBE-treated SH-SY5Y cells and human GD fibroblasts separately to induce GlcCer accumulation and investigate whether intracellular Cbl transport was affected in these conditions.

5.2.2. Methods

5.2.2.1 Induction of GlcCer accumulation

To examine whether GlcCer was induced and accumulated in the CBE-treated neuronal cells, total cellular lipid extraction was performed and GlcCer level was measured. The neuronal cells were seeded into 6-well cell culture plates and incubated with CBE (500 μM, Calbiochem, USA, Cat #234599) in DMEM supplemented with 10% (v/v) FCS for 1 week at 37°C. The cells were then rinsed

with PBS. The cells were treated with 50 µl mass spectrometry standards and 450 µl methanol for 15 min before transferring into Eppendorf tubes. The cells were then added to 1,500 µl methyl tert-butyl ether and sonicated in a water bath for 15 min. Next, the tubes were centrifuged at 16,000 × g for 5 min. The supernatant was removed and placed into clean Eppendorf tubes. Finally, the supernatant was dried completely with nitrogen gas. The GlcCer was extracted and quantified using liquid chromatography-mass spectrometry (LC-MS, Thermo Scientific, USA) analysis provided by Dr Anthony Don at the University of New South Wales (Hejazi *et al.*, 2011). In addition, total cellular lipids were also extracted and measured for the concentration of GlcCer in the human healthy foreskin fibroblasts and human GD fibroblasts.

5.2.2.2 [^{57}Co] Cbl labelling and western blotting

After GlcCer accumulation was observed in neuronal cells with CBE treatment and in GD cells, the neuronal cells were incubated with CBE (500 µM) for 1 week at 37°C, followed by incubation with 0.025 µCi/ml [^{57}Co] Cbl in DMEM with 10% (v/v) HS for 48 h at 37°C. The control and GD cells were grown separately until they reached approximately 80% confluence, they were then incubated with 0.025 µCi/ml [^{57}Co] Cbl in DMEM with 10% (v/v) HS and 1% (v/v) non-essential amino acid for 48 h at 37°C. All of the cells were then homogenised and cell fractions were collected, followed by subcellular fractionation as described previously (Chapter 2, section 2.4). Isolated cellular fractions containing lysosomes, mitochondria, and cytosol were probed for appropriate organelle markers by western blotting: lysosome: LAMP2; mitochondria: VDAC1; and cytosol: MS.

5.2.3. Results

5.2.3.1 GlcCer is induced in the CBE-treated neuronal cells but has no effect on lysosomal [^{57}Co] Cbl level

The GlcCer level was measured and analysed by LC-MS to examine whether GlcCer was induced and accumulated in the CBE-treated neuronal cells. The results demonstrated that total GlcCer level in the CBE-treated cells was dramatically increased more than 11-fold (from 35 pg/mol to 460 pg/mol) compared to the control cells. This indicates that GlcCer was induced by CBE treatment and lysosomal GlcCer accumulation may occur in the CBE-treated neuronal cells (Figure 5.3 A).

The western blot results from CBE-treated neuronal cells demonstrated a similar distribution of organelle markers compared to the cells incubated under control conditions (Figure 4.4 A and B). Pure lysosomes (LAMP2-positive fractions #1 – #5) were separated from mitochondria (VDAC1-positive fractions #6 – #9) in the CBE-treated neuronal cells (Figure 5.3 B). The organelle fractions were free of detectable MS whereas a clear MS signal was detected in the cytosolic fractions (#1 – #4).

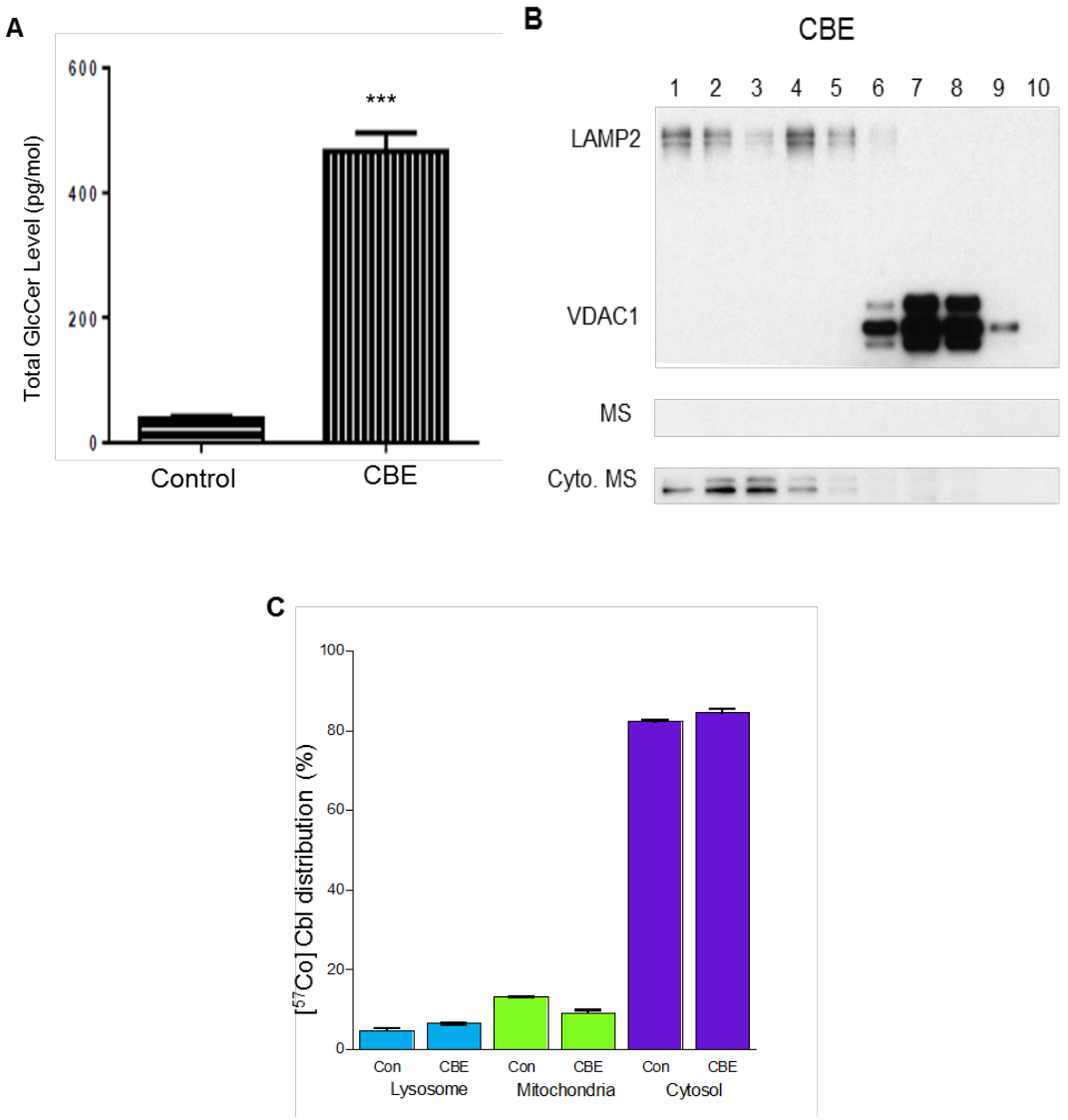

Figure 5.3 Subcellular [^{57}Co] Cbl distribution after CBE treatment. The GlcCer level was measured by LC-MS in the control and CBE-treated neuronal cells (A). The control and CBE-treated neuronal cells were incubated separately with 0.025 μCi/ml [^{57}Co] Cbl in DMEM with 10% (v/v) HS for 48 h. The lysosomal, mitochondrial, and cytosolic fractions were separated and probed for marker proteins LAMP2 (lysosomal), VDAC1 (mitochondrial), and MS (cytosolic) by western blotting (B). The proportional distribution of [^{57}Co] Cbl was expressed as the percentage of cpm values in each CBE-treated organelle fraction compared to the control cells (C). No significant change was observed in any fractions comparing the control and CBE-treated neuronal cells. Data are representative and expressed as mean ± SE (represented by the error bars) from three independent experiments. Con, control.

The data presented in Figure 5.3 C indicated the distribution of [^{57}Co] Cbl in each organelle fraction expressed as a percentage of cpm values between control and CBE-treated neuronal cells. The lysosomal [^{57}Co] Cbl level was slightly increased (from 4.8 ± 0.5% to 6.5 ± 0.2% of total cellular levels) in the CBE-treated neuronal cells compared to the control cells (mean ± SE, n = 3). This was associated with a slight decrease (from 13.1 ± 0.1% to 9.1 ± 0.8% of total cellular levels) in the cytosolic [^{57}Co] Cbl level. However, there was no significant change observed in lysosomal, mitochondrial, and cytosolic fractions between control and CBE-treated neuronal cells. The results suggest that GlcCer induced by CBE treatment in the neuronal cells does not affect intracellular [^{57}Co] Cbl transport, even though GlcCer may still accumulate in those cells.

5.2.3.2 GlcCer is accumulated in GD cells and increases lysosomal [^{57}Co] Cbl level

Next, I assessed whether intracellular [^{57}Co] Cbl transport is impaired in GD cells. It is predicted that lysosomal GlcCer is accumulated in these cells due to inherited deficiency in the lysosomal enzyme GCase. To test this hypothesis, the GlcCer level was measured and analysed by LC-MS in the control and GD cells. The results demonstrated that total GlcCer level in GD cells was significantly increased (from 1.0 x 10^7 pg/mol to 1.6 x 10^7 pg/mol) and was 56% higher than the control cells (Figure 5.4 A). Although the degree of the increase in the GlcCer level in GD cells (increased by 56%) is not as large as CBE-treated neuronal cells (increased by 11-fold), the amount of GlcCer in GD cells (1.6 x 10^7 pg/mol) is much larger than CBE-treated neuronal cells (460 pg/mol). The results show that lysosomal GlcCer is

increased and may accumulate in GD cells, which is consistent with previous studies (Jmoudiak and Futerman, 2005; Vitner and Futerman, 2013).

The western blot results from the GD cell fractions showed a distribution of organelle markers that was consistent with the control cell fractions (Figure 4.4 A and B). Pure lysosomes (LAMP2-positive fractions #1 – #5) were separated from mitochondria (VDAC1-positive fractions #6 – #8) in the control (Figure 5.4 B) and GD (Figure 5.4 C) cells. The appearance of GD cell fractions indicated higher intensity of LAMP2 and VDAC1 bands compared to the control cells. The organelle fractions were free from detectable MS. In the cytosolic fractions, LAMP2 and VDAC1 signals were not seen in any fraction, while a clear MS signal was detected in the fractions #2 – #5 (Figure 5.4 B and C).

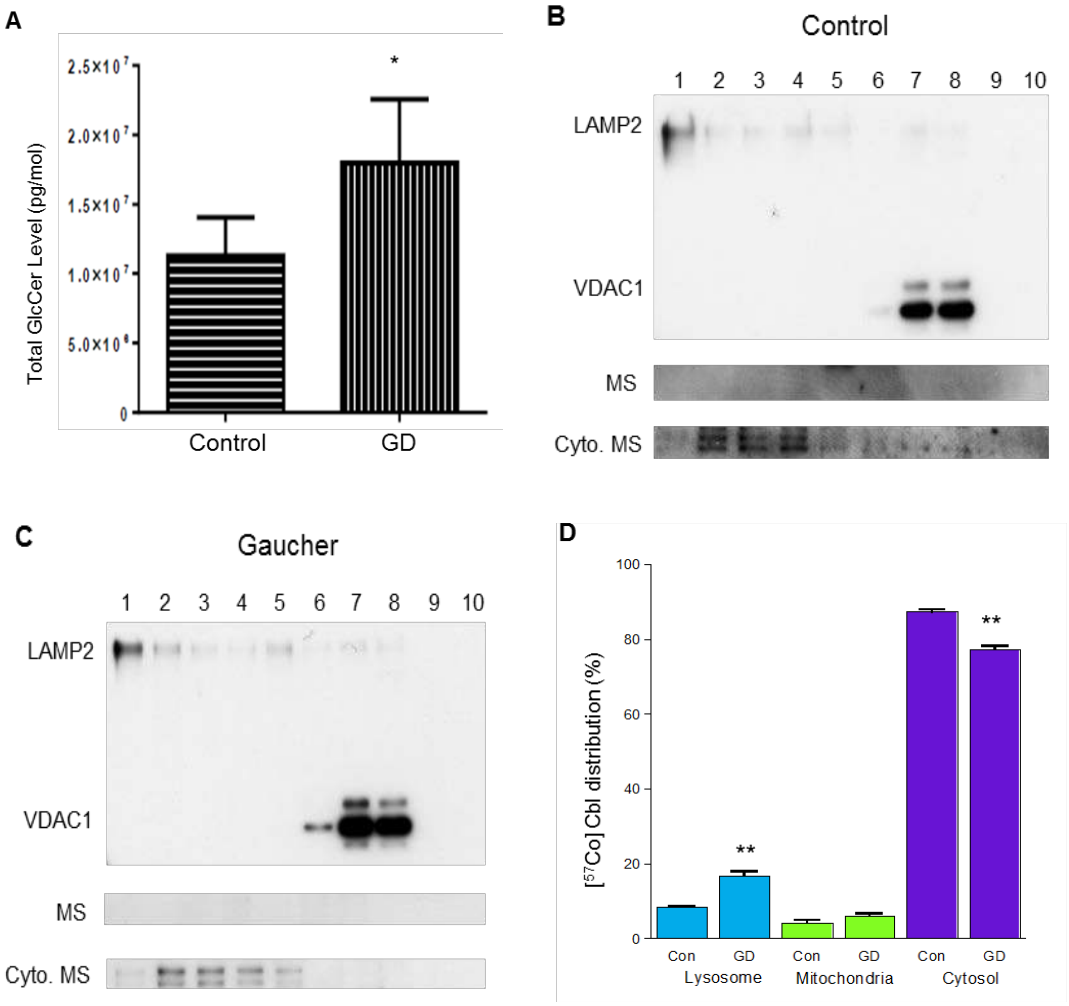

Figure 5.4 Subcellular [^{57}Co] Cbl distribution in GD cells. The GlcCer was measured by LC-MS in the control and GD cells (A). The control and GD cells were incubated separately with 0.025 µCi/ml [^{57}Co] Cbl in DMEM with 10% (v/v) HS for 48 h. The lysosomal, mitochondrial, and cytosolic fractions in the control (B) and GD (C) cells were separated and probed for marker proteins LAMP2 (lysosomal), VDAC1 (mitochondrial), and MS (cytosolic) by western blotting. The proportional distribution of [^{57}Co] Cbl was expressed as the percentage of cpm values in each GD cell organelle fraction compared to the control cells (D). The lysosomal [^{57}Co] Cbl level was significantly increased in GD cells. Data are representative and expressed as mean ± SE (represented by the error bars) from three independent experiments. *P < 0.05, ** P < 0.01. Con, control; GD, Gaucher disease.

The data presented in Figure 5.4 D indicated the distribution of [^{57}Co] Cbl in each organelle fraction expressed as a percentage of cpm values between control and GD cells. According to the distribution of lysosomes and mitochondria from the western blot, isolated lysosomes contained 8.4 ± 0.4% of total cellular [^{57}Co] Cbl in the control cells and the amount of [^{57}Co] Cbl was doubled to 17.6 ± 2.2 % in GD cells (mean ± SE, n = 3). This retention of [^{57}Co] Cbl in the lysosomes was associated with a significant 10% decrease (from 87.3 ± 1.1% to 77.3 ± 1.6% of total cellular levels) in the cytosolic [^{57}Co] Cbl level. There was no significant change in the mitochondrial [^{57}Co] Cbl level in GD cells compared to control cells. The results suggest that GlcCer accumulation in GD cells may cause lysosomal dysfunction that increases lysosomal [^{57}Co] Cbl level and impairs lysosomal Cbl transport.

5.2.4. Discussion

The GD cell model was selected for the current experiment because it is a known lysosomal glycosphingolipid storage disease, which has inherited deficiency in the lysosomal enzyme GCase, causing the accumulation of lysosomal GlcCer. This disease inhibits lysosomal function and GlcCer accumulation may increase lysosomal pH (Sillence, 2013). Consistent with previous results using lysosomal hydrolase inhibition in Chapter 4, the lysosomal [^{57}Co] Cbl level was doubled in the GD cells derived from a patient compared to the human healthy foreskin fibroblasts. This increase is possibly due to GlcCer accumulation in GD cells as total GlcCer level has a significant increase. The subcellular [^{57}Co] Cbl distribution is affected and lysosomal [^{57}Co] Cbl transport is impaired in GD cells. It is noteworthy that the lysosomal [^{57}Co] Cbl level in the healthy foreskin fibroblasts (8.4 ± 0.4%, all means

± SE, n = 3) is higher than SH-SY5Y neuronal cellal cells (4.8 ± 0.5%, all means ± SE, n = 3). As total GlcCer level in the healthy fibroblasts (1.0 x 10^7 pg/mol) is much greater than in the neuroblastoma cells (35 pg/mol), it is speculated that GlcCer may at least partly contribute to the increase of lysosomal [^{57}Co] Cbl level.

Surprisingly, although CBE treatment caused an acute remarkable increase in the GlcCer level in the SH-SY5Y cells as expected, the lysosomal [^{57}Co] Cbl levels in the CBE-treated cells remain statistically unchanged. This result may arise from two possible reasons. Firstly, the absolute value of total GlcCer level in the SH-SY5Y cells (460 pg/mol) is much less than in GD cells (1.0 x 10^7 pg/mol), which means that GlcCer is induced by CBE treatment compared to the control cells, but the GlcCer may not accumulate in the SH-SY5Y cells or the amount of GlcCer is not large enough to affect lysosomal function. Secondly, different from foreskin fibroblasts and GD fibroblasts, SH-SY5Y neuroblastoma cells are cancer cells that are in a constant proliferating and dividing state. The cell division and overturning rate is much faster than those post-mitotic cells. Different from GD cells that have a genetic defect in the lysosomal enzyme Gcase, CBE induces acute GlcCer accumulation by inhibiting Gcase. Once GlcCer is induced by CBE treatment in the SH-SY5Y cells, it is rapidly divided and distributed into newly synthesized daughter cells. Thus, during cell division, the divided relative small amount of GlcCer may not have enough time to accumulate in these proliferating active cells. Nonetheless, although other possible explanations can not be ruled out, CBE has an acute effect on inducing GlcCer, but GlcCer seems not to sufficiently accumulate in the SH-SY5Y cells and subsequently may not interrupt lysosomal [^{57}Co] Cbl transport.

5.3 Conclusions

As an inherited lysosomal glycosphingolipid storage disease, GD inhibits lysosomal function and causes the accumulation of lysosomal GlcCer. Lysosomal [^{57}Co] Cbl transport is impaired in GD cells and this effect is correlated with the increase of lysosomal GlcCer. However, exogenous intervention induced by the generation of either artificial lipofuscin or CBE-derived lysosomal GlcCer may perturb lysosomal function, but does not have a significant impact on lysosomal [^{57}Co] Cbl transport. The reason is not fully elucidated and may arise from inefficient penetration of these materials into the cells or due to the nature of cell itself in a constant proliferating and dividing state.

Chapter 6

Impaired lysosomal cobalamin transport in Alzheimer's disease

6 Impaired lysosomal cobalamin transport in Alzheimer's disease

6.1 Introduction

AD is a progressive neurodegenerative disorder characterised by a gradual loss of memory, orientation, judgment and reasoning. Several genetic mutations, in APP, PS1 and PS2 cause early-onset familial AD (Williamson *et al.*, 2009). The vast majority of AD is, however, of the late-onset type for which genes including *APOE* and *ABCA7* confer increased risk (Bettens *et al.*, 2013). Despite the increased AD risk associated with such genes, there are many aspects related to the initiation and progression of AD pathology that remain unclear. The characteristic neuropathological alterations of AD include neuronal loss in the cerebral cortex and hippocampus, the presence of abnormal neurofibrillary *tau* tangles within the neurons, and the accumulation of insoluble deposits of amyloid plaques surrounding the neurons (Williamson *et al.*, 2009; De-Paula *et al.*, 2012). The main component of amyloid plaques is the highly hydrophobic 39-43 amino acid Aβ peptide. Aβ is generated after sequential cleavage of APP by β- and γ- secretases (Wilquet and De Strooper, 2004; Nixon, 2007).

The incubation of cultured primary neurons with soluble $A\beta_{42}$ causes the accumulation of $A\beta_{42}$ in the lysosomes due to the fact that intracellular $A\beta_{42}$ is relatively resistant to protease degradation (Ditaranto *et al.*, 2001; Chafekar *et al.*, 2008). The increased levels of intralysosomal Aβ stimulate free radical generation within lysosomes, disrupt lysosomal membrane proton gradient, impair lysosomal

function which together result in a more rapid Aβ accumulation and aggregation (Ditaranto *et al.*, 2001). This may initate a vicious cycle as neuronal oxidative stress induces further lysosomal Aβ accumulation via increased autophagy induction and decreased lysosomal clearance (Zheng *et al.*, 2009; Zheng *et al.*, 2011). The accumulation of Aβ in the lysosome has also been reported in AD animal models (Langui *et al.*, 2004). In APPxPS1 transgenic AD mice, lysosomal function is continually up-regulated and the levels of lysosomal enzymes are increased in the hippocampus and frontal cortex (Amritraj *et al.*, 2009). This possibly reflects cellular responses to the failed degradation of the accumulating Aβ which results in a gradual accumulation of partially degraded "residual bodies" as neurons become compromised and AD progresses (Yang *et al.*, 2011). It is therefore clear that lysosomal function is disturbed in AD and lysosomal membrane becomes vulnerable and ruptures when accumulated Aβ combines with other undegraded material to induce oxidative stress (Yang *et al.*, 1998; Pasternak *et al.*, 2004; Zheng *et al.*, 2006).

I have demonstrated that inhibition of lysosomal proteolysis using both pH-dependent and -independent approaches impair lysosomal Cbl intracellular transport which leads to the accumulation of Cbl in the lysosomal compartment in fibroblasts and neuronal cells. Given the critical role that the lysosome plays in Cbl metabolism, and the fact that lysosomal function deteriorates in AD, it is possible that lysosomal Cbl transport may also be interrupted by dysfunctional lysosomes in AD (Zhao *et al.*, 2011). Lysosomal acidification is defective in AD and lysosomal proteolysis is disrupted by an AD-related PS1 mutation (Lee *et al.*, 2010; Wolfe *et al.*, 2013). I propose that this may be a significant factor responsible for the cognitive decline in

AD patients as the impaired transit of Cbl through lysosomes, particularly in long-lived post-mitotic cells such as neurons. If this hypothesis is correct it may explain why Cbl administration has not yielded a consistent therapeutic benefit in AD patients as the supplemented dose may not reach its correct intracellular targets. If such lysosomal dysfunction is present *in vivo*, this could identify a pathway that might be targeted to improve neuronal Cbl utilisation and reduce the production of neurotoxic metabolites that accumulate when the coenzyme forms of Cbl do not reach their correct enzyme targets.

In the present study, SH-SY5Y-APP mutant cells were treated with a reversible 20S and 26S proteasome inhibitor, MG-115, to induce lysosomal Aβ accumulation (Agholme *et al.*, 2012). The [^{57}Co] Cbl levels in the lysosomes, mitochondria, and cytosol were measured to assess whether lysosomal Cbl transport is affected in these cells. In the *in vivo* study, C57BL/6J WT mice and APPxPS1 transgenic AD mice were i.p. injected with [^{57}Co] Cbl. The amount of [^{57}Co] Cbl in the major organs of these mice was measured and the subcellular [^{57}Co] Cbl distribution in the brain was assessed.

6.2 Methods

6.2.1. Cell culture and induction of lysosomal Aβ accumulation

The SH-SY5Y-APP cells were generated in the laboratory of Prof Ashley Bush by transfecting SH-SY5Y neuroblastoma cells with an APP cDNA containing the

Swedish mutation (swAβPP695) cloned into the pIRESpuro2 vector (Li *et al.*, 2012). The cells were cultured in DMEM supplemented with 10% (v/v) FCS, 100 µg/ml penicillin/streptomycin, 2 mM L-glutamine, and 2µg/ml puromycin (Sigma, USA, Cat #P9620), at 37˚C in a humidified atmosphere containing 5% (v/v) CO_2 until they reached approximately 70% confluence.

To investigate whether the AD-derived lysosomal Aβ accumulation alters intracellular Cbl transport, the SH-SY5Y-APP cells were treated with proteasome inhibitor MG-115 (0.5 µM, Sigma, USA, Cat #SCP0005)) for 48 h at 37˚C, a technique previously shown to induce intralysosomal Aβ accumulation (Agholme *et al.*, 2012). The cells were then metabolically labeled with [^{57}Co] Cbl (0.025 µCi/ml) in DMEM with 10% (v/v) HS in the presence of MG-115 (0.5 µM) for 48 h at 37˚C. The cells were then homogenised and cell fractions were collected, followed by subcellular fractionation as described previously (Chapter 2, section 2.4).

6.2.2. Enzyme-linked immunosorbent assay (ELISA) analysis of intracellular $A\beta_{40}$ and $A\beta_{42}$ levels

The quantification of $A\beta_{40}$ and $A\beta_{42}$ in each lysosomal and mitochondrial fraction from SH-SY5Y-APP cells with the MG-115 treatment was achieved using Colorimetric BetaMark x-40 and x-42 ELISA kits (Covance, Cat #SIG-38954 and SIG-38956) following the manufacturer's instructions. Samples were diluted 1:8 ($A\beta_{40}$) or 1:4 ($A\beta_{42}$) and assayed in duplicate. The ELISA protocol involves three main steps:

A. Preparation of working incubation buffer

The incubation buffer (10 ml) was diluted in 10 ml of Milli-Q water in a 50 ml plastic tube. The HRP detection antibody (10 µl) was added to the mixture and vortexed thoroughly to ensure proper mixing.

B. Preparation of the samples

The fraction samples were diluted in PBS in 1:4 for $A\beta_{40}$ and 1:2 for $A\beta_{42}$. They were further diluted 1:2 in working incubation buffer and mixed well by inverting the tube.

C. Preparation of the standards

The standards were prepared in two steps:

a. Preparation of standard intermediates

Eppendorf tubes were labelled as intermediate 1 & 2 and 990 µl of the standard diluents were added to each tube. The x-40 and x-42 standards (20 µg) were reconstituted with 80 µl of the same standard diluents. The contents of the tubes were mixed well and then incubated for 30 min at 22°C. After incubation, the intermediate 1 & 2 were prepared as shown in Table 6.1.

Tube Number	Volume of Standard (µl)	Volume of Standard Diluent (µl)	Final Concentration (ng/ml)
Reconstituted Standard	0	80	250 000
Intermediate 1	10 of Reconstituted Standard	990	2 500
Intermediate 2	10 of Intermediate 1	990	25

Table 6.1 Preparation of ELISA standard intermediates.

b. Preparation of Standards

Eppendorf tubes were labelled as 1 to 8 for the preparation of the standards. The standard intermediate 2 and the working incubation buffer were aliquoted to make 1.8 fold serial dilutions as shown in Table 6.2.

Tube Number	Volume of Standard (µl)		Volume of Working Incubation Buffer (µl)		Final Concentration (pg/ml)
1	10 Intermediate 2		990		250.0
2	600 of 1	500 of 1	480	400	138.9
3	600 of 2	500 of 2	480	400	77.2
4	600 of 3	500 of 3	480	400	42.9
5	600 of 4	500 of 4	480	400	23.8
6	600 of 5	500 of 5	480	400	13.2
7	600 of 6	500 of 6	480	400	7.4
8	0	0	480	400	0

Volumes for $A\beta_{40}$, Volumes for $A\beta_{42}$

Table 6.2 Preparation of ELISA standards.

Next, an ELISA plate was prewashed with 300 µl of washing buffer. The standard and the samples (100 µl) were added to each well in using a multi-channel pipette. The ELISA plate was covered with plate sealer and incubated for 16 h at 37°C to allow the antigen-antibody binding to occur.

On the next day, the plate was emptied and washed with 300 µl of washing buffer 5 times. The washing process used a platform shaker for 5 min each time to ensure vigorous washing. The plate was patted dry after the washing. Next, the TMB substrate (3,3',5,5'-tetramethylbenzidine, 200 µl) was added to each well. The plate was covered and incubated for 45 min for $A\beta_{40}$ and 42 min for $A\beta_{42}$ at 22°C. After incubation, the absorbance was measured at 620 nm using a microtitre plate reader (Spectra Max, Bio Strategy, USA). The average absorbance of standards was used to plot the standard curve and the samples were quantified using the standard curve.

6.2.3. Western blotting

For SH-SY5Y-APP cultured cell fractions, the detail for identifying the fractions containing lysosomes, mitochondria, and cytosol using appropriate antibodies for marker proteins was described in Chapter 2, section 2.5. For mouse brain homogenates, proteins were probed with an anti-Aβ WO2 mouse monoclonal antibody (1:200; provided by Dr. Qiao-Xin Li and Prof. Colin Masters, University of Melbourne, Australia) and HRP-conjugated rabbit anti-mouse (1:4,000, Dako, Australia). The blots were rinsed in PBS, and the proteins were detected using enhanced chemiluminescence. The membranes were exposed to ECL hyperfilm,

which was developed and scanned, and the signal intensity was quantified using NIH Image software.

6.2.4. *In vivo* mouse study

To examine subcellular [^{57}Co] Cbl distribution in lysosomes, mitochondria, and cytosol obtained from the brain, an *in vivo* study was performed using three 12-month-old male C57BL/6J WT mice and three 12-month-old male APPxPS1 transgenic AD mice. APPxPS1 transgenic AD mice were purchased from Jackson lab (strain name: B6.Cg-Tg (AβPPswePSEN1dE9)85Dbo/J), and maintained at the Australian BioResources facility (Moss Vale, Australia). This study was approved by the University of Wollongong Animal Ethics Committee and was performed in accordance with the EU Directive 2010/63/EU for animal experiments.

The mice were i.p. injected with 4 μCi [^{57}Co] Cbl in a volume of 0.2 ml sterile saline (0.9%, (w/v) NaCl) for 72 h. As described previously (Zhao *et al.*, 2013), the mice were weighed immediately before the time of injection and again just prior to sacrifice. After 72 h, the mice were sacrificed, and blood samples were collected using a cardiac puncture. The mice were then transcardially perfused with PBS, and the brain, liver, kidneys, spleen, and heart were dissected and collected. The plasma was extracted from the blood by centrifuging at 3,000 g for 15 min at 4˚C. All of the tissues were weighed. The amount of [^{57}Co] Cbl radioactivity in each organ and plasma was measured as cpm values using a gamma counter. In the current experiment, only the brain was used to perform organelle separation. The quantification of $A\beta_{40}$ and $A\beta_{42}$ in each WT and APPxPS1 AD mouse brain was

measured by ELISA. The brains were rinsed with PBS and cut into small pieces (< 3 mm^3). The brain were then homogenised and cell fractions were collected, followed by subcellular fractionation as described previously (Chapter 2, section 2.4).

6.2.5. Histology and immunohistochemistry

To identify amyloid plaques in the WT and APPxPS1 AD mouse brains, free-floating sagittal sections (45 μm) were immersed in distilled H_2O (2 min) followed by Harris haemotoxylin (2 min), distilled H_2O (3 min), 1% (w/v) thioflavine S (ThS, Sigma, USA, Cat #T1892, 3 min), distilled H_2O (3 min), 1% (v/v) acetic acid (20 min), and distilled H_2O (3 min), and then mounted onto gelatin-coated slides as described previously (Kim *et al.*, 2013). Three sections per mouse were analysed from the hippocampal region between lateral 1 mm to lateral 2 mm from the midline as defined using a mouse brain atlas. Images were captured using a Nikon TE2000 microscope equipped with a SPOT digital camera (Diagnostic Instruments) and Image-Pro Plus 6.1 software (Media Cybernetics).

For amyloid immunohistochemistry, the mouse brain was fixed in 4% paraformaldehyde and was cut at 40 μm by a cryostat (Leica CM1860, USA). The sagittal sections were washed with PBS and blocked with 5% (v/v) donkey serum, then incubated with biotin-conjugated anti-Aβ 6E10 monoclonal antibody (1:5,000, Covance, USA, Cat #SIG39300) for 24 h at 4˚C. After washing with PBS, the sections were incubated with streptavidin-peroxidase polymer (1:4,000, Sigma, USA, Cat#S2438) for 2 h at 22˚C. The sections were developed using 3,3'-diaminobenzidine substrate with metal enhancer (Sigma, USA, Cat #D0426). Images

were taken using a Nikon Eclipse TS100 microscope equipped with a Nikon Coolpix 8400 digital camera (Coherent Scientific, Australia).

6.3 Results

6.3.1. Isolation of lysosomes, mitochondria and cytosol from SH-SY5Y-APP cells

SH-SY5Y-APP cell organelles were separated through an OptiPrep density gradient to yield pure lysosomes, mitochondria and cytosol. Western blot analysis of the organelle fractions revealed that pure lysosomes (LAMP2 positive fractions #1 – #6) were separated from mitochondria (VDAC1 positive fractions #7 – #9) in the control cells (Figure 6.1 A). In the MG-115-treated cells, pure lysosomes were located in fractions #1 – #6 and mitochondria were detected in fractions #7 – #9 with minor lysosome/mitochondria cross-contamination in fraction #7 (Figure 6.1 B). In this case the lysosome cpm value in that fraction was estimated based on the LAMP2 optical density and comparison with the closest "clean" LAMP2 fractions (i.e. fractions #5 and #6). After subtraction of the estimated lysosomal cpm in fractions #7, the remaining cpm was assigned as mitochondrial. The organelle fractions in both the control and SH-SY5Y-APP cells contained only trace amounts of β-actin and were free of detectable MS, whereas clear signals for both β-actin and MS were detected in the cytosolic fractions.

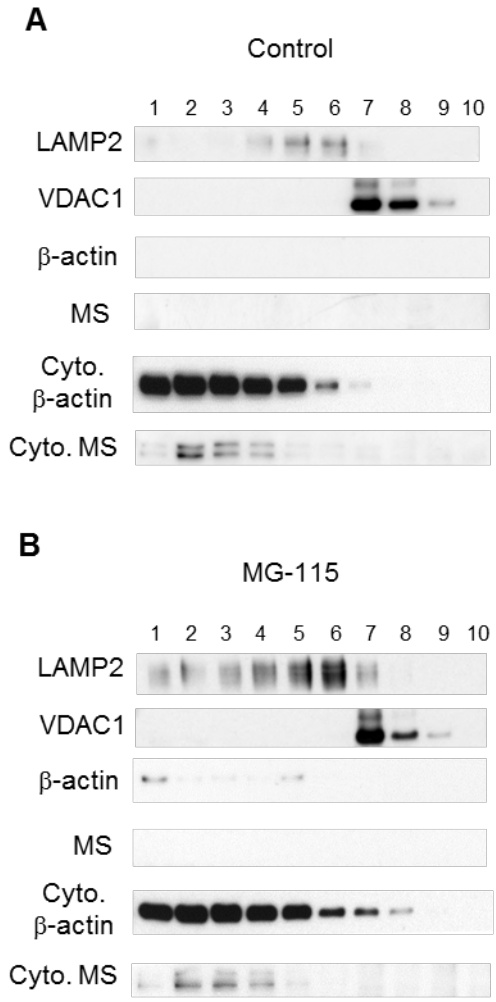

Figure 6.1 Isolation of lysosomes, mitochondria and cytosol fractions from SH-SY5Y-APP cells. The SH-SY5Y-APP cells were assessed under the standard 'Control' culture conditions (A) and after treatment with 0.5 μM MG-115 for 48 h (B). Cells were then metabolically labelled with [^{57}Co] Cbl for 48 h. The lysosomal, mitochondrial and cytosolic fractions were separated using an OptiPrep gradient. Intracellular marker proteins LAMP2 (lysosome), VDAC1 (mitochondria), β-actin and MS (cytosol) were probed by western blotting in all fractions.

6.3.2. Proteasome inhibition increases lysosomal Aβ levels and interrupts lysosomal Cbl transport

It has been previously reported that proteasome inhibition causes not only the accumulation of lysosomal Aβ, but also increased levels of intracellular and secreted Aβ (Agholme *et al.*, 2012). In our experiment, the SH-SY5Y-APP cells that stably express swAβPP695 were treated with the proteasome inhibitor MG-115 to induce $A\beta_{40}$ and $A\beta_{42}$ accumulation. The quantification of Aβ measured by the ELISA indicated that MG-115-treated cells had significantly higher levels of $A\beta_{40}$ and $A\beta_{42}$ in lysosomal fractions compared to the control cells (32% and 51%, respectively) (Figure 6.2 A and B). Although the mitochondrial $A\beta_{40}$ and $A\beta_{42}$ levels also had a significant increase (153% and 158%, respectively), the $A\beta_{40}$ and $A\beta_{42}$ levels in the lysosomes were much higher than in the mitochondria. In addition, lysosomal and mitochondrial fractions contained more $A\beta_{40}$ than $A\beta_{42}$ in both cells. These results suggest that $A\beta_{40}$ and $A\beta_{42}$ were induced and accumulated by MG-115 treatment resulting in a significant increase in the lysosomal $A\beta_{40}$ and $A\beta_{42}$ levels in the SH-SY5Y-APP cells.

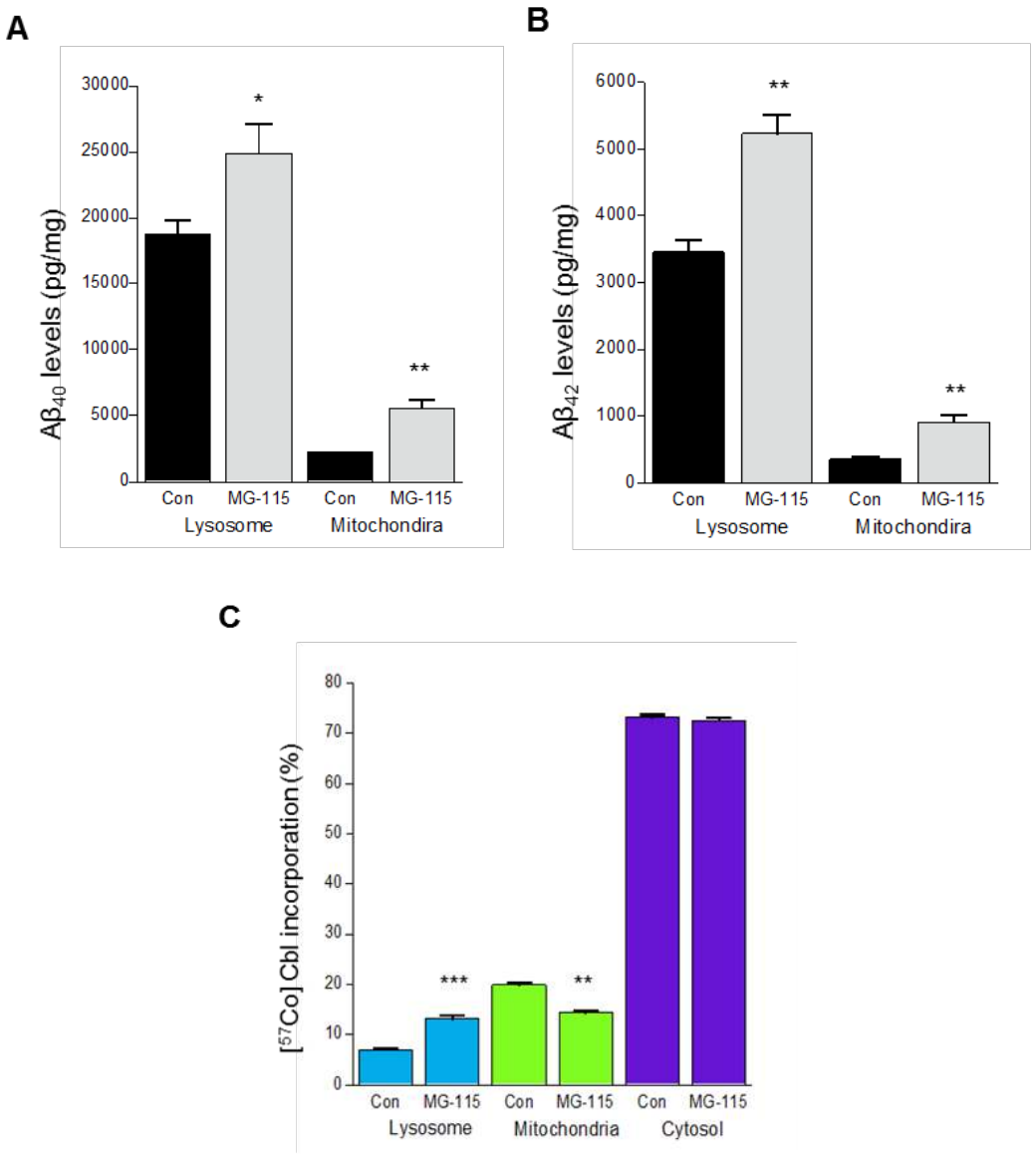

Figure 6.2 Proteasome inhibition increases lysosomal Aβ levels and impairs lysosomal Cbl transport. Quantification of $A\beta_{40}$ and $A\beta_{42}$ levels in lysosomal and mitochondrial fractions in the control (Con) and MG-115-treated SH-SY5Y-APP cells was measured by ELISA. The results demonstrated that the $A\beta_{40}$ (A) and $A\beta_{42}$ (B) levels were significantly increased in both lysosomal and mitochondrial fractions with MG-115 treatment. The proportional distribution of [^{57}Co] Cbl in both cells was assessed and expressed as a percentage of radioactivity in each fraction (C). The lysosomal [^{57}Co] Cbl level was significantly increased with MG-115 treatment. Data are expressed as mean ± SE (represented by the error bars) from three independent experiments. $^{**}P < 0.01$, $^{***}P < 0.001$.

Next, I assessed the impact that $A\beta_{40}$ and $A\beta_{42}$ accumulation induced by the proteasome inhibitor MG-115 may have on subcellular [^{57}Co] Cbl distribution. The incorporation of [^{57}Co] Cbl in each organelle was expressed as a percentage of cpm value. According to the distribution of lysosomes and mitochondria from the western blots, isolated lysosomes contained 7.0 ± 0.2% of the total cellular [^{57}Co] Cbl in the control cells, and this amount was almost doubled to 13.2 ± 0.7% with MG-115 treatment (mean ± SE, n = 3, Figure 6.2 C). This retention of [^{57}Co] Cbl in the lysosomes was concomitant with a significant reduction in mitochondrial [^{57}Co] Cbl levels (from 19.9 ± 0.4% to 14.3± 0.5% of the total cellular levels). Although the mitochondrial [^{57}Co] Cbl level in the MG-115-treated cells was decreased, there was no significant change observed in the cytosolic [^{57}Co] Cbl level. These results suggest that lysosomal Cbl transport in the MG-115-treated SH-SY5Y-APP cells was impaired, at least partly, due to increased Aβ accumulation that may perturb lysosomal function and prevent the release of Cbl from the lysosomes.

6.3.3. Aβ deposition and accumulation in the APPxPS1 AD mouse brain

To assess whether lysosomal Cbl transport is affected by Aβ accumulation in the AD brain *in vivo*, an APPxPS1 transgenic AD mouse model was used in the current experiment. To confirm the extent of Aβ deposition, cortical sections from 12-month-old WT and APPxPS1 AD mice were stained with ThS and 6E10 to identify plaque pathology. Numerous ThS-positive plaques were deposited in the hippocampus of APPxPS1 AD mice, whereas ThS-positive plaques were not observed in the WT mice (Figure 6.3 A). Similar to the result from ThS staining, the immunohistochemical staining demonstrated that 6E10-positive plaques were

detected in the hippocampus of APPxPS1 AD mice, but not found in WT mice (Figure 6.3 A). Expression of the human APP transgene in the brain homogenates was probed by anti-Aβ WO2 antibody using western blotting. The results showed that the human APP protein was detected at high levels in the APPxPS1 AD mouse brain (Figure 6.3 B). Furthermore, brain homogenates from WT and APPxPS1 AD mice were analysed by the ELISA for $A\beta_{40}$ and $A\beta_{42}$ quantification. The levels of $A\beta_{40}$ and $A\beta_{42}$ were much higher and significantly increased in the APPxPS1 AD mouse brains, whereas the signals of $A\beta_{40}$ and $A\beta_{42}$ from the WT mouse brains were at the lower range of detection (Figure 6.3 C). Together, these results confirm that $A\beta_{40}$ and $A\beta_{42}$ deposition and accumulation was clearly detected in the brain tissues derived from APPxPS1 AD mice.

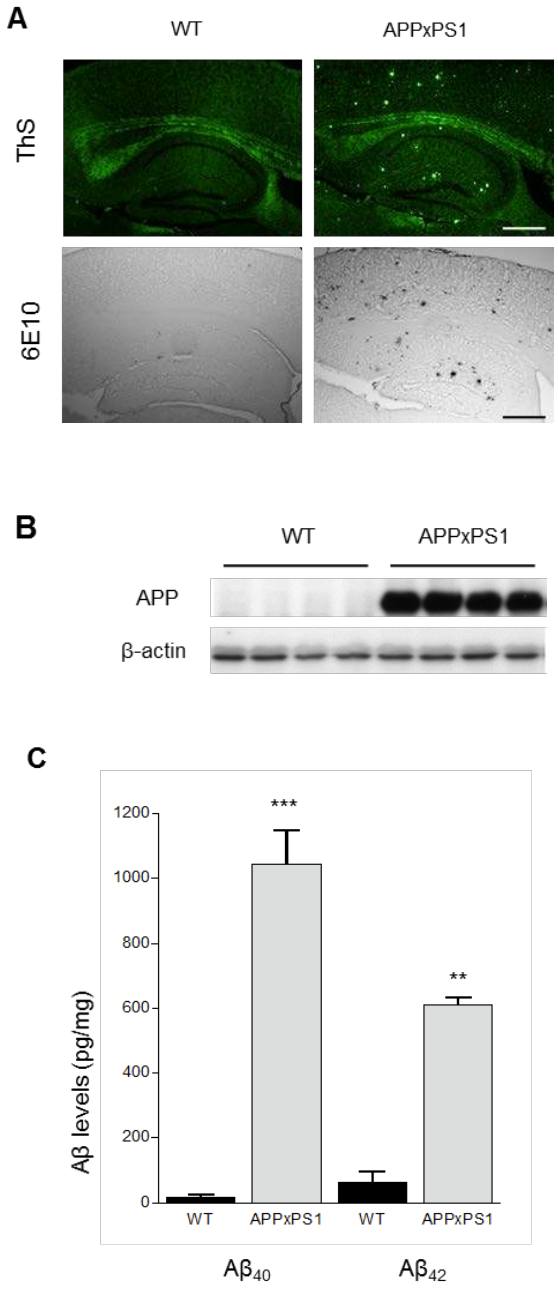

Figure 6.3 Aβ deposition and accumulation in the APPxPS1 AD mouse brain. Hippocampus section from WT and APPxPS1 AD mice was stained with ThS and 6E10 (A) to identify amyloid plaques. Plaques were only detected in the APPxPS1 AD mice. Human-specific APP transgene expression was probed by anti-Aβ WO2 antibody using western blotting (B). Aβ was only detected in the APPxPS1 AD mouse brains. Quantification of $A\beta_{40}$ and $A\beta_{42}$ levels in WT and APPxPS1 AD mouse brains were measured by the ELISA (C). Scale bars in "A" = 500 µm. ELISA data are expressed as mean ± SE (represented by the error bars) from three mice for each genotype. $^{**}P < 0.01$, $^{***}P < 0.001$.

6.3.4. [^{57}Co] Cbl incorporation in WT and APPxPS1 AD mice

To assess the incorporation of [^{57}Co] Cbl into major organs of the WT and APPxPS1 AD mice, three 12-month-old WT mice and three 12-month-old APPxPS1 AD mice were i.p. injected with 4 μCi [^{57}Co] Cbl for 72 h. A total of ~30% of the injected [^{57}Co] Cbl radioactivity was recovered from the collected organs and plasma. No significant difference was observed in [^{57}Co] Cbl radioactivity in the major organs when comparing WT and APPxPS1 AD mice (Figure 6.4). Similar to Cbl absorption in human, the majority of [^{57}Co] Cbl was contained in the kidneys (~15%) and liver (~11%), where excessive Cbl is known to be stored. The incorporation of [^{57}Co] Cbl in the brain, heart and spleen was minimal and less than 1% of total recovered [^{57}Co] Cbl radioactivity. Approximately 2.5% of [^{57}Co] Cbl was detected in the plasma, from where TC binds and transports Cbl to all target cells of the body. Intriguingly, and for reasons that remain unclear, plasma levels of [^{57}Co] Cbl were 24% lower ($P < 0.05$) in APPxPS1 AD mice compared to WT mice (Figure 4).

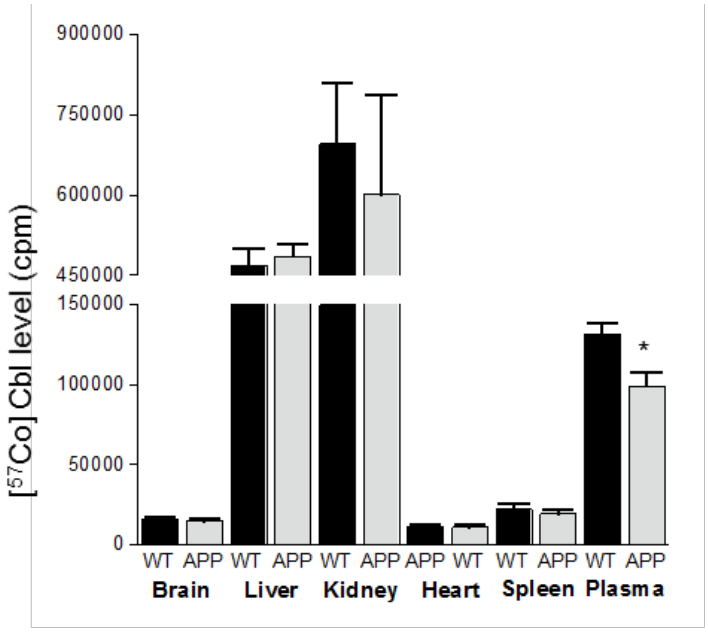

Figure 6.4 The [^{57}Co] Cbl level in WT and APPxPS1 transgenic AD mouse organs. Three WT and three APPxPS1 AD mice were i.p. injected with 4 µCi [^{57}Co] Cbl for 72 h. The brain, liver, kidneys, heart, spleen, and plasma were collected. The amount of [^{57}Co] Cbl radioactivity in these organs was measured using a gamma counter. The distribution of [^{57}Co] Cbl radioactivity was expressed as total cpm per organ. Data are expressed as mean ± SE (represented by the error bars) from three mice for each genotype. *P < 0.05.

6.3.5. Lysosomal Cbl transport is impaired in the APPxPS1 AD mouse brain

To examine subcellular [^{57}Co] Cbl distribution in lysosomes, mitochondria, and cytosol from the brain homogenates, the whole brain from WT and APPxPS1 AD mice was homogenised and processed by the subcellular fractionation method. Western blot analysis of the organelle fractions demonstrated that pure lysosomes (LAMP2 positive fractions #1 – #4) were separated from mitochondria (VDAC1 positive fractions #7 – #9) in the WT mouse brain (Figure 6.5 A). As the MS primary antibody was not suitable for use with mouse tissue, the cytosolic fractions were probed by the β-actin antibody only. The organelle fractions were free of detectable β-actin, whereas clear signals appeared in the cytosolic fractions (β-actin positive fractions #1 – #4) in the WT mouse brain. In the APPxPS1 AD mouse brain, pure lysosomes were localized at LAMP2 positive fractions #1 – #5 with intense signal on fraction #1, while mitochondria were distributed at VDAC1 positive fractions #7 – #9 (Figure 6.5 B). The organelle fractions were also free of detectable β-actin whereas a clear β-actin signal was detected in the cytosolic fractions (#1 – #5).

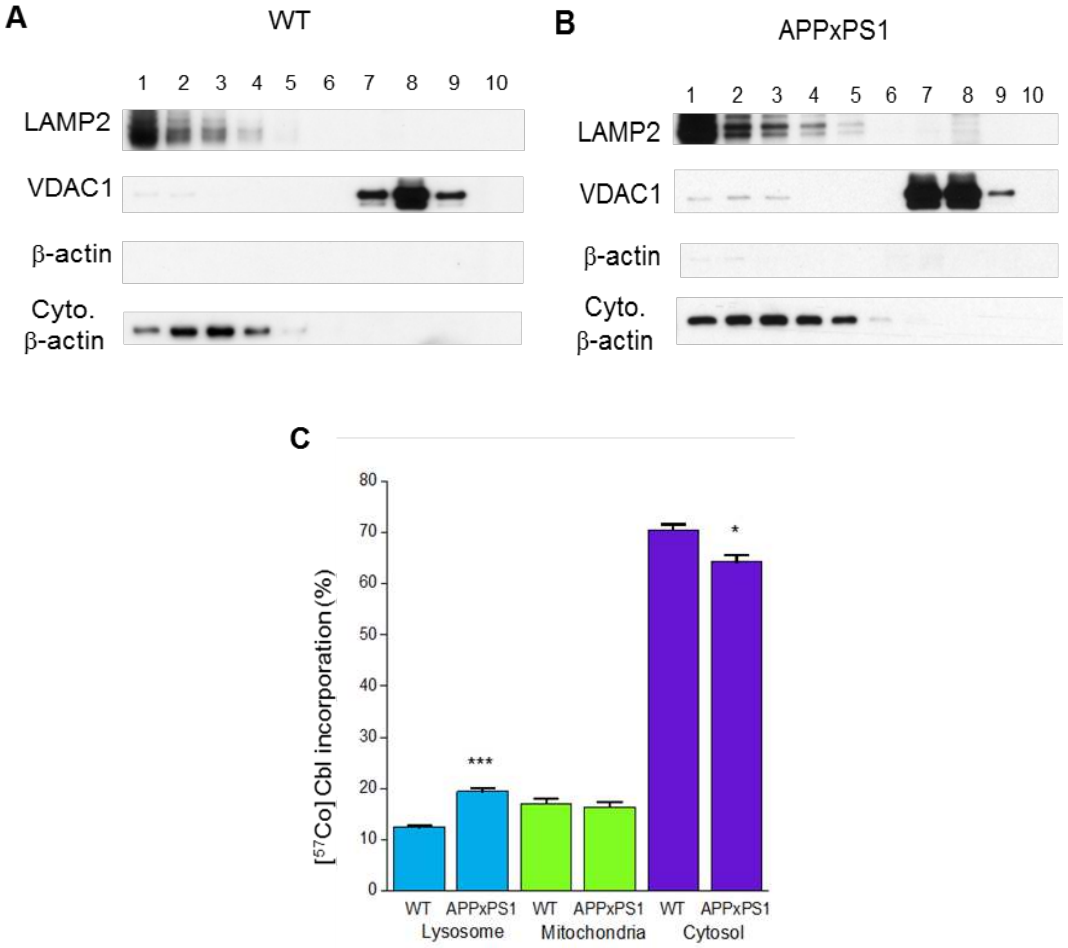

Figure 6.5 Subcellular Cbl transport is impaired in the APPxPS1 AD mouse brain. The whole brain from WT (A) and APPxPS1 AD (B) mice was homogenised and processed by subcellular fractionation. Intracellular marker proteins LAMP2 (lysosome), VDAC1 (mitochondria), and β-actin (cytosol) were probed by western blotting in all fractions. The proportional distribution of [^{57}Co] Cbl in brain homogenate organelles was assessed and expressed as a percentage of total radioactivity in each fraction (C). The lysosomal [^{57}Co] Cbl level was significantly increased in the APPxPS1 AD mouse brain. Data are expressed as mean ± SE (represented by the error bars) from three independent mouse experiments. *P < 0.05, ***P < 0.001.

Next, I investigated whether subcellular [^{57}Co] Cbl transport was altered in the APPxPS1 AD mouse brain. The incorporation of [^{57}Co] Cbl in each organelle expressed as a percentage of cpm values. According to the distribution of lysosomes and mitochondria from the western blots, the lysosomes contained 12.4 ± 0.6% of total cellular [^{57}Co] Cbl in the WT mouse brain, whereas the amount of lysosomal [^{57}Co] Cbl was increased to 19.4 ± 1.1% in the APPxPS1 AD mouse brain (mean ± SE, n = 3, Figure 5C). This represents a significant 56% increase in lysosomal [^{57}Co] Cbl level. This accumulation of [^{57}Co] Cbl in the lysosomes was associated with a significant 6% decrease (from 70.5 ± 1.9% to 64.0 ± 2.3% of total cellular levels) in the cytosolic [^{57}Co] Cbl level in the APPxPS1 AD mouse brain. Interestingly, there was no significant change observed in mitochondrial [^{57}Co] Cbl levels. Thus, lysosomal Cbl transport was interrupted in the APPxPS1 AD mouse brain with a 56% increase of [^{57}Co] Cbl entrapped in the lysosomal compartment.

6.4 Discussion

The ubiquitin-proteasome system and the autophagy-lysosome system are two major degradative pathways in eukaryotic cells. They are essential for many cellular processes, including misfolded protein degradation, the regulation of gene expression, and responses to oxidative stress (Lee *et al.*, 2013). In the present work, the results have demonstrated that the amount of lysosomal [^{57}Co] Cbl is almost doubled in the SH-SY5Y-APP cells with proteasome inhibitor treatment. Proteasome inhibition increases lysosomal Aβ levels and that the accumulation of Aβ is associated with impaired lysosomal Cbl transport *in vitro*.

When the proteasome system is inhibited by MG-115, autophagy is activated and up-regulated as a compensatory mechanism to degrade damaged organelles and protein aggregates. As more newly synthesised Aβ are delivered to the lysosomes, the progressively accumulated Aβ may combine with other undegradable materials to induce oxidative stress and abnormal proteolysis that impair lysosomal function, resulting in defective clearance of cellular molecules (Yang *et al.*, 1998). Lysosomes are rich in low mass redox-active iron and they are very sensitive to oxidative stress induced by ROS via the Fenton reaction (Kurz *et al.*, 2011). Thus, when TC-[^{57}Co] Cbl is transported to these dysfunctional lysosomes, TC may also fail to be degraded by lysosomal hydrolases and [^{57}Co] Cbl is therefore unable to be released and entrapped in the lysosomal compartment. However, from those experiments I did not determine whether the entrapped lysosomal [^{57}Co] Cbl remains bound to TC.

In the *in vivo* study, I used 12-month-old APPxPS1 transgenic AD mice as an AD model and found amyloid plaques and Aβ deposition in the hippocampus region of these mice. The results provide the first *in vivo* evidence that lysosomal [^{57}Co] Cbl level is significantly increased (by 56%) in association with AD pathology. It should be noted that the 56% increase in lysosomal [^{57}Co] Cbl trapping represent the average of all lysosomes from all cell types and brain regions. It is likely that post-mitotic cells such as neurons suffer more from an accumulation of "lysosomal garbage" as they are unable to divest themselves of their undegradable lysosomal material to daughter cells (Terman and Brunk, 2006; Terman *et al.*, 2006). This is predicted to be particularly pronounced under conditions associated with ageing and neurodegeneration (Zheng *et al.*, 2006; Kurz *et al.*, 2008; Zhao *et al.*, 2011). Thus a cell-specific roadblock in Cbl trafficking may occur in cell-specific manner or in

specific brain regions where Aβ levels are highest, and this would lead to a localised deficiency in MS and MMCM enzyme activity and concomitant increases in neurotoxic Hcy and MMA concentrations.

The exact mechanism responsible for lysosomal [^{57}Co] Cbl trapping in the APPxPS1 mouse brain is unknown. Based on the knowledge that lysosomal function gradually deteriorates in AD and that endogenous Aβ progressively accumulates in the dysfunctional lysosomes (Cataldo *et al.*, 1994; Agholme *et al.*, 2012; Wolfe *et al.*, 2013), it is plausible that excessive Aβ that cannot be degraded becomes aggregated and further compromises lysosomal function. It is possible that such lysosomes continue to receive newly synthesised hydrolases from primary lysosomes in a futile attempt to degrade indigestible material. These lysosomal enzymes would therefore be essentially lost for other useful purposes, e.g. for the degradation of newly autophagocytosed materials and releasing Cbl from TC (Terman *et al.*, 2006; Zhao *et al.*, 2011). This would be predicted to result in a delayed protein turnover, accumulation of waste products, and an impairment of Cbl transit through the lysosomal compartment.

Neither WT nor APPxPS1 AD mice had a significant change in body weight during injection period. All major organs were collected and no obvious weight change in those tissues was seen between two groups. Unlike humans which express Cbl carrier proteins TC and haptocorrin, TC is the only Cbl binding protein in mouse plasma that carries Cbl to the kidneys and liver (Hygum *et al.*, 2011). In our mouse studies, the kidneys contained the highest amount of [^{57}Co] Cbl among the organs examined, followed by the liver. The result is consistent with previous reports

(Lildballe *et al.*, 2012; Zhao *et al.*, 2013). It is noteworthy that although Cbl can rapidly pass through the blood-brain-barrier and is stored in human brain (Van den Berg *et al.*, 2003; Herrmann and Obeid, 2012), only ~ 0.4% of total [^{57}Co] Cbl radioactivity was recovered in the mouse brain. Nonetheless, this amount was adequate for the comparison of subcellular [^{57}Co] Cbl distribution in both WT and APPxPS1 AD mice. The mechanism regulating Cbl uptake into the brain needs to be elucidated and could be targeted in the AD context to increase the total CNS Cbl pool to help alleviate the lysosomal roadblock to Cbl transport that we have identified.

I also observed qualitatively that both MG-115 treatment (*in vitro*) and the accumulation of Aβ (*in vivo* in the APPxPS1 AD mice) that was associated with lysosomal [^{57}Co] Cbl trapping, also appeared to be associated with a change in LAMP2 distribution through the OptiPrep density gradient. In particular, I noted a tendency for the LAMP2 signal to be stronger in fractions of higher density. This is similar to the data obtained from cultured fibroblasts and neuronal cells that treated with lysosomal protease inhibitors to induce lysosomal [^{57}Co] Cbl trapping (Zhao *et al.*, 2014). This might indicate that lysosomal Cbl trapping is associated with an enlargement of the lysosomal compartment leading to an increase in average lysosome size and/or density distribution. This along with a failed release of Cbl from the TC-Cbl complex could together contribute to the impaired transit of [^{57}Co] Cbl through the lysosomal compartment. Although lysosomal morphology clearly changes in human AD tissues (Cataldo *et al.*, 1994; Cataldo *et al.*, 1996), future studies utilising electron microscopy techniques might clarify the extent to which lysosomal morphology changes under current experimental conditions.

The data derived from fibroblast and neuronal cell lines indicates that under standard culture conditions, only ~5.5% of cellular [^{57}Co] Cbl resides in the lysosomes. This is not surprising based on the fact that the major sites of Cbl utilisation in humans are the enzymes MS and MMCM located in the mitochondria and cytosol respectively. The relatively low level of lysosomal Cbl probably reflects the transient nature of this pool as it is released from the TC-Cbl complex and transported from the lysosome via LMBD1 and ABCD4 (Rutsch *et al.*, 2009; Coelho *et al.*, 2012). However, lysosomal [^{57}Co] Cbl level in WT mouse brain is much higher with ~ 12.4% of cellular [^{57}Co] Cbl was detected in the lysosomes. It is currently not clear why lysosomes isolated from the brain tissue are apparently enriched in [^{57}Co] Cbl compared to the cell lines. As it was unable to measure mouse MS using western blotting so it was possible that traces of cytosolic contamination in these fractions could contribute to the cpm values; although the very low levels of β-actin contamination would argue against this. Further rinse steps after the OptiPrep gradient may improve organelle purity; however, the challenge with the brain analysis is the relatively low amount of [^{57}Co] Cbl incorporation (~ 0.4%) and the possibility that further rinsing may reduce recovery of the lysosomes.

6.5 Conclusion

The previous results have demonstrated that lysosomal enzyme inhibition (either increasing lysosomal pH or inhibiting lysosomal proteases) surpresses lysosomal function, resulting in the accumulation of [^{57}Co] Cbl in lysosomes and impairment to lysosomal transport of Cbl to mitochondria and cytosol in the cultured cells. In this

Chapter, the results demonstrate that lysosomal [^{57}Co] Cbl level is significantly increased in association with AD-derived lysosomal Aβ accumulation both *in vitro* and *in vivo*. These results indicate that lysosomal [^{57}Co] Cbl transport is at least partly impaired when lysosomal function becomes defective due to AD-derived Aβ accumulation. Lysosomal dysfunction may significantly impact upon Cbl intracellular transport and utilisation.

Chapter 7

General discussion

7 General discussion

7.1 Project overview and major outcomes

Cbl is required for erythrocyte formation and DNA synthesis, and plays a crucial role in the maintenance of neurological function. MeCbl and AdoCbl are intracellular active forms in human metabolism. MeCbl is used to transform Hcy to Met via cytosolic MS, whereas AdoCbl is required for the conversion of MM-CoA to succinyl-CoA via mitochondrial MMCM. The reduction of MeCbl and AdoCbl causes elevated plasma Hcy and MMA concentrations that correlate positively with cognitive decline and brain atrophy (Herrmann *et al.*, 2000; Sachdev *et al.*, 2002). Thus, Cbl utilisation is critically dependent on Cbl efficient transit through the intracellular lysosomal compartment and subsequently being released into cytosol and mitochondria. Research evidence indicates that lysosomal function deteriorates in ageing post-mitotic cells such as neurons (Brunk and Terman, 2002; Double *et al.*, 2008). Importantly, it is also clear that lysosomal function is markedly perturbed in AD, and this is known to be a direct consequence of autophagy failure (Nixon *et al.*, 2008; Nixon and Yang, 2011). It is possible that lysosomal Cbl intracellular transport may be interrupted by aged or impaired lysosomes in ageing and AD (Zhao *et al.*, 2011).

Low serum Cbl levels are associated with neurodegenerative disease and cognitive impairment (Moore *et al.*, 2012). Increased plasma levels of Hcy are considered as a strong independent risk factor for developing AD and cognitive defect in the elderly (Seshadri *et al.*, 2002; Quadri *et al.*, 2004). Although animal studies indicate that Cbl

supplementation significantly improves cognitive performance (Zhang *et al.*, 2009; Zhuo and Pratico, 2010), human trials have failed to provide a consistent beneficial effect on cognitive performance with either oral or parenteral Cbl (McMahon *et al.*, 2006; Maron and Loscalzo, 2009; McCaddon and Hudson, 2010; Smith *et al.*, 2010). Malabsorption is a major cause of Cbl deficiency in the elderly. However, this is not likely to account for the lack of efficacy regarding cognitive improvement in clinical trials because both oral and parenteral delivery routes increase plasma circulating Cbl to the same degree in both young and aged subjects (Nilsson-Ehle, 1998; Andres *et al.*, 2005).

Lysosomes maintain cellular homeostasis by continually degrading and recycling misfolded cellular components. Lysosomes are essential subcellular organelles involved in the metabolism of intracellular Cbl utilisation. The importance of the role that the lysosome plays in the delivery of Cbl to MS and MMCM is described in the early study (Rosenblatt *et al.*, 1985) and has been highlighted by the later discovery of two inborn errors of Cbl metabolism referred to as *cblF* and *cblJ* (Rutsch *et al.*, 2009; Coelho *et al.*, 2012). These life-threatening conditions are caused by a loss of function in either LMBD1 or ABCD4, lysosomal membrane proteins that normally promote Cbl efflux from the lysosome to the cytosol (Rutsch *et al.*, 2009; Coelho *et al.*, 2012). In *cblF* and *cblJ* deficiencies, Cbl accumulates in lysosomes and levels of toxic metabolites Hcy and MMA increase. However, the significant impact of lysosomal dysfunction under neuropathological conditions on intracellular Cbl transport has been overlooked. It has been speculated that the role of lysosomes during Cbl utilisation is sole as transit station that transfer and release most lysosomal Cbl into cytosol and mitochondria.

The current project is designed on the basis of hypothesis that neuropathological conditions that impair lysosomal function, such as age-related lipofuscinosis, lysosomal storage diseases and AD, may interrupt lysosomal Cbl transport. This inhibition causes Cbl accumulation in the lysosomes, affects Cbl utilisation and may result in downstream cytotoxic metabolites accumulation. Suboptimal lysosomal processing of Cbl plays a significant role in age-related loss of neurological function associated with both ageing and AD. The impaired transit of Cbl through lysosomes, particularly in post-mitotic cells such as neurons is responsible for the lack of cognitive improvement in aged and AD patients. If this hypothesis is correct, it will explain why Cbl administration has not yielded a consistent therapeutic benefit in the ageing and dementia contexts, and may develop a clinical therapeutic target that improves neuronal Cbl utilisation to reduce the production of neurotoxic metabolites that accumulate when the coenzyme forms of Cbl do not reach their correct intracellular targets.

To investigate the Cbl intracellular distribution in three main compartments: lysosome, mitochondria and cytosol, I developed a subcellular fractionation technique that permits efficient and effective separation of the lysosomes from two major pools of intracellular Cbl (Silva *et al.*). This method builds on many previous studies that have separately analysed cellular [^{57}Co] Cbl metabolism in cells and mice (Mellman *et al.*, 1978; Youngdahl-Turner *et al.*, 1978; Yassin *et al.*, 2000; Hannibal *et al.*, 2008; Yamani *et al.*, 2008) or aspects of lysosome function in cells and mice (Manunta *et al.*, 2007; Yang *et al.*, 2011). The subcellular fractionation method provides a useful tool for isolating purified subcellular organelles and

investigating intracellular [^{57}Co] Cbl trafficking in fibroblast and neuronal cell lines. In addition, I assessed the levels of [^{57}Co] Cbl in lysosomes and other intracellular compartments and organelle markers throughout the separation gradients in the cell lines and animal models that are known to have impaired lysosome function due to, for example, accumulation of the age-related pigment lipofuscin, substrate accumulation in lysosomal storage diseases, and accumulation of Aβ in AD.

One major finding from this PhD study is to demonstrate that inhibition of lysosomal proteolysis using both pH-dependent (chloroquine) and -independent (leupeptin and vinblastine) approaches suppress lysosomal function, interrupt intracellular [^{57}Co] Cbl transit, and cause lysosomal [^{57}Co] Cbl accumulation in the HT1080 fibroblast and SH-SY5Y neuronal cells. Treating cells with these chemical compounds has acute impact on lysosomal morphology and significantly inhibit [^{57}Co] Cbl releasing from lysosomes. There is a close correlation when the [^{57}Co] Cbl cpm values were compared with LAMP2 signal in the pure lysosome fractions, however, the results cannot determine whether lysosomal trapping induced by either chloroquine or leupeptin is due to an expansion of the lysosomal compartment or an increase the amount of Cbl retained in each lysosome. As lysosomal protease inhibitors were reported to have a dual effect on autophagy when they initiate early autophagic processes while suppressing autophagic degradation (Li *et al.*, 2013). This is predicted to result in an expansion of the lysosomal compartment. Therefore I speculate that lysosomal Cbl accumulation that is induced by protease inhibition may due to a combination of both an enlargement of the lysosomal compartment and an increase in lysosomal Cbl concentration.

There is a marked difference in the amount of lysosomal [^{57}Co] Cbl accumulated in the fibroblasts compared to neuronal cells, which are more susceptible to these drugs and trap much more [^{57}Co] Cbl in the lysosomes. In the SH-SY5Y cells, I observed a very significant drop in cytosolic [^{57}Co] Cbl when lysosomal protease inhibitors are present. If the half-life of MS is shorter than the half-life of MMCM then one might predict a more rapid drop in the [^{57}Co] Cbl cytosolic pool; however, the predicted half-lives of these enzymes are 30 h and 5.5 h, respectively (Bachmair *et al.*, 1986; Gonda *et al.*, 1989). Therefore the differences in enzyme half-life are unlikely to account for the relative sensitivity of these pools. I am unaware of detailed studies on MS and MMCM turnover in neurons and the impact that Cbl deficiency may have on enzyme half-life. Nevertheless, based on the fact that Cbl deficiency includes a neurological phenotype (Healton *et al.*, 1991; Baik and Russell, 1999; Calvaresi and Bryan, 2001), these issues appear to be worthy of future study.

More importantly, lysosomal [^{57}Co] Cbl trapping caused by lysosomal dysfunction is connected with decreased incorporation of [^{14}C] propionate into cellular macromolecules, which is a physiological marker of mitochondrial MMCM activity (Willard *et al.*, 1976). The inhibition of lysosomal function disrupts intracellular Cbl utilisation and results in reduced level of mitochondrial [^{57}Co] Cbl that is correlated with impaired Cbl-dependent MMCM activity, which could lead to increased production of neurotoxic metabolites. To examine the impact of lysosomal dysfunction on the Cbl metabolic pathway, it is essential to define the relationship between altered intracellular Cbl distribution and changes in key downstream metabolites dependent on the availability of Cbl coenzyme forms: MeCbl and AdoCbl. It is predicted that neurotoxic levels of Hcy and MMA will increase when

MS and MMCM activities are inhibited due to reductions in MeCbl and AdoCbl supply. Thus, the Hcy and MMA levels in those lysosomal, mitochondrial, and cytosolic fractions are measured using established LC-MS and GC-MS methods (Guan *et al.*, 2003; Serot *et al.*, 2005). However, it seems that the amount of Hcy and MMA in each fraction was not enough to be accurately measured with the equipment in the lab. The results were variable and inconsistent in each condition, even after attempting several different measurement approaches. Due to this limited capability to accurately measure Hcy and MMA concentration, I chose to assess the Cbl metabolic pathway alteration under conditional lysosomal dysfunction. The reduced incorporation of [^{14}C] propionate into cellular macromolecules provides crucial information that impaired lysosomal function was associated with decreased Cbl-dependent mitochondrial MMCM activity.

Another finding from this study is to demonstrate that lysosomal Cbl transport is impeded under neuropathological conditions, such as lysosomal storage diseases. An *in vitro* experiment using human GD fibroblasts shows that lysosomal function was suppressed and lysosomal [^{57}Co] Cbl level was doubled in these cells. Lysosomal [^{57}Co] Cbl transport is impaired in GD cells and this effect was correlated with the increase of lysosomal GlcCer that is caused by inherited genetic defect in the lysosomal enzyme GCase. However, when SH-SY5Y cells were treated with CBE, an irreversible inhibitor of GCase, lysosomal [^{57}Co] Cbl level in these cells remained statistically unchanged, even though CBE induces rapid increase of GlcCer and pathologically mimics the GD phenotype. In addition, to examine whether age-related lipofuscin accumulation interrupts intracellular Cbl transport in the cultured cells, artificial lipofuscin was synthesised by exposing enriched lysosomes and

mitochondria cell lysates to UV light. HT180 fibroblasts and SH-SY5Y cells were treated with artificial lipofuscin and the cellular uptake was not efficient. Artificial lipofuscin had little impact on the lysosomal [^{57}Co] Cbl transport and lysosomal [^{57}Co] Cbl level in these cells was not statistically changed. It seems exogenous interventions induced by the generation of either artificial lipofuscin or CBE-derived lysosomal GlcCer may perturb lysosomal function, but do not have a significant impact on lysosomal [^{57}Co] Cbl transport. The reason is not fully elucidated and may arise from inefficient production of induced materials or due to the nature of cell itself in a constant proliferating and dividing state.

So far, I have examined the proposed hypothesis and proved that inhibition of lysosomal function (either increasing lysosomal pH, or inhibiting lysosomal proteases, or in the lysosomal storage disease) results in lysosomal [^{57}Co] Cbl accumulation and impedes lysosomal [^{57}Co] Cbl transport to mitochondria and cytosol in the cultured cells. Next, I investigated whether AD-derived lysosomal Aβ accumulation also interrupts intracellular [^{57}Co] Cbl transport, as defective intracellular Cbl utilisation is associated with cognitive decline and brain atrophy in AD patients (Levitt and Karlinsky, 1992; Douaud *et al.*, 2013). The results indicate that SH-SY5Y-APP cells with proteasome inhibitor MG-115 treatment induced Aβ accumulation in the lysosome compartment. The ubiquitin-proteasome system and the autophagy-lysosome system are two major independent degradative pathways in eukaryotic cells (Lee *et al.*, 2013). It has been reported that perturbations in the flux through either pathway affect the activity of the other system (Korolchuk *et al.*, 2010). When the proteasome system is inhibited by MG-115, autophagy is activated and up-regulated as a compensatory mechanism to mediate clearance of damaged

organelles and protein aggregates. As more newly synthesised Aβ are delivered to the lysosomes, they combine with other undegradable materials to induce oxidative stress and abnormal proteolysis that impairs lysosomal function, progressively resulting in defective clearance of cellular molecules (Yang *et al.*, 1998). Lysosomal [^{57}Co] Cbl level is almost doubled in the SH-SY5Y-APP cells with proteasome inhibitor treatment. Thus, proteasome inhibition increases lysosomal Aβ levels and replicates AD-derived lysosomal Aβ accumulation, which possibly leads to impaired lysosomal Cbl transport *in vitro*.

Another major outcome from this study is that I provide the first *in vivo* evidence that lysosomal [^{57}Co] Cbl transport in the 12-month-old APPxPS1 transgenic AD mouse brain is interrupted in association with AD pathology. Amyloid plaques and Aβ accumulation was clearly detected in hippocampus region of these mice. There was no obvious difference in terms of [^{57}Co] Cbl incorporation in the major organs of WT and APPxPS1 AD mice. Consistent with previous reports (Lildballe *et al.*, 2012; Zhao *et al.*, 2013), the kidneys contain the highest amount of [^{57}Co] Cbl among those organs, followed by the liver in these WT and APPxPS1 AD mice. However, when subcellular [^{57}Co] Cbl distribution is examined from the brain homogenates, lysosomal [^{57}Co] Cbl level in the APPxPS1 AD mouse brain is significantly increased by 56% compared to WT mouse brain. It should be noted that the 56% increase in lysosomal [^{57}Co] Cbl trapping represent the average of all lysosomes from all cell types and brain regions. It is likely that post-mitotic cells such as neurons suffer more from an accumulation of "lysosomal garbage" as they are unable to divest themselves of their undegradable lysosomal material to daughter cells (Terman and Brunk, 2006; Terman *et al.*, 2006).

The detailed mechanism responsible for lysosomal [^{57}Co] Cbl accumulation in the APPxPS1 AD brain is unknown. It has been reported that lysosomal function gradually deteriorates in AD and that endogenous Aβ progressively accumulates in the dysfunctional lysosomes (Cataldo *et al.*, 1994; Agholme *et al.*, 2012; Wolfe *et al.*, 2013). It is plausible that excessive Aβ becomes aggregated or misfolded, while newly formed lysosomal hydrolases are in a futile attempt to degrade these indigestible materials and thus may lose for other useful purposes, e.g. for the degradation of newly autophagocytosed other materials or releasing Cbl from TC (Terman *et al.*, 2006; Zhao *et al.*, 2011). This would be speculated to result in a delayed protein turnover, aggravate waste product accumulation, and eventually initate a vicious cycle. Therefore, the release of [^{57}Co] Cbl from lysosomal compartment is inhibited in the APPxPS1 AD brain and the impairment of lysosomal Cbl transit is closely correlated with AD-derived lysosomal Aβ accumulation in the defective lysosomes.

7.2 Future directions

Chloroquine is an effective anti-malarial drug to prevent the development of malaria parasites in the blood and it has long been used in the treatment or prevention of malaria infection. The side effects of chloroquine treatment include gastrointestinal problems, stomach ache, itch, headache, postural hypotension, and cognitive impairment (Albright *et al.*, 2002; Boivin *et al.*, 2007). Clinical studies reported that malaria patients developed with retinal toxicity secondary to the use of chloroquine (Reis *et al.*, 2010; Michaelides *et al.*, 2011). In addition, chloroquine raises intralysosomal pH above its physical level by disrupting the H^+ gradient across the

lysosomal membrane (Gonzalez-Noriega *et al.*, 1980). Chloroquine alters the lysosomal acidic compartments, causes inhibition of lysosomal hydrolase activities, and induces accumulation of autophagosomes (Geng *et al.*, 2010; Chen *et al.*, 2011). In the current study, the results demonstrate that the cells with chloroquine treatment have a significant impact on the lysosomal [^{57}Co] Cbl transport. Chloroquine causes the increase of lysosomal [^{57}Co] Cbl and simultaneously reduces [^{57}Co] Cbl to be released into mitochondria and cytosol, and thereby impeding intracellular [^{57}Co] Cbl transit. Lower cytosolic Cbl level causes increased plasma levels of Hcy, which is a strong independent risk factor for cognitive decline in the elderly. Therefore, cognitive impairment caused by chloroquine treatment is possibly linked with impaired intracellular Cbl utilisation due to mutual defect: dysfunctional lysosomes (Lie and Schofield, 1973). Further investigation is necessory to provide insight into cellular and molecular mechanisms underlying the impact of lysosomal protective function and its regulation on chloroquine treatment and Cbl utilisation. It is conceivable that approaches to preserve lysosomal function or by-pass the dysfunctional lysosome roadblock may be explored in the future as novel strategies to escort Cbl to its correct intracellular targets and with the possibility to alleviate the side effects of chloroquine on cognitive decline.

The current study examines the subcellular Cbl distribution in the cells that are induced with age-related lysosomal artificial lipofuscin by exposing enriched lysosomes and mitochondria cell lysates to UV light for 24 h. It seems that induced artificial lipofuscin in fibroblasts and neuronal cells have not obviously affected lysosomal [^{57}Co] Cbl transport. It is noteworthy that this method is not efficient for the induction of artificial lipofuscin in this experiment. Lipofuscin formation can be

induced under various experimental conditions. It has been shown that oxidative stress promotes lipofuscin formation, whereas antioxidant treatment prevents it (Thaw *et al.*, 1984; Terman and Brunk, 1998). In order to generate large amount of lipofuscin, human fibroblasts can be cultured for 6 months under hyperoxic conditions (40% ambient oxygen) in the future experiment to induce lipofuscin accumulation. Studies find that intermediate lipofuscin accumulation occurs at 8 weeks via established methods (Quinn *et al.*, 2004). However, the disadvantage of this method is time-consuming and may not be practically conducted in most laboratories.

In the *in vivo* APPxPS1 AD mouse study, the mice are i.p. injected with 4 μCi [^{57}Co] Cbl in a volume of 0.2 ml sterile saline (0.9%, (w/v) NaCl) for 72 h. Although Cbl can rapidly pass through the blood-brain-barrier and store in the brain (Van den Berg *et al.*, 2003; Herrmann and Obeid, 2012), only ~0.4% of total [^{57}Co] Cbl radioactivity was detected in the mouse brain. The mechanism regulating Cbl uptake into the brain is still unknown. However, to increase the total CNS Cbl pool, stereotaxic instruments can be applied to precisely locate lateral ventricle and less amount of [^{57}Co] Cbl can be directly injected into the brain. By this method it will efficiently promote the uptake of [^{57}Co] Cbl into the brain and may attenuate the effect of dysfunctional lysosomal roadblock on intracellular Cbl transport under neuropathological conditions. Investigations into the volume of administration of [^{57}Co] Cbl cerebral injection required to affect lysosomal Cbl transport and possibly improve Cbl utilisation would be informative.

7.3 Conclusion

Lysosomes play a vital intracellular role maintaining cellular homeostasis by continually degrading cytoplasmic contents, abnormal protein aggregates and excess or damaged organelles. Lysosomes are essential subcellular organelles involved in the metabolism of intracellular Cbl utilisation. However, the important role of lysosomes that may play on intracellular Cbl transport in aging and AD has been overlooked. The current study systematically examines the proposed hypothesis that lysososmal dysfunction impairs lysosomal Cbl transport and has a significant impact on intracellular Cbl utilisation. A series of experiments were conducted to suppress lysosomal function by inhibition of lysosomal proteolysis using both pH-dependent and -independent approaches; generation of artificial lipofuscin and feeding to cultured cells; using cell model of lysosomal storage disease; applying AD-related SH-SY5Y-APP cell model and APPxPS1 AD transgenic mice. These results demonstrate that lysosomal [^{57}Co] Cbl transport is impaired under these conditions and that increased lysosomal [^{57}Co] Cbl level is concomitant with reduced lysosomal [^{57}Co] Cbl release into mitochondria and cytosol. The results also show that reduced level of mitochondrial [^{57}Co] Cbl is closely correlated with impaired Cbl-dependent MMCM activity, suggesting that inhibition of lysosomal function possibly disrupts intracellular Cbl utilisation and contributes to the deleterious increases in Hcy and MMA levels that occur in the aging brain and thereby directly accelerates neurodegeneration. Taken together, the results from the *in vitro* and *in vivo* experiments provide a detailed understanding of the impact of lysosomal dysfunction in relation to brain ageing and AD on lysosomal Cbl transport at the subcellular level. These results may explain why Cbl administration has not yielded a consistent

cognitive improvement in the ageing and AD patients because of the impaired transit of Cbl through lysosome compartment, particularly in long-lived post-mitotic cells such as neurons. More importantly, this thesis sheds light on this crucial issue and is a step towards identifying a clinical therapeutic target to improve neuronal Cbl utilisation and thus reduce the production of neurotoxic metabolites that accumulate when the coenzyme forms of Cbl do not reach their intracellular targets.

REFERENCES

Agholme, L., M. Hallbeck, E. Benedikz, J. Marcusson and K. Kagedal (2012). "Amyloid-beta secretion, generation, and lysosomal sequestration in response to proteasome inhibition: involvement of autophagy." J Alzheimers Dis **31**(2): 343-358.

Albright, T. A., H. J. Binns and B. Z. Katz (2002). "Side effects of and compliance with malaria prophylaxis in children." Journal of travel medicine **9**(6): 289-292.

Allen, L. H. (2009). "How common is vitamin B-12 deficiency?" Am J Clin Nutr **89**(2): 693S-696S.

Amagasaki, T., R. Green and D. W. Jacobsen (1990). "Expression of transcobalamin II receptors by human leukemia K562 and HL-60 cells." Blood **76**(7): 1380-1386.

Amano, T., H. Nakanishi, T. Kondo, T. Tanaka, M. Oka and K. Yamamoto (1995). "Age-related changes in cellular localization and enzymatic activities of cathepsins B, L and D in the rat trigeminal ganglion neuron." Mech Ageing Dev **83**(3): 133-141.

Amritraj, A., C. Hawkes, A. L. Phinney, H. T. Mount, C. D. Scott, D. Westaway and S. Kar (2009). "Altered levels and distribution of IGF-II/M6P receptor and lysosomal enzymes in mutant APP and APP + PS1 transgenic mouse brains." Neurobiol Aging **30**(1): 54-70.

Andres, E., S. Affenberger, S. Vinzio, J. E. Kurtz, E. Noel, G. Kaltenbach, F. Maloisel, J. L. Schlienger and J. F. Blickle (2005). "Food-cobalamin malabsorption in elderly patients: clinical manifestations and treatment." Am J Med **118**(10): 1154-1159.

Andres, E., E. Noel, G. Kaltenbach, A. E. Perrin, S. Vinzio, B. Goichot, J. L. Schlienger and J. F. Blickle (2003). "[Vitamin B12 deficiency with normal Schilling test or non-dissociation of vitamin B12 and its carrier proteins in elderly patients. A study of 60 patients]." Rev Med Interne **24**(4): 218-223.

Avila, J. (2006). "Tau phosphorylation and aggregation in Alzheimer's disease pathology." FEBS letters **580**(12): 2922-2927.

Bach, G., C. S. Chen and R. E. Pagano (1999). "Elevated lysosomal pH in Mucolipidosis type IV cells." Clin Chim Acta **280**(1-2): 173-179.

Bachmair, A., D. Finley and A. Varshavsky (1986). "In vivo half-life of a protein is a function of its amino-terminal residue." Science **234**(4773): 179-186.

Baik, H. W. and R. M. Russell (1999). "Vitamin B12 deficiency in the elderly." Annu Rev Nutr **19**: 357-377.

Ballhausen, D., L. Mittaz, O. Boulat, L. Bonafe and O. Braissant (2009). "Evidence for catabolic pathway of propionate metabolism in CNS: expression pattern of methylmalonyl-CoA mutase and propionyl-CoA carboxylase alpha-subunit in developing and adult rat brain." Neuroscience **164**(2): 578-587.

Banerjee, R. (2006). "B12 Trafficking in Mammals: A Case for Coenzyme Escort Service." ACS Chemical Biology **1**(3): 149-159.

Banerjee, R. (2006). "B12 trafficking in mammals: A for coenzyme escort service." ACS Chem Biol **1**(3): 149-159.

Banerjee, R., C. Gherasim and D. Padovani (2009). "The tinker, tailor, soldier in intracellular B12 trafficking." Curr Opin Chem Biol **13**(4): 484-491.

Beedholm-Ebsen, R., K. van de Wetering, T. Hardlei, E. Nexo, P. Borst and S. K. Moestrup (2010). "Identification of multidrug resistance protein 1 (MRP1/ABCC1) as a molecular gate for cellular export of cobalamin." Blood **115**(8): 1632-1639.

Berliner, N. and L. E. Rosenberg (1981). "Uptake and metabolism of free cyanocobalamin by cultured human fibroblasts from controls and a patient with transcobalamin II deficiency." Metabolism **30**(3): 230-236.

Bettens, K., K. Sleegers and C. Van Broeckhoven (2013). "Genetic insights in Alzheimer's disease." Lancet Neurol **12**(1): 92-104.

Beutler, E. (2004). "Enzyme replacement in Gaucher disease." PLoS Med **1**(2): e21.

Boers, G. H. (1994). "Hyperhomocysteinaemia: a newly recognized risk factor for vascular disease." Neth J Med **45**(1): 34-41.

Boivin, M. J., P. Bangirana, J. Byarugaba, R. O. Opoka, R. Idro, A. M. Jurek and C. C. John (2007). "Cognitive impairment after cerebral malaria in children: a prospective study." Pediatrics **119**(2): e360-e366.

Boland, B., A. Kumar, S. Lee, F. M. Platt, J. Wegiel, W. H. Yu and R. A. Nixon (2008). "Autophagy induction and autophagosome clearance in neurons: relationship to autophagic pathology in Alzheimer's disease." J Neurosci **28**(27): 6926-6937.

Bose, S., S. Seetharam and B. Seetharam (1995). "Membrane expression and interactions of human transcobalamin II receptor." J Biol Chem **270**(14): 8152-8157.

Brunk, U. and J. L. Ericsson (1972). "Electron microscopical studies on rat brain neurons. Localization of acid phosphatase and mode of formation of lipofuscin bodies." J Ultrastruct Res **38**(1): 1-15.

Brunk, U., J. L. Ericsson, J. Ponten and B. Westermark (1973). "Residual bodies and "aging" in cultured human glia cells. Effect of entrance into phase 3 and prolonged periods of confluence." Exp Cell Res **79**(1): 1-14.

Brunk, U. T. and A. Terman (2002). "Lipofuscin: mechanisms of age-related accumulation and influence on cell function." Free Radic Biol Med **33**(5): 611-619.

Calvaresi, E. and J. Bryan (2001). "B vitamins, cognition, and aging: a review." J Gerontol B Psychol Sci Soc Sci **56**(6): P327-339.

Carmel, R. (1995). "Malabsorption of food cobalamin." Baillieres Clin Haematol **8**(3): 639-655.

Carter, J. and C. F. Lippa (2001). "Beta-amyloid, neuronal death and Alzheimer's disease." Current molecular medicine **1**(6): 733-737.

Cataldo, A. M., J. L. Barnett, C. Pieroni and R. A. Nixon (1997). "Increased neuronal endocytosis and protease delivery to early endosomes in sporadic Alzheimer's disease: neuropathologic evidence for a mechanism of increased beta-amyloidogenesis." The Journal of neuroscience : the official journal of the Society for Neuroscience **17**(16): 6142-6151.

Cataldo, A. M., D. J. Hamilton, J. L. Barnett, P. A. Paskevich and R. A. Nixon (1996). "Properties of the endosomal-lysosomal system in the human central nervous system: disturbances mark most neurons in populations at risk to degenerate in Alzheimer's disease." J Neurosci **16**(1): 186-199.

Cataldo, A. M., D. J. Hamilton and R. A. Nixon (1994). "Lysosomal abnormalities in degenerating neurons link neuronal compromise to senile plaque development in Alzheimer disease." Brain Res **640**(1-2): 68-80.

Cataldo, A. M., P. A. Paskevich, E. Kominami and R. A. Nixon (1991). "Lysosomal hydrolases of different classes are abnormally distributed in brains of patients with Alzheimer disease." Proc Natl Acad Sci U S A **88**(24): 10998-11002.

Chafekar, S. M., F. Baas and W. Scheper (2008). "Oligomer-specific Abeta toxicity in cell models is mediated by selective uptake." Biochimica et biophysica acta **1782**(9): 523-531.

Chafekar, S. M., F. Baas and W. Scheper (2008). "Oligomer-specific Abeta toxicity in cell models is mediated by selective uptake." Biochim Biophys Acta **1782**(9): 523-531.

Chen, P. M., Z. J. Gombart and J. W. Chen (2011). "Chloroquine treatment of ARPE-19 cells leads to lysosome dilation and intracellular lipid accumulation: possible implications of lysosomal dysfunction in macular degeneration." Cell Biosci **1**(1): 10-10.

Clarke, R., A. D. Smith, K. A. Jobst, H. Refsum, L. Sutton and P. M. Ueland (1998). "Folate, vitamin B12, and serum total homocysteine levels in confirmed Alzheimer disease." Arch Neurol **55**(11): 1449-1455.

Clifford, P. M., S. Zarrabi, G. Siu, K. J. Kinsler, M. C. Kosciuk, V. Venkataraman, M. R. D'Andrea, S. Dinsmore and R. G. Nagele (2007). "Abeta peptides can enter the brain through a defective blood-brain barrier and bind selectively to neurons." Brain Res **1142**: 223-236.

Coelho, D., J. C. Kim, I. R. Miousse, S. Fung, M. du Moulin, I. Buers, T. Suormala, P. Burda, M. Frapolli, M. Stucki, P. Nurnberg, H. Thiele, H. Robenek, W.

Hohne, N. Longo, M. Pasquali, E. Mengel, D. Watkins, E. A. Shoubridge, J. Majewski, D. S. Rosenblatt, B. Fowler, F. Rutsch and M. R. Baumgartner (2012). "Mutations in ABCD4 cause a new inborn error of vitamin B12 metabolism." Nat Genet **44**(10): 1152-1155.

Coelho, D., J. C. Kim, I. R. Miousse, S. Fung, M. du Moulin, I. Buers, T. Suormala, P. Burda, M. Frapolli, M. Stucki, P. Nurnberg, H. Thiele, H. Robenek, W. Hohne, N. Longo, M. Pasquali, E. Mengel, D. Watkins, E. A. Shoubridge, J. Majewski, D. S. Rosenblatt, B. Fowler, F. Rutsch and M. R. Baumgartner (2012). "Mutations in ABCD4 cause a new inborn error of vitamin B(12) metabolism." Nat Genet **44**(10): 1152-1155.

Coelho, D., T. Suormala, M. Stucki, J. P. Lerner-Ellis, D. S. Rosenblatt, R. F. Newbold, M. R. Baumgartner and B. Fowler (2008). "Gene identification for the cblD defect of vitamin B12 metabolism." N Engl J Med **358**(14): 1454-1464.

Copper, G. (2000). "The Cell: A Molecular Approach. 2nd edition " Boston University.

Coutinho, M. F., M. J. Prata and S. Alves (2012). "Mannose-6-phosphate pathway: a review on its role in lysosomal function and dysfunction." Molecular genetics and metabolism **105**(4): 542-550.

Cuervo, A. M., L. Stefanis, R. Fredenburg, P. T. Lansbury and D. Sulzer (2004). "Impaired degradation of mutant alpha-synuclein by chaperone-mediated autophagy." Science **305**(5688): 1292-1295.

Dali-Youcef, N. and E. Andres (2009). "An update on cobalamin deficiency in adults." QJM **102**(1): 17-28.

Daniels, L. B., R. H. Glew, N. S. Radin and R. R. Vunnam (1980). "A revised fluorometric assay for Gaucher's disease using conduritol-beta-epoxide with liver as the source of Beta-glucosidase." Clin Chim Acta **106**(2): 155-163.

Das, P. K., G. J. Murray, A. E. Gal and J. A. Barranger (1987). "Glucocerebrosidase deficiency and lysosomal storage of glucocerebroside induced in cultured macrophages." Exp Cell Res **168**(2): 463-474.

De-Paula, V. J., M. Radanovic, B. S. Diniz and O. V. Forlenza (2012). "Alzheimer's disease." Sub-cellular biochemistry **65**: 329-352.

De Duve, C., B. C. Pressman, R. Gianetto, R. Wattiaux and F. Appelmans (1955). "Tissue fractionation studies. 6. Intracellular distribution patterns of enzymes in rat-liver tissue." Biochem J **60**(4): 604-617.

Dhamodharan, R., M. A. Jordan, D. Thrower, L. Wilson and P. Wadsworth (1995). "Vinblastine suppresses dynamics of individual microtubules in living interphase cells." Molecular biology of the cell **6**(9): 1215-1229.

Ditaranto, K., T. L. Tekirian and A. J. Yang (2001). "Lysosomal membrane damage in soluble Abeta-mediated cell death in Alzheimer's disease." Neurobiol Dis **8**(1): 19-31.

Douaud, G., H. Refsum, C. A. de Jager, R. Jacoby, T. E. Nichols, S. M. Smith and A. D. Smith (2013). "Preventing Alzheimer's disease-related gray matter atrophy by B-vitamin treatment." Proceedings of the National Academy of Sciences of the United States of America **110**(23): 9523-9528.

Double, K. L., V. N. Dedov, H. Fedorow, E. Kettle, G. M. Halliday, B. Garner and U. T. Brunk (2008). "The comparative biology of neuromelanin and lipofuscin in the human brain." Cell Mol Life Sci **65**(11): 1669-1682.

Dunlop, R. A., U. T. Brunk and K. J. Rodgers (2009). "Oxidized proteins: mechanisms of removal and consequences of accumulation." IUBMB life **61**(5): 522-527.

Fedosov, S. N., L. Berglund, N. U. Fedosova, E. Nexo and T. E. Petersen (2002). "Comparative analysis of cobalamin binding kinetics and ligand protection for intrinsic factor, transcobalamin, and haptocorrin." The Journal of biological chemistry **277**(12): 9989-9996.

Ferguson, P. J., J. R. Phillips, M. Selner and C. E. Cass (1984). "Differential activity of vincristine and vinblastine against cultured cells." Cancer research **44**(8): 3307-3312.

Fernandes-Costa, F. and J. Metz (1982). "Vitamin B12 binders (transcobalamins) in serum." Crit Rev Clin Lab Sci **18**(1): 1-30.

Fernandez-Roig, S., S. C. Lai, M. M. Murphy, J. Fernandez-Ballart and E. V. Quadros (2012). "Vitamin B12 deficiency in the brain leads to DNA hypomethylation in the TCblR/CD320 knockout mouse." Nutr Metab (Lond) **9**: 41.

Ferrari, G., A. M. Knight, C. Watts and J. Pieters (1997). "Distinct intracellular compartments involved in invariant chain degradation and antigenic peptide loading of major histocompatibility complex (MHC) class II molecules." J Cell Biol **139**(6): 1433-1446.

Fiskerstrand, T., B. Riedel, P. M. Ueland, B. Seetharam, E. H. Pezacka, S. Gulati, S. Bose, R. Banerjee, R. K. Berge and H. Refsum (1998). "Disruption of a regulatory system involving cobalamin distribution and function in a methionine-dependent human glioma cell line." J Biol Chem **273**(32): 20180-20184.

Fuso, A., L. Seminara, R. A. Cavallaro, F. D'Anselmi and S. Scarpa (2005). "S-adenosylmethionine/homocysteine cycle alterations modify DNA methylation status with consequent deregulation of PS1 and BACE and beta-amyloid production." Mol Cell Neurosci **28**(1): 195-204.

Gailus, S., W. Hohne, B. Gasnier, P. Nurnberg, B. Fowler and F. Rutsch (2010). "Insights into lysosomal cobalamin trafficking: lessons learned from cblF disease." J Mol Med **88**(5): 459-466.

Geng, Y., L. Kohli, B. J. Klocke and K. A. Roth (2010). "Chloroquine-induced autophagic vacuole accumulation and cell death in glioma cells is p53 independent." Neuro-oncology **12**(5): 473-481.

Gonda, D. K., A. Bachmair, I. Wunning, J. W. Tobias, W. S. Lane and A. Varshavsky (1989). "Universality and structure of the N-end rule." J Biol Chem **264**(28): 16700-16712.

Gonzalez-Noriega, A., J. H. Grubb, V. Talkad and W. S. Sly (1980). "Chloroquine inhibits lysosomal enzyme pinocytosis and enhances lysosomal enzyme secretion by impairing receptor recycling." J Cell Biol **85**(3): 839-852.

Grabowski, G. A. (2008). "Phenotype, diagnosis, and treatment of Gaucher's disease." Lancet **372**(9645): 1263-1271.

Guan, X., B. Hoffman, C. Dwivedi and D. P. Matthees (2003). "A simultaneous liquid chromatography/mass spectrometric assay of glutathione, cysteine, homocysteine and their disulfides in biological samples." Journal of pharmaceutical and biomedical analysis **31**(2): 251-261.

Hall, C. A. (1977). "The carriers of native vitamin B12 in normal human serum." Clin Sci Mol Med **53**(5): 453-457.

Hall, C. A. (1984). "The uptake of vitamin B12 by human lymphocytes and the relationships to the cell cycle." J Lab Clin Med **103**(1): 70-81.

Hannibal, L., A. Axhemi, A. V. Glushchenko, E. S. Moreira, N. E. Brasch and D. W. Jacobsen (2008). "Accurate assessment and identification of naturally occurring cellular cobalamins." Clin Chem Lab Med **46**(12): 1739-1746.

Hannibal, L., J. Kim, N. E. Brasch, S. Wang, D. S. Rosenblatt, R. Banerjee and D. W. Jacobsen (2009). "Processing of alkylcobalamins in mammalian cells: A role for the MMACHC (cblC) gene product." Mol Genet Metab **97**(4): 260-266.

Healton, E. B., D. G. Savage, J. C. Brust, T. J. Garrett and J. Lindenbaum (1991). "Neurologic aspects of cobalamin deficiency." Medicine (Baltimore) **70**(4): 229-245.

Hejazi, L., J. W. Wong, D. Cheng, N. Proschogo, D. Ebrahimi, B. Garner and A. S. Don (2011). "Mass and relative elution time profiling: two-dimensional analysis of sphingolipids in Alzheimer's disease brains." The Biochemical journal **438**(1): 165-175.

Herrmann, W. and R. Obeid (2012). "Cobalamin deficiency." Subcell Biochem **56**: 301-322.

Herrmann, W., H. Schorr, M. Bodis, J. P. Knapp, A. Muller, G. Stein and J. Geisel (2000). "Role of homocysteine, cystathionine and methylmalonic acid measurement for diagnosis of vitamin deficiency in high-aged subjects." European journal of clinical investigation **30**(12): 1083-1089.

Hodgkin, D. C., J. Kamper, M. Mackay, J. Pickworth, K. N. Trueblood and J. G. White (1956). "Structure of vitamin B12." Nature **178**(4524): 64-66.

Hygum, K., D. L. Lildballe, E. H. Greibe, A. L. Morkbak, S. S. Poulsen, B. S. Sorensen, T. E. Petersen and E. Nexo (2011). "Mouse transcobalamin has features resembling both human transcobalamin and haptocorrin." PLoS One **6**(5): e20638.

Ivy, G. O., S. Kanai, M. Ohta, G. Smith, Y. Sato, M. Kobayashi and K. Kitani (1989). "Lipofuscin-like substances accumulate rapidly in brain, retina and internal organs with cysteine protease inhibition." Adv Exp Med Biol **266**: 31-45; discussion 45-37.

Ivy, G. O., F. Schottler, J. Wenzel, M. Baudry and G. Lynch (1984). "Inhibitors of lysosomal enzymes: accumulation of lipofuscin-like dense bodies in the brain." Science **226**(4677): 985-987.

Jacobsen, D. W. (2000). "Hyperhomocysteinemia and oxidative stress: time for a reality check?" Arterioscler Thromb Vasc Biol **20**(5): 1182-1184.

Jacobsen, D. W. and A. V. Glushchenko (2009). "The transcobalamin receptor, redux." Blood **113**: 3-4.

Jmoudiak, M. and A. H. Futerman (2005). "Gaucher disease: pathological mechanisms and modern management." Br J Haematol **129**(2): 178-188.

Kim, J., J. M. Basak and D. M. Holtzman (2009). "The role of apolipoprotein E in Alzheimer's disease." Neuron **63**(3): 287-303.

Kim, W. S., H. Li, K. Ruberu, S. Chan, D. A. Elliott, J. K. Low, D. Cheng, T. Karl and B. Garner (2013). "Deletion of Abca7 increases cerebral amyloid-beta accumulation in the J20 mouse model of Alzheimer's disease." J Neurosci **33**(10): 4387-4394.

Koo, E. H., S. L. Squazzo, D. J. Selkoe and C. H. Koo (1996). "Trafficking of cell-surface amyloid beta-protein precursor. I. Secretion, endocytosis and

recycling as detected by labeled monoclonal antibody." Journal of cell science **109**(5): 991-998.

Korolchuk, V. I., F. M. Menzies and D. C. Rubinsztein (2010). "Mechanisms of cross-talk between the ubiquitin-proteasome and autophagy-lysosome systems." FEBS letters **584**(7): 1393-1398.

Krasinski, S. D., R. M. Russell, I. M. Samloff, R. A. Jacob, G. E. Dallal, R. B. McGandy and S. C. Hartz (1986). "Fundic atrophic gastritis in an elderly population. Effect on hemoglobin and several serum nutritional indicators." J Am Geriatr Soc **34**(11): 800-806.

Kruman, II, T. S. Kumaravel, A. Lohani, W. A. Pedersen, R. G. Cutler, Y. Kruman, N. Haughey, J. Lee, M. Evans and M. P. Mattson (2002). "Folic acid deficiency and homocysteine impair DNA repair in hippocampal neurons and sensitize them to amyloid toxicity in experimental models of Alzheimer's disease." J Neurosci **22**(5): 1752-1762.

Kurz, T., J. W. Eaton and U. T. Brunk (2011). "The role of lysosomes in iron metabolism and recycling." The international journal of biochemistry & cell biology **43**(12): 1686-1697.

Kurz, T., A. Terman, B. Gustafsson and U. T. Brunk (2008). "Lysosomes and oxidative stress in aging and apoptosis." Biochim Biophys Acta **1780**(11): 1291-1303.

Kurz, T., A. Terman, B. Gustafsson and U. T. Brunk (2008). "Lysosomes in iron metabolism, ageing and apoptosis." Histochemistry and cell biology **129**(4): 389-406.

Langui, D., N. Girardot, K. H. El Hachimi, B. Allinquant, V. Blanchard, L. Pradier and C. Duyckaerts (2004). "Subcellular topography of neuronal Abeta peptide in APPxPS1 transgenic mice." Am J Pathol **165**(5): 1465-1477.

Langui, D., N. Girardot, K. H. El Hachimi, B. Allinquant, V. Blanchard, L. Pradier and C. Duyckaerts (2004). "Subcellular topography of neuronal Abeta peptide in APPxPS1 transgenic mice." The American journal of pathology **165**(5): 1465-1477.

Lee, J. H., W. H. Yu, A. Kumar, S. Lee, P. S. Mohan, C. M. Peterhoff, D. M. Wolfe, M. Martinez-Vicente, A. C. Massey, G. Sovak, Y. Uchiyama, D. Westaway, A. M. Cuervo and R. A. Nixon (2010). "Lysosomal proteolysis and autophagy require presenilin 1 and are disrupted by Alzheimer-related PS1 mutations." Cell **141**(7): 1146-1158.

Lee, M. J., J. H. Lee and D. C. Rubinsztein (2013). "Tau degradation: the ubiquitin-proteasome system versus the autophagy-lysosome system." Progress in neurobiology **105**: 49-59.

Lehmann, M., C. G. Gottfries and B. Regland (1999). "Identification of cognitive impairment in the elderly: homocysteine is an early marker." Dement Geriatr Cogn Disord **10**(1): 12-20.

Levine, B. and G. Kroemer (2008). "Autophagy in the pathogenesis of disease." Cell **132**(1): 27-42.

Levitt, A. J. and H. Karlinsky (1992). "Folate, vitamin B12 and cognitive impairment in patients with Alzheimer's disease." Acta psychiatrica scandinavica **86**(4): 301-305.

Li, H., G. Evin, A. F. Hill, Y. H. Hung, A. I. Bush and B. Garner (2012). "Dissociation of ERK signalling inhibition from the anti-amyloidogenic action of synthetic ceramide analogues." Clin Sci (Lond) **122**(9): 409-419.

Li, M., B. Khambu, H. Zhang, J. H. Kang, X. Chen, D. Chen, L. Vollmer, P. Q. Liu, A. Vogt and X. M. Yin (2013). "Suppression of lysosome function induces autophagy via a feedback down-regulation of MTOR complex 1 (MTORC1) activity." J Biol Chem **288**(50): 35769-35780.

Lie, S. O. and B. Schofield (1973). "Inactivation of lysosomal function in normal cultured human fibroblasts by chloroquine." Biochemical pharmacology **22**(23): 3109-3114.

Lildballe, D. L., E. Mutti, H. Birn and E. Nexo (2012). "Maximal load of the vitamin B12 transport system: a study on mice treated for four weeks with high-dose vitamin B12 or cobinamide." PLoS One **7**(10): e46657.

Linnell, J. C. and H. R. Bhatt (1995). "Inherited errors of cobalamin metabolism and their management." Baillieres Clin Haematol **8**(3): 567-601.

Manunta, M., L. Izzo, R. Duncan and A. T. Jones (2007). "Establishment of subcellular fractionation techniques to monitor the intracellular fate of polymer therapeutics II. Identification of endosomal and lysosomal compartments in HepG2 cells combining single-step subcellular fractionation with fluorescent imaging." J Drug Target **15**(1): 37-50.

Maric, M. A., M. D. Taylor and J. S. Blum (1994). "Endosomal aspartic proteinases are required for invariant-chain processing." Proc Natl Acad Sci U S A **91**(6): 2171-2175.

Maron, B. A. and J. Loscalzo (2009). "The treatment of hyperhomocysteinemia." Annu Rev Med **60**: 39-54.

Martin, B. M., E. Sidransky and E. I. Ginns (1989). "Gaucher's disease: advances and challenges." Adv Pediatr **36**: 277-306.

Martins, A. M., E. R. Valadares, G. Porta, J. Coelho, J. Semionato Filho, M. A. Pianovski, M. S. Kerstenetzky, F. Montoril Mde, P. C. Aranda, R. F. Pires, R. M. Mota and T. C. Bortolheiro (2009). "Recommendations on diagnosis, treatment, and monitoring for Gaucher disease." J Pediatr **155**(4 Suppl): S10-18.

Marzella, L., P. O. Sandberg and H. Glaumann (1980). "Autophagic degradation in rat liver after vinblastine treatment." Experimental cell research **128**(2): 291-301.

McBride, H. M., M. Neuspiel and S. Wasiak (2006). "Mitochondria: more than just a powerhouse." Curr Biol **16**(14): R551-560.

McCaddon, A. (2006). "Homocysteine and cognition--a historical perspective." J Alzheimers Dis **9**(4): 361-380.

McCaddon, A. and P. R. Hudson (2010). "L-methylfolate, methylcobalamin, and N-acetylcysteine in the treatment of Alzheimer's disease-related cognitive decline." CNS Spectr **15**(1 Suppl 1): 2-5; discussion 6.

McMahon, J. A., T. J. Green, C. M. Skeaff, R. G. Knight, J. I. Mann and S. M. Williams (2006). "A controlled trial of homocysteine lowering and cognitive performance." N Engl J Med **354**(26): 2764-2772.

Mellman, I. (1996). "Endocytosis and molecular sorting." Annu Rev Cell Dev Biol **12**: 575-625.

Mellman, I., H. F. Willard and L. E. Rosenberg (1978). "Cobalamin binding and cobalamin-dependent enzyme activity in normal and mutant human fibroblasts." J Clin Invest **62**(5): 952-960.

Michaelides, M., N. B. Stover, P. J. Francis and R. G. Weleber (2011). "Retinal toxicity associated with hydroxychloroquine and chloroquine: risk factors, screening, and progression despite cessation of therapy." Archives of ophthalmology **129**(1): 30-39.

Mindell, J. A. (2012). "Lysosomal acidification mechanisms." Annu Rev Physiol **74**: 69-86.

Mizushima, N., T. Yoshimori and B. Levine (2010). "Methods in mammalian autophagy research." Cell **140**(3): 313-326.

Moestrup, S. K. and P. J. Verroust (2001). "Megalin- and cubilin-mediated endocytosis of protein-bound vitamins, lipids, and hormones in polarized epithelia." Annu Rev Nutr **21**: 407-428.

Molano, A., Z. Huang, M. G. Marko, A. Azzi, D. Wu, E. Wang, S. L. Kelly, A. H. Merrill, Jr., S. C. Bunnell and S. N. Meydani (2012). "Age-dependent changes in the sphingolipid composition of mouse CD4+ T cell membranes and immune synapses implicate glucosylceramides in age-related T cell dysfunction." PloS one **7**(10): e47650.

Moore, E., A. Mander, D. Ames, R. Carne, K. Sanders and D. Watters (2012). "Cognitive impairment and vitamin B12: a review." International psychogeriatrics / IPA **24**(4): 541-556.

Moras, E., A. Hosack, D. Watkins and D. S. Rosenblatt (2007). "Mitochondrial vitamin B12-binding proteins in patients with inborn errors of cobalamin metabolism." Mol Genet Metab **90**(2): 140-147.

Morris, M. S. (2003). "Homocysteine and Alzheimer's disease." Lancet Neurol **2**(7): 425-428.

Mueller-Steiner, S., Y. Zhou, H. Arai, E. D. Roberson, B. Sun, J. Chen, X. Wang, G. Yu, L. Esposito, L. Mucke and L. Gan (2006). "Antiamyloidogenic and neuroprotective functions of cathepsin B: implications for Alzheimer's disease." Neuron **51**(6): 703-714.

Munnell, J. F. and R. Getty (1968). "Rate of accumulation of cardiac lipofuscin in the aging canine." J Gerontol **23**(2): 154-158.

Murphy, M. P. and H. LeVine, 3rd (2010). "Alzheimer's disease and the amyloid-beta peptide." Journal of Alzheimer's disease : JAD **19**(1): 311-323.

Myers, B. M., P. S. Tietz, J. E. Tarara and N. F. LaRusso (1995). "Dynamic measurements of the acute and chronic effects of lysosomotropic agents on hepatocyte lysosomal pH using flow cytometry." Hepatology **22**(5): 1519-1526.

Nakano, M. and S. Gotoh (1992). "Accumulation of cardiac lipofuscin depends on metabolic rate of mammals." J Gerontol **47**(4): B126-129.

Newburg, D. S., T. B. Shea, S. Yatziv, S. S. Raghavan and R. H. McCluer (1988). "Macrophages exposed in vitro to conduritol B epoxide resemble Gaucher cells." Exp Mol Pathol **48**(3): 317-323.

Nilsson-Ehle, H. (1998). "Age-related changes in cobalamin (vitamin B12) handling. Implications for therapy." Drugs Aging **12**(4): 277-292.

Nilsson, E. and D. Yin (1997). "Preparation of artificial ceroid/lipofuscin by UV-oxidation of subcellular organelles." Mech Ageing Dev **99**(1): 61-78.

Nixon, R. A. (2007). "Autophagy, amyloidogenesis and Alzheimer disease." J Cell Sci **120**(Pt 23): 4081-4091.

Nixon, R. A., A. M. Cataldo and P. M. Mathews (2000). "The endosomal-lysosomal system of neurons in Alzheimer's disease pathogenesis: a review." Neurochem Res **25**(9-10): 1161-1172.

Nixon, R. A., J. Wegiel, A. Kumar, W. H. Yu, C. Peterhoff, A. Cataldo and A. M. Cuervo (2005). "Extensive involvement of autophagy in Alzheimer disease: an immuno-electron microscopy study." J Neuropathol Exp Neurol **64**(2): 113-122.

Nixon, R. A. and D. S. Yang (2011). "Autophagy failure in Alzheimer's disease--locating the primary defect." Neurobiol Dis **43**(1): 38-45.

Nixon, R. A., D. S. Yang and J. H. Lee (2008). "Neurodegenerative lysosomal disorders: a continuum from development to late age." Autophagy **4**(5): 590-599.

Nothwang, H. G., M. Becker, K. Ociepka and E. Friauf (2003). "Protein analysis in the rat auditory brainstem by two-dimensional gel electrophoresis and mass spectrometry." Brain Res Mol Brain Res **116**(1-2): 59-69.

Obeid, R. (2013). "The metabolic burden of methyl donor deficiency with focus on the betaine homocysteine methyltransferase pathway." Nutrients **5**(9): 3481-3495.

Oliva, O., G. Rez, Z. Palfia and E. Fellinger (1992). "Dynamics of vinblastine-induced autophagocytosis in murine pancreatic acinar cells: influence of cycloheximide post-treatments." Experimental and molecular pathology **56**(1): 76-86.

Pacheco-Quinto, J., E. B. Rodriguez de Turco, S. DeRosa, A. Howard, F. Cruz-Sanchez, K. Sambamurti, L. Refolo, S. Petanceska and M. A. Pappolla (2006). "Hyperhomocysteinemic Alzheimer's mouse model of amyloidosis

shows increased brain amyloid β peptide levels." Neurobiology of disease **22**(3): 651-656.

Pasternak, S. H., J. W. Callahan and D. J. Mahuran (2004). "The role of the endosomal/lysosomal system in amyloid-beta production and the pathophysiology of Alzheimer's disease: reexamining the spatial paradox from a lysosomal perspective." J Alzheimers Dis **6**(1): 53-65.

Powell, S. R., P. Wang, A. Divald, S. Teichberg, V. Haridas, T. W. McCloskey, K. J. Davies and H. Katzeff (2005). "Aggregates of oxidized proteins (lipofuscin) induce apoptosis through proteasome inhibition and dysregulation of proapoptotic proteins." Free radical biology & medicine **38**(8): 1093-1101.

Quadri, P., C. Fragiacomo, R. Pezzati, E. Zanda, G. Forloni, M. Tettamanti and U. Lucca (2004). "Homocysteine, folate, and vitamin B-12 in mild cognitive impairment, Alzheimer disease, and vascular dementia." Am J Clin Nutr **80**(1): 114-122.

Quadros, E. V., A. L. Regec, K. M. Khan, E. Quadros and S. P. Rothenberg (1999). "Transcobalamin II synthesized in the intestinal villi facilitates transfer of cobalamin to the portal blood." Am J Physiol **277**(1 Pt 1): G161-166.

Quinn, C. M., K. Kagedal, A. Terman, U. Stroikin, U. T. Brunk, W. Jessup and B. Garner (2004). "Induction of fibroblast apolipoprotein E expression during apoptosis, starvation-induced growth arrest and mitosis." Biochem J **378**(Pt 3): 753-761.

Refsum, H., P. M. Ueland, O. Nygard and S. E. Vollset (1998). "Homocysteine and cardiovascular disease." Annu Rev Med **49**: 31-62.

Reis, P. A., C. M. Comim, F. Hermani, B. Silva, T. Barichello, A. C. Portella, F. C. Gomes, I. M. Sab, V. S. Frutuoso, M. F. Oliveira, P. T. Bozza, F. A. Bozza,

F. Dal-Pizzol, G. A. Zimmerman, J. Quevedo and H. C. Castro-Faria-Neto (2010). "Cognitive dysfunction is sustained after rescue therapy in experimental cerebral malaria, and is reduced by additive antioxidant therapy." PLoS pathogens **6**(6): e1000963.

Reynolds, E. (2006). "Vitamin B12, folic acid, and the nervous system." Lancet Neurol **5**(11): 949-960.

Rosenberg, L. E., L. Patel and A. C. Lilljeqvist (1975). "Absence of an intracellular cobalamin-binding protein in cultured fibroblasts from patients with defective synthesis of 5'-deoxyadenosylcobalamin and methylcobalamin." Proc Natl Acad Sci U S A **72**(11): 4617-4621.

Rosenblatt, D. S., A. Hosack, N. V. Matiaszuk, B. A. Cooper and R. Laframboise (1985). "Defect in vitamin B12 release from lysosomes: newly described inborn error of vitamin B12 metabolism." Science **228**(4705): 1319-1321.

Rubinsztein, D. C. (2006). "The roles of intracellular protein-degradation pathways in neurodegeneration." Nature **443**(7113): 780-786.

Rutsch, F., S. Gailus, I. R. Miousse, T. Suormala, C. Sagne, M. R. Toliat, G. Nurnberg, T. Wittkampf, I. Buers, A. Sharifi, M. Stucki, C. Becker, M. Baumgartner, H. Robenek, T. Marquardt, W. Hohne, B. Gasnier, D. S. Rosenblatt, B. Fowler and P. Nurnberg (2009). "Identification of a putative lysosomal cobalamin exporter altered in the cblF defect of vitamin B12 metabolism." Nat Genet **41**(2): 234-239.

Sachdev, P. S., M. Valenzuela, X. L. Wang, J. C. Looi and H. Brodaty (2002). "Relationship between plasma homocysteine levels and brain atrophy in healthy elderly individuals." Neurology **58**(10): 1539-1541.

Scarlett, J. D., H. Read and K. O'Dea (1992). "Protein-bound cobalamin absorption declines in the elderly." Am J Hematol **39**(2): 79-83.

Schwarz, A., E. Rapaport, K. Hirschberg and A. H. Futerman (1995). "A regulatory role for sphingolipids in neuronal growth. Inhibition of sphingolipid synthesis and degradation have opposite effects on axonal branching." J Biol Chem **270**(18): 10990-10998.

Seetharam, B. and R. R. Yammani (2003). "Cobalamin transport proteins and their cell-surface receptors." Expert Rev Mol Med **5**(18): 1-18.

Selhub, J. (1999). "Homocysteine metabolism." Annu Rev Nutr **19**: 217-246.

Serot, J. M., F. Barbe, E. Arning, T. Bottiglieri, P. Franck, P. Montagne and J. P. Nicolas (2005). "Homocysteine and methylmalonic acid concentrations in cerebrospinal fluid: relation with age and Alzheimer's disease." J Neurol Neurosurg Psychiatry **76**(11): 1585-1587.

Seshadri, S., A. Beiser, J. Selhub, P. F. Jacques, I. H. Rosenberg, R. B. D'Agostino, P. W. Wilson and P. A. Wolf (2002). "Plasma homocysteine as a risk factor for dementia and Alzheimer's disease." N Engl J Med **346**(7): 476-483.

Seshadri, S., P. A. Wolf, A. S. Beiser, J. Selhub, R. Au, P. F. Jacques, M. Yoshita, I. H. Rosenberg, R. B. D'Agostino and C. DeCarli (2008). "Association of plasma total homocysteine levels with subclinical brain injury: cerebral volumes, white matter hyperintensity, and silent brain infarcts at volumetric magnetic resonance imaging in the Framingham Offspring Study." Arch Neurol **65**(5): 642-649.

Sillence, D. J. (2007). "New insights into glycosphingolipid functions—storage, lipid rafts, and translocators." International review of cytology **262**: 151-189.

Sillence, D. J. (2013). "Glucosylceramide modulates endolysosomal pH in Gaucher disease." Mol Genet Metab **109**(2): 194-200.

Sillence, D. J. and F. M. Platt (2003). "Storage diseases: new insights into sphingolipid functions." Trends in cell biology **13**(4): 195-203.

Silva, D. F., A. R. Esteves, D. M. Arduino, C. R. Oliveira and S. M. Cardoso (2011). "Amyloid-beta-induced mitochondrial dysfunction impairs the autophagic lysosomal pathway in a tubulin dependent pathway." J Alzheimers Dis **26**(3): 565-581.

Sitte, N., M. Huber, T. Grune, A. Ladhoff, W. D. Doecke, T. Von Zglinicki and K. J. Davies (2000). "Proteasome inhibition by lipofuscin/ceroid during postmitotic aging of fibroblasts." FASEB J **14**(11): 1490-1498.

Smith, A. D. (2008). "The worldwide challenge of the dementias: a role for B vitamins and homocysteine?" Food Nutr Bull **29**(2 Suppl): S143-172.

Smith, A. D., S. M. Smith, C. A. de Jager, P. Whitbread, C. Johnston, G. Agacinski, A. Oulhaj, K. M. Bradley, R. Jacoby and H. Refsum (2010). "Homocysteine-lowering by B vitamins slows the rate of accelerated brain atrophy in mild cognitive impairment: a randomized controlled trial." PLoS One **5**(9): e12244.

Sohal, R. S. and U. T. Brunk (1989). "Lipofuscin as an indicator of oxidative stress and aging." Adv Exp Med Biol **266**: 17-26; discussion 27-19.

Stadtman, E. R. (1992). "Protein oxidation and aging." Science **257**(5074): 1220-1224.

Strehler, B. L. (1964). "On the Histochemistry and Ultrastructure of Age Pigment." Adv Gerontol Res **18**: 343-384.

Terman, A. and U. T. Brunk (1998). "Ceroid/lipofuscin formation in cultured human fibroblasts: the role of oxidative stress and lysosomal proteolysis." Mech Ageing Dev **104**(3): 277-291.

Terman, A. and U. T. Brunk (1998). "Lipofuscin: mechanisms of formation and increase with age." APMIS **106**(2): 265-276.

Terman, A. and U. T. Brunk (1998). "On the degradability and exocytosis of ceroid/lipofuscin in cultured rat cardiac myocytes." Mech Ageing Dev **100**(2): 145-156.

Terman, A. and U. T. Brunk (2004). "Lipofuscin." Int J Biochem Cell Biol **36**(8): 1400-1404.

Terman, A. and U. T. Brunk (2006). "Oxidative stress, accumulation of biological 'garbage', and aging." Antioxid Redox Signal **8**(1-2): 197-204.

Terman, A., H. Dalen, J. W. Eaton, J. Neuzil and U. T. Brunk (2004). "Aging of cardiac myocytes in culture: oxidative stress, lipofuscin accumulation, and mitochondrial turnover." Ann N Y Acad Sci **1019**: 70-77.

Terman, A., B. Gustafsson and U. T. Brunk (2006). "The lysosomal-mitochondrial axis theory of postmitotic aging and cell death." Chem Biol Interact **163**(1-2): 29-37.

Terman, A., T. Kurz, M. Navratil, E. A. Arriaga and U. T. Brunk (2010). "Mitochondrial turnover and aging of long-lived postmitotic cells: the mitochondrial-lysosomal axis theory of aging." Antioxid Redox Signal **12**(4): 503-535.

Terman, A. and S. Sandberg (2002). "Proteasome inhibition enhances lipofuscin formation." Ann N Y Acad Sci **973**: 309-312.

Thaw, H. H., V. P. Collins and U. T. Brunk (1984). "Influence of oxygen tension, pro-oxidants and antioxidants on the formation of lipid peroxidation products (lipofuscin) in individual cultivated human glial cells." Mech Ageing Dev **24**(2): 211-223.

Troen, A. M., M. Shea-Budgell, B. Shukitt-Hale, D. E. Smith, J. Selhub and I. H. Rosenberg (2008). "B-vitamin deficiency causes hyperhomocysteinemia and vascular cognitive impairment in mice." Proc Natl Acad Sci U S A **105**(34): 12474-12479.

Van den Berg, M. P., P. Merkus, S. G. Romeijn, J. C. Verhoef and F. W. Merkus (2003). "Hydroxocobalamin uptake into the cerebrospinal fluid after nasal and intravenous delivery in rats and humans." J Drug Target **11**(6): 325-331.

van Meerloo, J., G. J. Kaspers and J. Cloos (2011). "Cell sensitivity assays: the MTT assay." Methods in molecular biology **731**: 237-245.

Vitner, E. B. and A. H. Futerman (2013). "Neuronal forms of Gaucher disease." Handb Exp Pharmacol(216): 405-419.

von Zglinicki, T., E. Nilsson, W. D. Docke and U. T. Brunk (1995). "Lipofuscin accumulation and ageing of fibroblasts." Gerontology **41 Suppl 2**: 95-108.

Walker, J. M. (1994). "The bicinchoninic acid (BCA) assay for protein quantitation." Methods in molecular biology **32**: 5-8.

Willard, H. F., L. M. Ambani, A. C. Hart, M. J. Mahoney and L. E. Rosenberg (1976). "Rapid prenatal and postnatal detection of inborn errors of propionate, methylmalonate, and cobalamin metabolism: a sensitive assay using cultured cells." Human genetics **34**(3): 277-283.

Williams, J. H., E. A. Pereira, M. M. Budge and K. M. Bradley (2002). "Minimal hippocampal width relates to plasma homocysteine in community-dwelling older people." Age and ageing **31**(6): 440-444.

Williamson, J., J. Goldman and K. S. Marder (2009). "Genetic aspects of Alzheimer disease." The neurologist **15**(2): 80-86.

Wilquet, V. and B. De Strooper (2004). "Amyloid-beta precursor protein processing in neurodegeneration." Current opinion in neurobiology **14**(5): 582-588.

Wolfe, D. M., J. H. Lee, A. Kumar, S. Lee, S. J. Orenstein and R. A. Nixon (2013). "Autophagy failure in Alzheimer's disease and the role of defective lysosomal acidification." Eur J Neurosci **37**(12): 1949-1961.

Wolfe, D. M., J. H. Lee, A. Kumar, S. Lee, S. J. Orenstein and R. A. Nixon (2013). "Autophagy failure in Alzheimer's disease and the role of defective lysosomal acidification." The European journal of neuroscience **37**(12): 1949-1961.

Yamani, L., B. F. Gibbs, B. M. Gilfix, D. Watkins, A. Hosack and D. S. Rosenblatt (2008). "Transcobalamin in cultured fibroblasts from patients with inborn errors of vitamin B12 metabolism." Mol Genet Metab **95**(1-2): 104-106.

Yang, A. J., D. Chandswangbhuvana, L. Margol and C. G. Glabe (1998). "Loss of endosomal/lysosomal membrane impermeability is an early event in amyloid Abeta1-42 pathogenesis." J Neurosci Res **52**(6): 691-698.

Yang, D. S., P. Stavrides, P. S. Mohan, S. Kaushik, A. Kumar, M. Ohno, S. D. Schmidt, D. Wesson, U. Bandyopadhyay, Y. Jiang, M. Pawlik, C. M. Peterhoff, A. J. Yang, D. A. Wilson, P. St George-Hyslop, D. Westaway, P. M. Mathews, E. Levy, A. M. Cuervo and R. A. Nixon (2011). "Reversal of autophagy dysfunction in the TgCRND8 mouse model of Alzheimer's disease

ameliorates amyloid pathologies and memory deficits." Brain **134**(Pt 1): 258-277.

Yassin, M. S., J. Ekblom, M. Xilinas, C. G. Gottfries and L. Oreland (2000). "Changes in uptake of vitamin B(12) and trace metals in brains of mice treated with clioquinol." J Neurol Sci **173**(1): 40-44.

Yatziv, S., D. S. Newburg, N. Livni, G. Barfi and E. H. Kolodny (1988). "Gaucher-like changes in human blood-derived macrophages induced by beta-glucocerebrosidase inhibition." J Lab Clin Med **111**(4): 416-420.

Youngdahl-Turner, P., L. E. Rosenberg and R. H. Allen (1978). "Binding and uptake of transcobalamin II by human fibroblasts." J Clin Invest **61**(1): 133-141.

Yu, Z., H. L. Persson, J. W. Eaton and U. T. Brunk (2003). "Intralysosomal iron: a major determinant of oxidant-induced cell death." Free Radic Biol Med **34**(10): 1243-1252.

Yuan, X. M., W. Li, H. Dalen, J. Lotem, R. Kama, L. Sachs and U. T. Brunk (2002). "Lysosomal destabilization in p53-induced apoptosis." Proc Natl Acad Sci U S A **99**(9): 6286-6291.

Zhang, C. E., W. Wei, Y. H. Liu, J. H. Peng, Q. Tian, G. P. Liu, Y. Zhang and J. Z. Wang (2009). "Hyperhomocysteinemia increases beta-amyloid by enhancing expression of gamma-secretase and phosphorylation of amyloid precursor protein in rat brain." Am J Pathol **174**(4): 1481-1491.

Zhao, H., U. T. Brunk and B. Garner (2011). "Age-related lysosomal dysfunction: an unrecognized roadblock for cobalamin trafficking?" Cell Mol Life Sci **68**(24): 3963-3969.

Zhao, H., K. Ruberu, H. Li and B. Garner (2013). "Analysis of subcellular [57Co] cobalamin distribution in SH-SY5Y neurons and brain tissue." J Neurosci Methods **217**(1-2): 67-74.

Zhao, H., K. Ruberu, H. Li and B. Garner (2013). "Analysis of subcellular [Co] cobalamin distribution in SH-SY5Y neurons and brain tissue." J Neurosci Methods **217**(1-2): 67-74.

Zhao, H., K. Ruberu, H. Li and B. Garner (2014). "Perturbation of neuronal cobalamin transport by lysosomal enzyme inhibition." Bioscience reports.

Zheng, L., K. Kagedal, N. Dehvari, E. Benedikz, R. Cowburn, J. Marcusson and A. Terman (2009). "Oxidative stress induces macroautophagy of amyloid beta-protein and ensuing apoptosis." Free Radic Biol Med **46**(3): 422-429.

Zheng, L., J. Marcusson and A. Terman (2006). "Oxidative stress and Alzheimer disease: the autophagy connection?" Autophagy **2**(2): 143-145.

Zheng, L., K. Roberg, F. Jerhammar, J. Marcusson and A. Terman (2006). "Autophagy of amyloid beta-protein in differentiated neuroblastoma cells exposed to oxidative stress." Neurosci Lett **394**(3): 184-189.

Zheng, L., K. Roberg, F. Jerhammar, J. Marcusson and A. Terman (2006). "Oxidative stress induces intralysosomal accumulation of Alzheimer amyloid beta-protein in cultured neuroblastoma cells." Ann N Y Acad Sci **1067**: 248-251.

Zheng, L., A. Terman, M. Hallbeck, N. Dehvari, R. F. Cowburn, E. Benedikz, K. Kagedal, A. Cedazo-Minguez and J. Marcusson (2011). "Macroautophagy-generated increase of lysosomal amyloid beta-protein mediates oxidant-induced apoptosis of cultured neuroblastoma cells." Autophagy **7**(12): 1528-1545.

Zhuo, J. M., G. S. Portugal, W. D. Kruger, H. Wang, T. J. Gould and D. Pratico (2010). "Diet-induced hyperhomocysteinemia increases amyloid-beta formation and deposition in a mouse model of Alzheimer's disease." Curr Alzheimer Res **7**(2): 140-149.

Zhuo, J. M. and D. Pratico (2010). "Acceleration of brain amyloidosis in an Alzheimer's disease mouse model by a folate, vitamin B6 and B12-deficient diet." Exp Gerontol **45**(3): 195-201.

Zhuo, J. M. and D. Pratico (2010). "Normalization of hyperhomocysteinemia improves cognitive deficits and ameliorates brain amyloidosis of a transgenic mouse model of Alzheimer's disease." FASEB J **24**(10): 3895-3902.